

GEMS & GEMOLOGY

VOLUME XXXIV

FALL 1998



THE QUARTERLY JOURNAL OF THE GEMOLOGICAL INSTITUTE OF AMERICA

GEMS & GEMOLOGY

FALL 1998

VOLUME 34 NO. 3

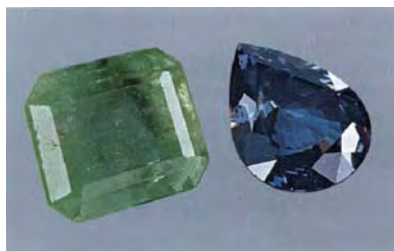
T A B L E O F C O N T E N T S



pg. 159



pg. 198



pg. 210

pg. 217



EDITORIAL

- 157** Demystifying Diamond Cut
William E. Boyajian

FEATURE ARTICLES

- 158** Modeling the Appearance of the Round Brilliant Cut Diamond: An Analysis of Brilliance
T. Scott Hemphill, Ilene M. Reinitz, Mary L. Johnson, and James E. Shigley
- 184** Cultured Abalone Blister Pearls from New Zealand
Cheryl Y. Wentzell

NOTES AND NEW TECHNIQUES

- 202** Estimating Weights of Mounted Colored Gemstones
Charles I. Carmona

REGULAR FEATURES

- 212** Gem Trade Lab Notes
218 Gem News
231 1998 Challenge Winners
232 Book Reviews
234 Gemological Abstracts

ABOUT THE COVER: Because abalone pearls are admired for their rarity, attractive colors, and striking iridescence, efforts have been made to culture them for more than a century. Only recently has commercial production of cultured abalone blister pearls been achieved. A feature article in this issue examines the history, production, marketing, and identifying characteristics of assembled cultured blister pearls from one major producer, Empress Abalone Ltd., using New Zealand's Haliotis iris. These abalone "mabés" are being incorporated into distinctive jewelry designs, together with colored stones and diamonds. The gold pendants and rings shown here contain abalone "mabés" ranging from 12.5 to 17.3 mm in diameter. Jewelry courtesy of designer Ian Henderson, Dunedin, New Zealand.

Photo © Harold & Erica Van Pelt—Photographers, Los Angeles, California.

Color separations for Gems & Gemology are by Pacific Color, Carlsbad, California.

Printing is by Fry Communications, Inc., Mechanicsburg, Pennsylvania.

© 1998 Gemological Institute of America All rights reserved. ISSN 0016-626X



DEMYSTIFYING DIAMOND CUT



The proper assessment of cut in diamonds has long been an elusive, but intriguing, goal. As the authors point out in the lead article, most diamond grading systems in use today establish parameters for cut grades in round brilliants based on a variation of proportions devised by Marcel Tolkowsky in 1919. For nearly 80 years now, there have been few, if any, rigorous attempts to shed more light on the subject.

Recognizing this fact, several years ago the Gemological Institute of America made a long-term commitment to establish a comprehensive understanding of the effects of cut and proportions on diamond appearance. Our goal was, and is, to develop modern criteria for cut assessment using today's sophisticated technology, and to integrate this knowledge into our diamond education and training courses. When the study has been successfully completed, this knowledge may even be applied to our laboratory reporting and instrument development.

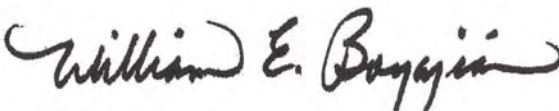

This much-anticipated first article on GIA's three-dimensional, ray-tracing computer model addresses the most

important appearance concept, brilliance, based on what the authors call "weighted light return." As the authors state, a brilliance measurement is one of several important pieces of the "cut" puzzle; dispersion, scintillation, and perhaps symmetry and color, are others. Since a polished diamond should display a pleasing combination of brilliance, fire, and scintillation, the elusive "best" overall appearance might not be found among just the brightest round brilliant cuts. Thus, we caution you to read this article fully and carefully, and to refrain from drawing unequivocal conclusions from this initial work.

So what *do* we know at this point? Certainly, we know that cut is the most complex of the 4 C's, even when isolated to one cutting style: the round brilliant. We know that the success of cutting for weighted light return has more to do with the interrelationship between three critical proportions—table size, crown angle, and pavilion angle—than on a selection of isolated proportion measurements. We know that one cannot, and must not, assess the cut of a diamond by examining any one of these proportion parameters alone.

We also know that there are many combinations of proportions that yield equally attractive round-brilliant-cut diamonds. In fact, we know that diamonds can be cut in a fairly wide range of proportions to yield the same high light return, which can lead to better utilization of the rough and a better fit with the myriad tastes that exist in the global marketplace.

Finally, we know from our extensive historical research on cut that there have been numerous claims to a single set of "Ideal" proportions in round-brilliant-cut diamonds. These have ranged from Wade's American Ideal in 1916 (with a 45.3% table, a 35° crown angle, and a 41° pavilion angle) to Watermeyer's Modern Ideal in 1991 (with a 61% table, a 34° crown, and a 41° pavilion). The derivation and use of the term "Ideal" is thus confusing at best, somewhat like "blue-white" and "perfect" decades ago. Although it is not GIA's role to discredit the concept of an "Ideal" cut, on the basis of our research to date we cannot recommend its use in modern times.



William E. Boyajian, President
Gemological Institute of America

MODELING THE APPEARANCE OF THE ROUND BRILLIANT CUT DIAMOND: AN ANALYSIS OF BRILLIANCE

By T. Scott Hemphill, Ilene M. Reinitz, Mary L. Johnson, and James E. Shigley

Of the “four C’s,” cut has historically been the most complex to understand and assess. This article presents a three-dimensional mathematical model to study the interaction of light with a fully faceted, colorless, symmetrical round-brilliant-cut diamond. With this model, one can analyze how various appearance factors (brilliance, fire, and scintillation) depend on proportions. The model generates images and a numerical measurement of the optical efficiency of the round brilliant—called weighted light return (WLR)—which approximates overall brilliance. This article examines how WLR values change with variations in cut proportions, in particular crown angle, pavilion angle, and table size. The results of this study suggest that there are many combinations of proportions with equal or higher WLR than “Ideal” cuts. In addition, they do not support analyzing cut by examining each proportion parameter independently. However, because brilliance is just one aspect of the appearance of a faceted diamond, ongoing research will investigate the added effects of fire and scintillation.

ABOUT THE AUTHORS

Mr. Hemphill is research associate, and Dr. Shigley is director, of GIA Research, Carlsbad, California. Dr. Reinitz is manager of Research and Development at the GIA Gem Trade Laboratory (GIA GTL), New York. Dr. Johnson is manager of Research and Development at GIA GTL, Carlsbad.

Please see acknowledgments at the end of the article.

Gems & Gemology, Vol. 34, No. 3, pp. 158–183
© 1998 Gemological Institute of America

The quality and value of faceted gem diamonds are often described in terms of the “four C’s”: carat weight, color, clarity, and cut. Weight is the most objective, because it is measured directly on a balance. Color and clarity are factors for which grading standards have been established by GIA, among others. Cut, however, is much less tractable. Clamor for the standardization of cut, and calls for a simple cut grading system, have been heard sporadically over the last 25 years, gaining strength recently (Shor, 1993, 1997; Nestlebaum, 1996, 1997). Unlike color and clarity, for which diamond trading, consistent teaching, and laboratory practice have created a general consensus, there are a number of different systems for grading cut in round brilliants. As discussed in greater detail later in this article, these systems are based on relatively simple assumptions about the relationship between the proportions and appearance of the round brilliant diamond. Inherent in these systems is the premise that there is *one* set (or a narrow range) of preferred proportions for round brilliants, and that any deviation from this set of proportions diminishes the attractiveness of a diamond. In this article, we present and discuss our findings with regard to the rather complex relationship between cut proportions and brilliance.

Diamond manufacturing has undergone considerable change during this century. For the most part, diamonds are cut within very close proportion tolerances, both to save weight while maximizing appearance and to account for local market preferences (Caspi, 1997). As shown in figure 1 and table 1, however, differences in proportions can produce noticeable differences in appearance in round-brilliant-cut diamonds. Within this single cutting style, there is substantial debate—and some strongly held views—about which proportions yield the best face-up appearance (Federman, 1997). Yet face-up appearance depends as well on many intrinsic physical and optical properties of diamond as a

Figure 1. These round-brilliant-cut diamonds illustrate how cut affects face-up appearance. Of the three larger stones (1.07–1.50 ct), the one on the lower right (F color) is obviously less bright than the other two (above, H color, and lower left, E color). All three 0.35–0.38 ct diamonds in the inset are brighter, on average; but the F-color diamond on the lower right, which could be marketed as an “Ideal” cut, is less bright than the F- and G-color stones with larger tables and small crown angles. See table 1 for the proportions and other data on these diamonds. Photo © GIA and Tino Hammid.



material, and on the way these properties govern the paths of light through the faceted gemstone. (Also important are properties particular to each stone, such as polish quality, symmetry, and the presence of inclusions.)

Diamond appearance is described chiefly in terms of *brilliance* (white light returned through the crown), *fire* (the visible extent of light dispersion into spectral colors), and *scintillation* (flashes of light reflected from the crown). Yet each of these terms represents a complex appearance concept that has not been defined rigorously, and that cannot be expressed mathematically without making some assumptions and qualifications (see below).

Despite the widespread perception in the trade that diamond appearance has been extensively addressed, there is limited information in the literature, and some aspects have never been examined. Several analyses of the round brilliant cut have been published, starting with Wade (1916). Best known are Tolokowsky's (1919) calculations of the proportions that he believed would optimize the appearance of the round-brilliant-cut diamond. However, Tolokowsky's calculations, as well as most others since then, involved two-dimensional images as graphical and mathematical models. These were

used to solve sets of relatively simple equations that described what was considered to be the brilliance of a polished round brilliant diamond. (Tolokowsky did include a simple analysis of fire, but it was not central to his model and it will not be discussed at any length in this article.) For the most part, the existing cut grading systems are based on Tolokowsky's research.

We believe that diamond cut, as a matter of such importance to the trade, deserves a more thorough and thoughtful investigation. The issues raised can only be resolved by considering the complex combination of physical factors that influence the appearance of a faceted diamond (i.e., the interaction of light with diamond as a material, the shape of a given polished diamond, the quality of its surface polish, the type of light source, and the illumination and viewing conditions), and incorporating these into an analysis of that appearance.

The initial goal of this research project was to develop a theoretical model for the interaction of light with a faceted diamond that could serve as the basis for exploring many aspects of the effect of cut on appearance. Computer graphics simulation techniques were used to develop the model presented here, in conjunction with several years of research

TABLE 1. Proportions and calculated WLR values for the diamonds photographed in figure 1.

Position	Color	Weight (ct)	Table size (%)	Crown angle (°)	Pavilion angle (°)	Calculated WLR ^a
Main photo						
Top	H	1.21	62	29.4	41.7	0.279
Lower right	F	1.50	63	39.8	41.7	0.257
Lower left	E	1.07	57	34.6	40.9	0.282
Inset						
Top	G	0.38	60	26.5	42.6	0.288
Lower right	F	0.35	56	34.7	41.2	0.281
Lower left	F	0.35	59	27.0	41.4	0.290

^a WLR, our metric for overall brightness, is calculated from the given crown angle, pavilion angle, and table size, using our standard reference proportions (given in table 4) for the other five parameters.

on how to express mathematically the interaction of light with diamond and also the various appearance concepts (i.e., brilliance, fire, and scintillation). Our model serves as a general framework for examining cut issues; it includes mathematical representations of both the shape of a faceted diamond and the physical properties governing the movement of light within the diamond. We plan to analyze the appearance aspects one at a time and then, ultimately, assemble the results in order to examine how proportions affect the balance of brilliance, fire, and scintillation.

The *general* mathematical model presented in this article uses computer graphics to examine the interaction of light with a standard (58 facet) round-brilliant-cut diamond with a fully faceted girdle. For any chosen set of proportions, our model can produce images and numerical results for an appearance concept (by way of a mathematical expression). To compare the appearance concepts of brilliance, fire, and scintillation in round brilliants of different proportions, we need a quantity to measure and a relative scale for each concept. A *specific* mathematical expression (with its built-in assumptions and qualifications) that aids the measurement and comparison of a concept such as brilliance is known as a *metric*. In this study, we derived a metric for brilliance that quantifies the amount of light returned from a modeled diamond for averaged illumination and viewing arrangements, as described

below. Although other factors (e.g., bodycolor or inclusions) may also influence how bright a particular round brilliant appears, light return is an essential feature of diamond brilliance.

In future reports on this project, we plan to address how fire and scintillation are affected by proportions. We also intend to examine how symmetry, lighting conditions, and other factors affect all three of these appearance concepts. The overall goal of this research is to provide a comprehensive understanding of how cut affects the appearance of a faceted diamond.

BACKGROUND

Early History. Diamond faceting began in about the 1400s and progressed in stages toward the round brilliant we know today (see Tillander, 1966, 1995). In his early mathematical model of the behavior of light in fashioned diamonds, Tolkowsky (1919) used principles from geometric optics to explore how light rays behave in a prism that has a high refractive index. He then applied these results to a two-dimensional model of a round brilliant with a knife-edge girdle, using a single refractive index (that is, only one color of light), and plotted the paths of some illustrative light rays.

Tolkowsky assumed that a light ray is either totally internally reflected or totally refracted out of the diamond, and he calculated the pavilion angle needed to internally reflect a ray of light entering the stone vertically through the table. He followed that ray to the other side of the pavilion and found that a shallower angle is needed there to achieve a second internal reflection. Since it is impossible to create substantially different angles on either side of the pavilion in a symmetrical round brilliant diamond, he next considered a ray that entered the table at a shallow angle. Ultimately, he chose a pavilion angle that permitted this ray to exit through a bezel facet at a high angle, claiming that such an exit direction would allow the dispersion of that ray to be seen clearly. Tolkowsky also used this limiting case of the ray that enters the table at a low angle and exits through the bezel to choose a table size that he claimed would allow the most fire. He concluded by proposing angles and proportions for a round brilliant that he believed best balanced the brilliance and fire of a polished diamond, and then he compared them to some cutting proportions that were typical at that time. However, since Tolkowsky only considered one refractive index, he could not verify the extent to which any of his rays

would be dispersed. Nor did he calculate the light loss through the pavilion for rays that enter the diamond at high angles.

Over the next 80 years, other researchers familiar with this work produced their own analyses, with varying results (see table 2). It is interesting (and somewhat surprising) to realize that despite the numerous possible combinations of proportions for a standard round brilliant, in many cases each researcher arrived at a *single* set of proportions that he concluded produced an appearance that was superior to all others. Currently, many gem grading laboratories and trade organizations that issue cut grades use narrow ranges of proportions to classify cuts, including what they consider to be best (table 3).

Several cut researchers, but not Tolokowsky, used "Ideal" to describe their sets of proportions, which vary significantly, as seen in table 2. Today, in addition to systems that incorporate "Ideal" in their names, many people use this term to refer to measurements similar to Tolokowsky's proportions, but with a somewhat larger table (which, at the same crown angle, yields a smaller crown height percentage). This is what we mean when we use "Ideal" in this article.

Recent Appearance Models and Measurements. We found thorough descriptions of three computer models of round brilliant diamonds in the literature. One model explored light return numerically (Tognoni, 1990); another produced a number of monochromatic images, each using a different refractive index, and some numerical output (Astric et al., 1992); but the third (Dodson, 1979) was similar to our work in several ways. Using a three-dimensional model of a fully faceted round brilliant diamond, Dodson devised metrics for brilliance, fire, and "sparkliness" (scintillation). His mathematical model employed a full sphere of approximately diffuse illumination centered on the diamond's table. His results were presented as graphs of brilliance, fire, and sparkliness for 120 proportion combinations. They show the complex interdependence of all three appearance aspects on pavilion angle, crown height, and table size. His model (as well as that of Shannon and Wilson, as best we can determine from the little published on it [Lawrence, 1998; Shor, 1998]) is distinct from ours in that all rays emerging from the diamond were weighted equally. Three of Dodson's results are given in table 2.

There are also computer-aided-design (CAD) software programs for creating gemstone cuts and

analyzing the effect of cut on the appearance of the finished gemstone. (One of these, Gem-Cad, is marketed by Gemsoft Enterprises, Austin, Texas.)

These computer programs and mathematical models use ray-tracing algorithms to produce visual images of gemstones or numerical data about their appearance, or both. However, each of the programs described above excludes one or more of the starting assumptions that we employ here (e.g., wavelength-dependent refractive index, accounting for secondary rays, weighing observer angles; see below and Box A). Because of these differences, our computer graphics program is not directly comparable to these other programs. However, the optimal proportions predicted by those models can be assessed and compared using our metric for brilliance.

Commercial services are currently available that claim to measure the brilliance of fashioned stones. The measurements of brilliance provided by Diamond Profile (Portland, Oregon) are based on digital video images through the crown of the diamond under a few controlled lighting conditions, which are then combined to generate graphic results for that particular stone (Gilbertson and Walters, 1997; Gilbertson, 1998).

DESCRIPTION OF OUR MODEL

In general, within a mathematical model, all of the factors we consider important to diamond appearance—the diamond itself, its proportions and facet arrangement, and the lighting and observation conditions—can be carefully controlled, and fixed for a given set of analyses. Such control is nearly impossible to achieve with actual diamonds. Furthermore, with this model we can examine thousands of sets of diamond proportions that would not be economically feasible to create from diamond rough. Thus, use of a model allows us to explore how cut proportions affect diamond appearance in a more comprehensive way than would be possible through observation of actual round brilliants. However, every mathematical model incorporates some assumptions, and these built-in conditions affect the nature of the results. (The modeled diamond used in Tolokowsky's [1919] analysis, for example, was two-dimensional and had a knife-edge girdle, which limited the number and paths of light rays he could consider.)

Real diamonds will inevitably differ from the model conditions because of inclusions, symmetry deviations, and the like. Nevertheless, a theoretical model provides a goal to reach toward: What is the

best result—best brilliance, best fire, best balance of the two, best scintillation, best weight retention, best combination—that can be achieved from a particular piece of rough? In addition, a theoretical understanding of the behavior of light in a faceted diamond could help in the design of any instrument intended to measure optical performance in real diamonds.

Finally, a model of the interaction of light with a faceted diamond can be used to compare and contrast different metrics and different lighting and observation conditions, as well as evaluate the dependence of those metrics on proportions, symmetry, or any other property of diamond included in the model. In the following sections, we present the assumptions and methods on which our model is based, and introduce our metric for brilliance.

Assumptions and Methods. The mathematical model presented here creates a fresh structure for examining nearly all aspects of the influence that cut has on a diamond's appearance. Box A provides the assumptions on which the model is based: a detailed list of the physical properties included in the model, a mathematical description of the proportions of the round brilliant, and a description of the lighting condition used in this study. The inclusion of these many physical properties distinguishes this model from previous work, and the details of the lighting conditions affect the specific numerical values we present here. The model traces rays from the modeled light source through a mathematical representation of a round brilliant of any chosen proportions (referred to hereafter as the "virtual" diamond) to produce two kinds of results: (1) digital images of the virtual diamond, and (2) a numerical evaluation of an appearance concept (in this case, brilliance).

A digital image (see, e.g., figure 2), drawn from the perspective of our choice, is a two-dimensional array of picture elements (pixels), each of which comprises a small area of the virtual diamond. We traced up to one million rays of various colors for each pixel in an image, to obtain convergence of the color and total brightness for that small area. As the computer traces the first few hundred rays, randomly selecting wavelengths and angles of incidence, the computed brightness and color for a given pixel change rapidly. Eventually, when enough different directions and wavelengths have been traced, the computed brightness and color settle down, or converge, to particular values, and tracing more rays

does not change these values. The resolution of the image depends on our choice of the number of pixels to compute for a particular image size. For most of the images presented in this article, we calculated the color and brightness of 65,536 pixels, requiring up to 65,000,000,000 traced rays.

The computer program employed is not a commercial product, but was written specifically for this work by the first author. It was written in C, a scientific programming language. The program has been run on a Pentium personal computer, on two models of Digital Equipment Corp.'s Alpha workstation, and on a dual Pentium II. If the convergence thresholds and choice of resolution are maintained, the hardware used to run the program does not alter the results. The accuracy of the program, in general and on different kinds of hardware, was verified with a simple test problem for which we had computed a result manually. Further details of the ray tracing and computational methods will be given by Hemphill et al. (in preparation). These techniques extend the methods described by Foley (1996).

Defining Metrics: Brilliance. Our aim is to use this model to explore how brilliance, fire, and scintillation vary with the proportions of a round brilliant diamond. We begin with brilliance for several reasons. First, brilliance is the aspect of diamond appearance that is most immediately noticed. Second, it is an aspect for which the desired outcome is obvious: Bright is good and dark is not. Last, most of the previous work investigating cut focused on brilliance (see references in table 2), and it is this work that has fueled the current trade debate about cut.

One advantage of using a computer model is the capability it gives us to examine thousands of proportion variations. To make sense of so much data, however, we needed to define a metric for brilliance, and use it to compare the performance of the different proportion combinations. The *GIA Diamond Dictionary* (1993, p. 28) defines brilliance as the "intensity of the internal and external reflections of white light from the crown. . . ." A variety of mathematical expressions can be created to describe such light return. Each expression requires explicit or implicit assumptions about what constitutes brilliance and about light sources, viewing geometry, response of the human eye, and response of the human brain. As an example of this last consideration, should a mathematical definition of brilliance represent one viewing geometry—that is, a

TABLE 2. Superior proportions for a round-brilliant-cut diamond, as suggested by previous investigators.

Name	Investigator	Year	Table size (%)	Crown angle (Crown height)	Pavilion angle (Pavilion height)	Total depth (%)	Girdle thickness (%)	Calculated WLR ^a
American Ideal	Wade	1916	45.3	35° (19.2%)	41° (43.5%)	62.7	0	0.266
(None)	Tolkowsky ^b	1919	53	34.5° (16.2%)	40.75° (43.1%)	59.3	0	0.281
Ideal	Johnsen	1926	56.1	41.1° (19.2%)	38.7° (40%)	59.2	nd ^c	0.252
Ideal	Rösch	1926, 1927	56	41.1° (19%)	38.5° (40%)	59	0	0.251
Normal Universal	Stoephasius	1931	54	38° (18%)	36.5° (37%)	56 ^d	1	0.262
(None)	Stoephasius	1931	52	41° (21%)	39.4° (41%)	64	2	0.248
(None)	Stoephasius	1931	50	43.8° (24%)	41.4° (44%)	72	4	0.216
Total Reflection	Maier	1936, 1938	nd	40.8°–41.3°	38.6°	nd	nd	0.237–0.251 ^a
Ideal	Bergheimer	1938	nd	41.1°	38.7°	nd	nd	0.238–0.243 ^a
Ideal	Eppler	1933, 1938	56	41.1° (19%)	38.5° (40%)	59	2	0.251
Practical Fine	Eppler	1939	56	33.2° (14.4%)	40.8° (43.2%)	57.6	nd	0.284
Ideal Type I	Eppler	1939, 1940	56.1	41.1° (19.2%)	38.7° (40%)	59.2	2	0.252
Ideal Type II	Eppler ^b	1940	57.1	33.1° (14%)	40.1° (42.1%)	57.6	1.5	0.281
Ideal	Eppler and Klüppelberg	1940	56.1	41.1° (19.2%)	38.7° (40%)	59.2	nd	0.252
Practical Fine I	Eppler and Klüppelberg	1940	55.3	35.6° (16%)	38.6° (39.9%)	55.9	2	0.274
Practical Fine II	Eppler and Klüppelberg	1940	57.1	33.1° (14%)	40.1° (42.1%)	56.1	1.5	0.281
Practical Fine III	Eppler and Klüppelberg ^b	1940	69	32.8° (10%)	41.7° (44.6%)	54.6	1	0.264
(None)	Parker (cited by Eppler, 1973)	1951	55.9	25.5° (10.5%)	40.9° (43.4%)	53.9	nd	0.297
Practical Fine	Schlossmacher	1969	56.4	33.2° (14.4%)	40.8° (43.2%)	57.6	nd	0.284
Standard Cut	ScanDN ^e	1979	57.5	34.5° (14.6%)	40.75° (43.1%)	57.7	2 to 3	0.282
Brilliance Design	Suzuki ^f	1970	56	41.1° (19%)	38.7° (40%)	59	nd	0.252
Dispersion Design	Suzuki ^f	1970	58	48.6° (23%)	38.9° (40%)	63 ^d	nd	0.205
(None)	Elbe	1972	nd	(14.6%)	47° (53.7%)	68.3	nd	nc ^g
Optical Symmetrical	Eulitz	1972	56.5	33.6° (14.45%)	40.8° (43.15%)	59.1	1.5	0.283
(Brightest)	Dodson ^{b,f}	1979	40	26.5° (15%)	43°	nd	nd	0.277
(Most fire)	Dodson ^{b,f}	1979	60	26.5° (10%)	43°	nd	nd	0.287
(Most sparkliness)	Dodson ^{b,f}	1979	50	31.0° (15%)	52°	nd	nd	0.247
Australian Ideal	Connellan and Pozzibon	1984	56	33.75° (14.3%)	39.66° (41.45%)	55.75	nd	0.281
Modern Ideal	Watermeyer	1991	61	34.0°	41.0°	nd	nd	0.279
(None)	Shannon and Wilson ^f (Shor, 1998)	1998	61	32°	(41%)	nd	nd	0.275
(None)	Shannon and Wilson ^f (Shor, 1998)	1998	57	32°	(42%)	nd	nd	0.281
(None)	Shannon and Wilson ^f (Shor, 1998)	1998	58	33.5°	(43.1%)	nd	nd	0.282
(None)	Shannon and Wilson ^f (Shor, 1998)	1998	50	33°	(46%)	nd	nd	0.279

^a WLR, our metric for overall brightness, is calculated from the given crown angle, pavilion angle, and table size, using our standard reference proportions (given in table 4) for the other five parameters. For Maier's "Total Reflection" and Bergheimer's "Ideal" cuts, where no table size was specified, we calculated WLR for tables ranging from 50% to 70%.

^b Used broad illumination across the entire crown rather than the vertical illumination used by others.

^c nd = not defined.

^d The measurements given are not consistent with this depth percentage.

^e Scandinavian Diamond Nomenclature Committee.

^f Used three-dimensional analysis rather than the two-dimensional analyses used by other investigators.

^g nc = not calculated (not enough information to calculate the WLR value).

TABLE 3. Proportions for some of the cut grading systems for round brilliant diamonds used today.^a

Cut grading system ^b	Category ^a	Table size (%)		Crown angle (°)		Pavilion angle (°)		Pavilion depth (%)	
		Min.	Max.	Min.	Max.	Min.	Max.	Min.	Max.
AGA	*1A	53	58	34.3	34.7	40.5 ^d	40.8 ^d	42.8	43.2
	1B	52.0–52.9	58.1–60.0	34.01–34.2	34.81–35.0	40.36–40.5 ^d	40.9–41.0 ^d	42.5–42.7	43.3–43.5
	2A	51.5–51.9	60.1–63.0	32.1–33.9	35.1–35.8	40.03–40.03 ^d	41.08–41.3 ^d	42.0–42.4	43.6–44.0
	3A	50.5–50.9	64.1–67.0	29.6–30.0	38.0–39.4	39.35–39.6 ^d	42.0–42.3 ^d	41.0–41.4	45.0–45.5
AGJ	* Excellent	53	58	33	35	40.0 ^d	41.3 ^d	42	44
	Very Good	52	63	32	36	40.0 ^d	42.0 ^d	42	45
	Good	50	67	30	38	39.3 ^d	43.2 ^d	41	47
AGS	*0	52.4	57.5	33.7	35.8	40.16 ^d	41.2 ^d	42.2	43.8
	1	51.4–52.3	57.6–59.5	32.7–33.6	35.9–36.3	40.16 ^d	41.3–41.5 ^d	42.2	43.9–44.3
	3	50.4–51.3	61.6–63.5	31.7–32.1	36.9–37.3	40.16 ^d	41.3–41.5 ^d	42.2	43.9–44.3
	5	49.4–50.3	65.6–67.5	30.7–31.1	37.9–38.3	39.1–39.4 ^d	42.2–42.5 ^d	40.7–41.1	45.4–45.8
AGT	* Excellent	53	60	33	35	40.7 ^d	40.7 ^d	43	43
	Very Good	52	64	32	36	40.0 ^d	41.3 ^d	42	44
	Good	51	68	30	38	39.3 ^d	42.6 ^d	41	46
CGL	* Excellent	52	58	33	35	40.0 ^d	41.3 ^d	42	44
EGL	* Exceptional	54	57	34	35	40.5	41.0	42.5	43.5
HRD	* Very Good	53	66	30.7	37.7	39.6 ^f	42.2 ^f	41.5 ^f	45 ^f
IGI	* Ideal	53	60	33	36	40.0 ^d	41.3 ^d	42	44
Rap	* Specification A	55	64	30	35	nd	nd	nd	nd
ScanDN	* Good	52	65	30	39	40	42	42	45

^a Asterisk (*) indicates top grade. Generally all parameters must be in the specified ranges for the stone to receive the top grade; variation in any parameter reduces the grade accordingly. Abbreviations: Max. = maximum, Min. = minimum, med. = medium, sl. = slightly, ex. = extra, v. = very.

^b The full names and countries of the organizations are indicated below. For some organizations, only the top grade is provided. All of the information provided in this table was obtained from the respective organizations:

AGA = As reported in *Fine Make, Accredited Gem Appraisers, 1997, U.S.* (Class 1A and 1B = "American Ideal Cut," Class 2A = "International Fine Cut," Class 3A = "U.S. Domestic Average Cut." Values given for stones ≥ 0.5 ct)

AGJ = Association of Gemological Laboratories, 1993, Japan

AGS = American Gem Society, 1997, U.S.

AGT = Association of Japan Gem Trust, 1995, Japan

CGL = Central Gem Laboratory, 1993, Japan

EGL = European Gemological Laboratory, U.S. (G. Sherman, pers. comm., 1997)

HRD = Hoge Raad voor Diamant, 1993, Belgium

IGI = International Gemological Institute, 1997, U.S.

"snapshot"—or an average over many viewing situations? We chose the latter approach.

Weighted Light Return. The metric we discuss in this article is called *weighted light return* (WLR); it is specific to each set of modeled diamond proportions with the chosen illumination. After examining a variety of possible metrics for brilliance, we developed WLR to best represent the way the experienced viewer sees a diamond, especially one

mounted in jewelry, with lighting that illuminates the stone from all around without excessive glare or shadow.

The WLR is a weighted sum of the amount of light returned through the crown of the virtual diamond to all positions of observation above the girdle. Rather than using the total fraction of light returned through the crown for a fixed arrangement of the light source, diamond, and viewer, we weighed the relative importance of returned light

Total depth (%)		Girdle thickness (%) ^a		Calculated WLR ^c	
Min.	Max.	Min.	Max.	Min.	Max.
58.7	62.3	thin (1.7%)	med. (3.0%)	0.281	0.283
58.3–58.69	62.31–62.99	thin (1.5%)	sl. thick (4.5%)	0.278	0.284
57.9–58.29	63.0–63.5	thin (1.0%)	sl. thick (4.5%)	0.271	0.286
57.0–57.49	63.81–64.1	v. thin (0.4%)	v. thick (7.0%)	0.245	0.289
59.2	62.4	thin	sl. thick	0.279	0.285
58	63.8	ex. thin	sl. thick	0.270	0.286
56.8	65.9	ex. thin	v. thick	0.248	0.289
nd ^e	nd	thin	sl. thick	0.275	0.284
nd	nd	v. thin	nd	0.271	0.285
nd	nd	nd	thick	0.262	0.286
nd	nd	nd	v. thick	0.250	0.288
59	63	thin	sl. thick	0.279	0.284
58	64	thin	thick	0.269	0.286
56	66	v. thin	v. thick	0.252	0.289
59.2	62.4	thin	sl. thick	0.278	0.285
nd	nd	thin	med.	0.284	0.284
55.5	63.9	thin	med.	0.262	0.288
58.5	62.5	thin	sl. thick	0.274	0.285
57.5	62.5	v. thin	thick	nc ^g	nc
nd	nd	v. thin	sl. thick	0.251	0.288

Rap = Rapaport Diamond Report, ©1998, U.S.

ScanDN = Scandinavian Diamond Nomenclature Committee, 1979, Denmark

^c Minimum and maximum WLR values were calculated for the entire range of properties listed. See text.

^d Converted from pavilion depth using the formula given in Box A.

^e nd = not defined.

^f The given pavilion angle and pavilion depth do not correlate exactly.

^g nc = not calculated (not enough information to calculate the WLR values).

rays based on their exit direction. An experienced diamond observer assesses the diamond primarily on the basis of its face-up appearance, but also “rocks” the stone both to minimize the effect of glare and to consider the stone from various angles, with the views closest to vertical (face-up) weighing the most in this evaluation. We wanted the metric we chose to behave like this assessment. Therefore, we wanted the contribution from rays that emerged straight up to be much greater than that from rays

that exited horizontally, with a smooth variation as the exit angle changed. We chose the square of the cosine function, applied to the exit angle measured from the vertical, as a weighting factor (figure 3). In contrast to this, both Dodson (1979) and Shannon and Wilson (Shor, 1998) considered all views of the diamond’s crown to be equally important, and so they weighed much larger angles from the vertical far more heavily than our metric does (or than experienced observers do).

With this weighting function, we constrained the scale of the numbers for our metric between values of 0 and 1. For instance, if we could construct a virtual diamond in which all light that entered left the crown straight up, it would have a WLR equal to 1.000; but if all the light that entered left the crown at an angle of 25° to the horizontal, the WLR would be 0.179. If light only exited from the crown horizontally (or no light left through the crown), the WLR would be 0. Similarly, if half the light passed out of the crown at 45°, one fourth exited at 25°, and the remaining fourth was horizontal, the WLR would equal 0.294. This weighting function emphasizes the angle at which a light ray exits the virtual diamond, rather than which facet the ray exits.

Note that we excluded glare—that is, any light directly reflected from the top surface—from the WLR value (a difference from the *GIA Diamond Dictionary* definition of brilliance). We made this simple change in our computer program to guarantee that any trends in the WLR data were not simply due to an increased area of the crown acting like a front-surface reflector. However, this is also a reasonable change to the metric, since when experienced observers “rock” a diamond, they mentally correct for the effects of glare. (We also checked our results with glare included and found that although the WLR values increased across the whole range of proportions, the relative variation was essentially unchanged.)

We systematically explored the dependence of WLR on the eight proportion parameters that define the perfectly symmetrical round brilliant diamond (again, see Box A) by changing one or more of these parameters across the ranges given in table 4 and computing the WLR for each set of proportions. Although ideally we would have liked to examine all the interactions between WLR and the eight parameters, this was not practical given existing computer hardware. If we were interested in the co-variation of, say, 20 values for each of the eight parameters, we would require 20⁸ =

BOX A: BASIC DESCRIPTION OF OUR MODEL

We describe a faceted diamond as a convex polyhedron, a three-dimensional object with a surface that is bounded by flat planes and straight edges, with no indentations or clefs. The model requires that all surfaces be faceted, including the girdle, and currently excludes consideration of indented naturals or cavities. To date, we have focused our calculations on the round brilliant cut because of its dominant position in the market, but this model can be used for nearly any fully faceted shape. Our modeled round brilliant has mathematically perfect symmetry; all facets are perfectly shaped, pointed, and aligned. Also, all facet junctions are modeled with the same sharpness and depth.

Because our modeled round brilliant has perfect eight-fold symmetry, only eight numbers (parameters) are required to specify the convex polyhedron that describes its shape (figure A-1). (Modeling other shapes or including asymmetries requires additional parameters.) We defined these eight parameters as:

Crown angle	Angle (in degrees) between the bezel facets and the girdle plane
Pavilion angle	Angle (in degrees) between the pavilion mains and the girdle plane
Table size	Table width (as percent of girdle diameter)
Culet size	Culet width (as percent of girdle diameter)
Star length	The ratio of the length of the star facets to the distance between the table edge and girdle edge
Lower-girdle length	The ratio of the length of the lower-girdle facets to the distance between the center of the culet and girdle edge
Girdle thickness	Measured between bezel and pavilion main facets (the thick part of the girdle) and expressed as a percentage of girdle diameter. This differs from the typical use of the term <i>girdle thickness</i> (see, e.g., <i>GIA Diamond Dictionary</i> , 1993)
Girdle facets	Total number of girdle facets

Other proportions, such as the crown height, pavilion depth, and total depth (expressed as percentages of the girdle diameter) can be directly calculated from these eight parameters, using these formulas:

$$\begin{aligned} \text{Crown height} &= \frac{1}{2}(100 - \text{table size}) \times \tan(\text{crown angle}) \\ \text{Pavilion depth} &= \frac{1}{2}(100 - \text{culet size}) \times \tan(\text{pavilion angle}) \\ \text{Total depth} &= (\text{Crown height} + \text{pavilion depth} + \text{girdle thickness}) \end{aligned}$$

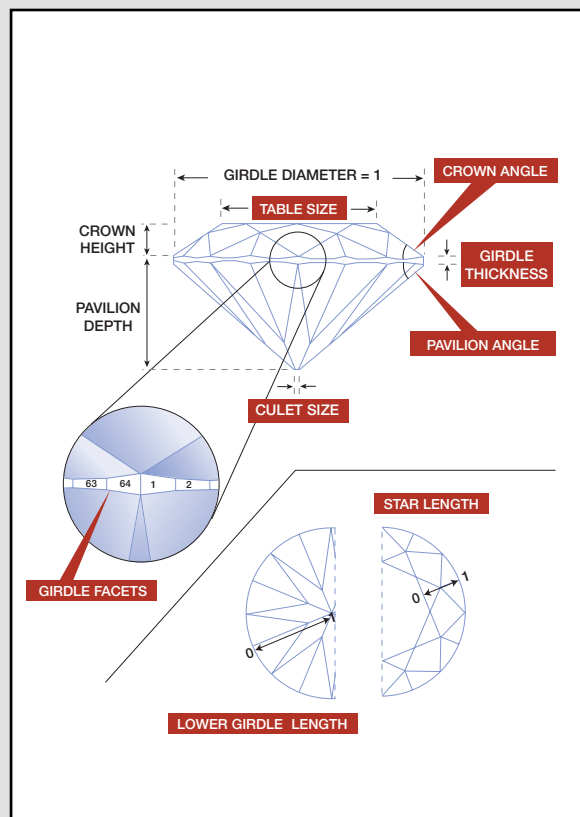
For the results in this article, the diamond simulated in our calculations (called a “virtual” diamond) has no inclusions, is perfectly polished, and is completely colorless. It has a polished girdle, not a bruted one, so that the girdle facets refract light rays in the same way that other facets do. The virtual diamond has relative proportions but no absolute size—that is, no specific carat weight. (The principles governing the way light moves through a colorless diamond do not vary with size.)

We then chose a light source to illuminate our virtual diamond. Most of our results to date, and all the results presented here, used a diffuse hemisphere of even, white light (D65 daylight illumination) shining on the crown. Light rays from every position on the hemisphere point in every direction, not just toward the center of the stone (as in focused light). We selected this illumination condition to best average over the many different ambient light conditions in which diamonds are seen and worn, from the basic trading view of a diamond face-up in a tray next to large north-facing windows, to the common consumer experience of seeing a diamond worn outdoors or in a well-lit room. Diffuse illumination emphasizes the return of white light, although it is a poor lighting condition for examining other aspects, such as fire. This geometry also eliminated the need to consider the shadow that a viewer’s head might cast on a diamond. (In addition, although many mountings, such as a Tiffany setting, allow some light to enter the diamond’s pavilion, the amount of light coming from this direction has not been included in the model.)

Next we examined mathematically how millions of rays of light from the source interact with the transparent, three-dimensional, colorless, fully faceted round brilliant specified by our choice of proportion parameters. Diamond is a dispersive material; the refractive index is different for different wavelengths of light. Since the angle of refraction depends on the refractive index, white light entering the virtual diamond is spread (dispersed) into rays of different colors, and each of these variously colored rays takes a slightly different path through the stone. We used Sellmeier’s formula (see Nassau, 1983 [p. 211]; or, for a more thorough explanation, see Papadopoulos and Anastassakis, 1991) to incorporate this dispersion into the model. With this formula, we obtained the correct refractive index for each of the different colored rays (taken at 1

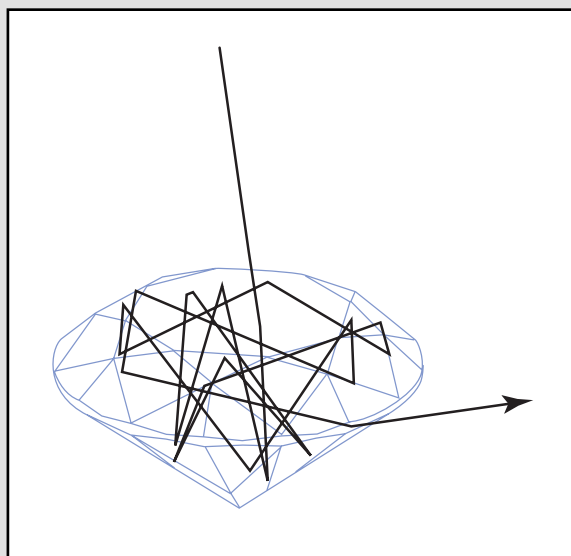
nm intervals from 360 to 830 nm), so that each ray could be traced (followed) individually as it moved through the stone. Some rays follow simple paths with only a few internal reflections, while others follow complex three-dimensional paths (figure A-2). The color distribution of these rays was scaled to the response of the human eye, using "CIE X,Y,Z" color functions as part of the convergence criteria (Wright, 1969).

Figure A-1. We used eight parameters—varied across the range given in table 4—to define our geometric model of the round brilliant shape. (a) All linear distances in this profile view can be described as a percentage of the girdle diameter. The enlarged view of the girdle is centered on the position where we measured the girdle thickness. (b) In this view of the table, the star length is shown at 50%, so that the star facets extend halfway from the table to the girdle (when viewed from straight above). (c) In this view of the pavilion, the lower-girdle length is shown at 75%, so that the lower girdle facets extend three-fourths of the distance from the girdle to the culet (when viewed from straight below).



Each time a ray strikes a facet, some combination of reflection and refraction takes place, depending on the angle between the ray and the facet, the refractive index at the wavelength of the ray, and the polarization state of the ray. Although the rays from our diffuse hemisphere light source are initially unpolarized, a light ray becomes polarized each time it bounces off a facet. The degree and direction of polarization affect how much of the ray is internally reflected, rather than refracted out the next time it intersects a facet. (For example, about 18% of a light ray approaching a diamond facet from the inside at an angle of 5° from the perpendicular is reflected, regardless of the polarization. But at an incidence of 70° , rays with polarization parallel to the plane of incidence are completely lost from the stone, while 55% of a ray polarized perpendicular to the plane of incidence is reflected back into the stone.) The model traces each ray until 99.95% of its incident energy has exited the diamond. The end result of this ray tracing can be either an image of the virtual diamond or the value of a metric for that stone, or both.

Figure A-2. Some of the light rays that pass through the virtual diamond follow complicated paths. Here, we show the track of one light ray within a round brilliant diamond, as calculated by our mathematical model. This ray reflects in multiple directions. Not all light rays reflect this many times, but most take a three-dimensional path through the diamond. The chief inadequacy of a two-dimensional analysis is that light rays must be confined to a single plane.



$20 \times 20 \times 20 \times 20 \times 20 \times 20 \times 20 \times 20 = 25.6$ billion computations, which was not feasible at this time. (Note that each of these computations would require tracing the previously mentioned 65 billion light rays.)

Direct observation of actual diamonds indicates that the overall shape of the round brilliant is primarily determined by three parameters: *crown angle*, *pavilion angle*, and *table size*. (These were the only parameters Tolokowsky considered in his analysis.) Therefore, we examined in detail the changes in WLR as these three important parameters varied together, while holding the others constant. We used about 20 values for each parameter, within the ranges given in table 4. This yielded almost 20,000 proportion combinations, with each calculation requiring several minutes of computer time. We also analyzed the extent to which the other five parameters affect diamond appearance by varying each of them individually while holding the other seven parameters constant at the reference values (again, see table 4).

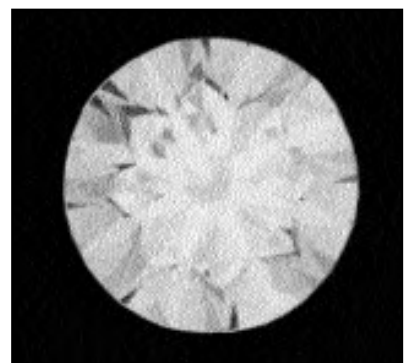
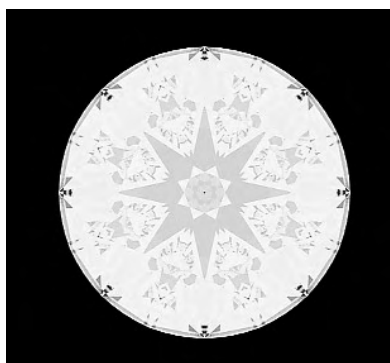
For each chosen set of cut parameters, our computer program can calculate a single WLR value or

an image of the virtual diamond (or both). The WLR values can be compared to one another for different sets of proportions. The bulk of this discussion will focus on the analysis of these WLR values for various ranges of parameters taken singly and in combination. Table 4 lists these ranges for the 20,122 combinations of cut proportions that we have examined for this study. In addition to the WLR values generated for these virtual diamonds, we also examined proportion data obtained from 67,621 actual diamonds measured and graded in the GIA Gem Trade Laboratory (GIA GTL), and we calculated WLR values for virtual diamonds with these combinations of proportions (see Box B).

As a convenience for the readers of this article, for comparison purposes only, we have placed WLR values into five general categories:

High (bright):	WLR values above 0.285
Moderately high:	WLR values from 0.280 to 0.285
Typical:	WLR values from 0.270 to 0.280
Moderately low:	WLR values from 0.265 to 0.270
Low (dark):	WLR values below 0.265

Figure 2. Left: This oblique profile view of a standard round brilliant—a “virtual” diamond (1024 × 1024 pixels)—with commercially acceptable proportions was calculated with our mathematical model using a partial sphere of white light for illumination. This computer-generated image shows how the model captures many of the appearance aspects of an actual diamond, such as three-dimensionality, transparency, facet arrangement, overall light return (brilliance), pattern of light and dark reflections, and dispersion (fire). Center: This digital image (512 × 512 pixels) of a standard round brilliant was calculated face-up with a diffuse hemisphere of white light for illumination. The proportions, used for reference throughout this paper, are: 34° crown angle, 40.5° pavilion angle, 56% table, 3% girdle (at the thickest places, which corresponds to a medium girdle thickness) with 64 girdle facets, 50% star length, 75% lower-girdle length, and 0.5% (“very small”) culet. Right: An actual diamond with proportions comparable to the virtual diamond in the center was photographed in diffuse white light using a hemispherical reflector. This diamond has a 34.5° crown angle, 40.9° pavilion angle, 55% table, faceted girdle of medium thickness, 38.7% star length, very small culet, and excellent symmetry. The lower girdle length was not measured. The diffuse illumination reduces the overall contrast, allowing us to examine brilliance separately from the other appearance aspects. Photo by Vincent Cracco.



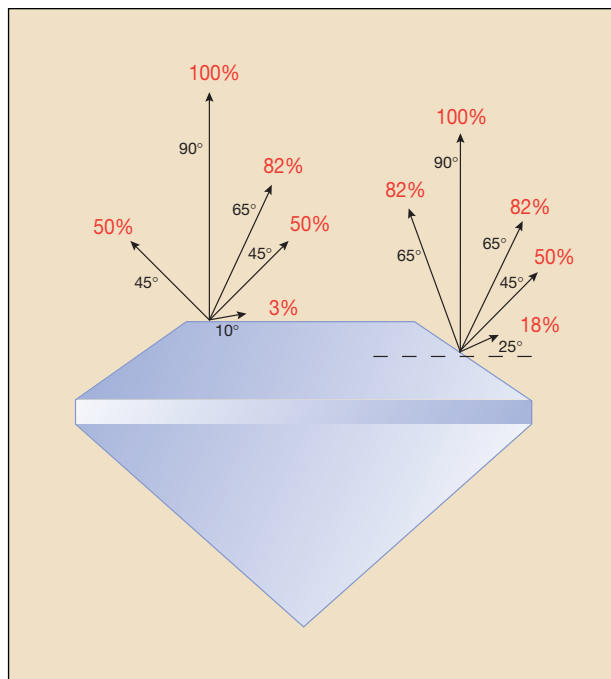


Figure 3. The weighting function used to calculate weighted light return (WLR)—the sum of the squares of the cosines of the angles (from the vertical) at which light rays emerge from the diamond—depends on the angle of the emerging ray to the table plane, regardless of which crown facet it exits. As the relative lengths of the arrows on this illustration indicate, light rays that emerge straight up (perpendicular to the table) are given 100% weight, rays that exit at 45° to the table are given 50% weight, and the rays that exit at 0° (parallel to the girdle plane) are given zero weight (i.e., they do not contribute to the total WLR).

These groups should *not* be taken as WLR or brilliance “grades.” The authors strongly caution against such usage. These terms are provided as a convenience only, to compare the relative brightness of the virtual diamonds in the different WLR ranges.

As seen in figure 1, large differences in WLR correlate to perceptible differences in the overall brightness of actual diamonds. Even over the restricted WLR range in the inset to figure 1, the darkest and brightest stones differ by almost 0.010; this difference is also easily perceived by a trained viewer. In our experience, WLR differences of 0.005 are discernable among stones with the same color and clarity grades when examined with controlled observation environments and lighting conditions.

RESULTS

Images and WLR. The calculations made with our model produced realistic digital images of virtual diamonds (again, see figure 2). These computer-generated images reproduce the patterns of light and dark seen in actual round brilliant diamonds under lighting conditions similar to those used with the model, although the light-and-dark patterns are more symmetrical than those seen in most real diamonds. During the course of this research, we generated a variety of digital images, from different perspectives and with different lighting conditions. However, the details of how brilliance changes with proportions can be better studied by comparing a metric, such as WLR values, than by visually examining thousands of images.

Results for Key Individual Parameters. Our investigation of the dependence of WLR on crown angle, pavilion angle, and table size began with an examination of how WLR varies with each of these three parameters while the remaining seven parameters (again, see Box A) are held constant. Except where otherwise noted in the text, we fixed these parameters at the reference proportions that are provided in table 4.

TABLE 4. The eight proportion parameters used for calculating the WLR values.

Round-brilliant-cut parameters ^a	Range ^b	Increment	Reference proportions
Table size ^c	50% – 75%	1%	56%
Crown angle ^c	19° – 50°	1°	34°
Pavilion angle ^c	38° – 43°	0.25°	40.5°
Girdle facets ^d	16 – 144	16	64
Girdle thickness ^d	1.8% – 4.0%	0.2%	3.0%
Star length ^d	5% – 95%	1%	50%
Lower-girdle length ^d	50% – 95%	5%	75%
Culet size ^d	0% – 20%	0.5%	0.5%

^a These eight parameters are defined in Box A.

^b These ranges extend beyond the widest range for diamonds normally encountered in the trade today.

^c These three parameters were varied together while the other five were held at the reference proportions. A set of calculations was also made at the reference proportions with crown angle varying from 1° to 50°.

^d These five parameters were varied individually. For each one, the other seven parameters were held constant at the reference proportions.

BOX B: COMPARISON OF MODELED RESULTS TO ACTUAL DIAMOND PROPORTIONS

To get an idea of the range of WLR values for stones seen in the diamond trade, we collected information on the proportions of 67,621 round brilliants graded by GIA GTL. (This data set included all the D-to-Z-color round brilliant diamonds seen during a span of months.) This population of diamonds had crown angles ranging from 19.4° to 45.0°, pavilion angles from 39.9° to 43°, and table sizes from 50% to 74%. More than 80% of this group of diamonds fell within the smaller proportion range of 30°–40° crown angles, 40.2°–42.4° pavilion angles, and table sizes from 53% to 70%. The WLR values calculated for all of the diamonds ranged from 0.235 to 0.306, with a mean and standard deviation of 0.274 ± 0.005 . The stones with average proportions for this sample set (represented by 29% of the sample) had crown angles between 31° and 35.9°, pavilion angles between 41.0° and 42.4°, and table sizes of 61%–63%; the WLR values calculated for this relatively small range of proportions varied from 0.269 to 0.279.

In the entire data set, the diamonds with the highest calculated WLR values had the smallest crown angles: only eight of the 67,621 stones had WLR values above 0.295 (far into the high range), and of these, the largest crown angle was 25.5°. However, crown angle alone does not determine WLR; the 61 stones with crown angles less than 25° had WLR values ranging from 0.261 to 0.306 (low to high), with an average of 0.288 (high). Another 3,494 stones had crown angles between 25° and 30°, with more than half of these falling between 29.0° and 29.9°, and WLR values from 0.261 to 0.296 (low to high). In contrast, round bril-

liants with high crown angles have lower WLR values on average, although the brightest such stones yield WLR values slightly higher than the mean for the whole population; 7,617 diamonds had crown angles of 36° or more, with WLR values that ranged from 0.235 to 0.278 (low to typical). There were 275 round brilliants that had crown angles of 40° or more, with WLR values ranging from 0.235 to 0.259 (all low); these values indicate diamonds that are considerably darker than the average.

This sample of 67,621 diamonds contained very few with proportions that would qualify for a top grade in most of the systems shown in table 3. Only 3% of the sample (2,051 round brilliants) had crown angles between 34.0° and 34.9°, pavilion angles between 40.2° and 41.3°, and table sizes between 53% and 57%.

Of these 2,051 round brilliants, only 76, or less than 4% of this group, had tables of 53%, and nearly twice as many diamonds had pavilion angles of 41°–41.3°, rather than 40.2°–40.9°. Thus, even manufacturers who strive to cut "Ideal" proportions often choose to cut a larger table or steeper pavilion angle than Tolkowsky recommended, presumably for greater weight retention. However, there is as yet no clear evidence whether either of these changes significantly alters the balance between brilliance and fire that Tolkowsky proposed. As shown in table 3, the proportion ranges that define the top grades in existing systems yield WLR values of 0.275–0.285 (typical to moderately high); yet some proportions that receive lower grades in these same systems have higher calculated WLR values.

Crown Angle. Of the three parameters, changing the crown angle produced the greatest variation in WLR. In general, WLR increases as crown angle decreases; but, as figure 4 shows, there are three local maxima in WLR across the range of angles (that is, WLR varies up and down with changes in crown angle). These results suggest that, at the reference proportions, a diamond with a 23° crown angle is brighter than a stone with any other crown angle greater than 10°. However, other considerations may dictate that a diamond must have a crown angle above a certain value (such as reduced durability with a thin to medium girdle and a crown

flatter than, say, 25°; see, e.g., Crowningshield and Moses, 1997). Ironically, the highest WLR values are obtained for a round brilliant with no crown at all. It is interesting to note that the question of reduced durability with a shallower crown was discussed in *Gems & Gemology* in 1936, although at that time it was the "modern" trend toward angles of 34.5° (from the steeper angles cut previously) that raised concern (Ware, 1936).

Figure 4 also shows images of virtual diamonds that have crown angles of 25°, 35°, and 45°, with all other parameters at the reference proportions listed in table 4. The overall brightness clearly decreases

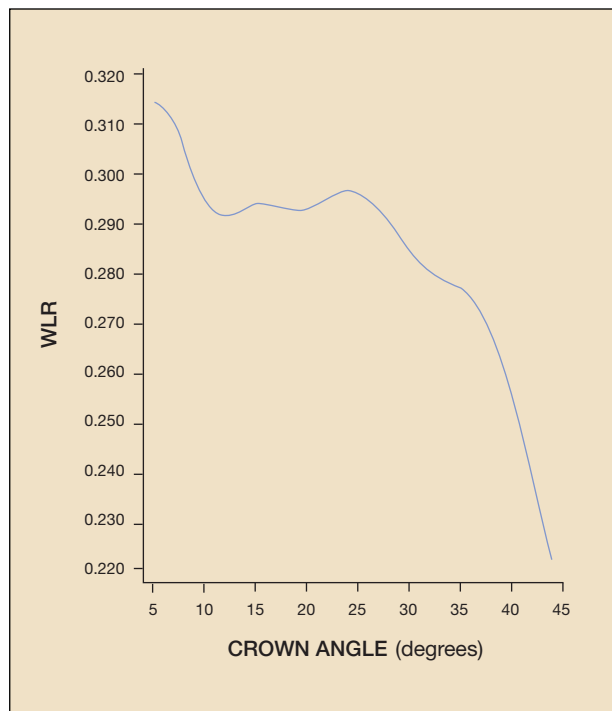
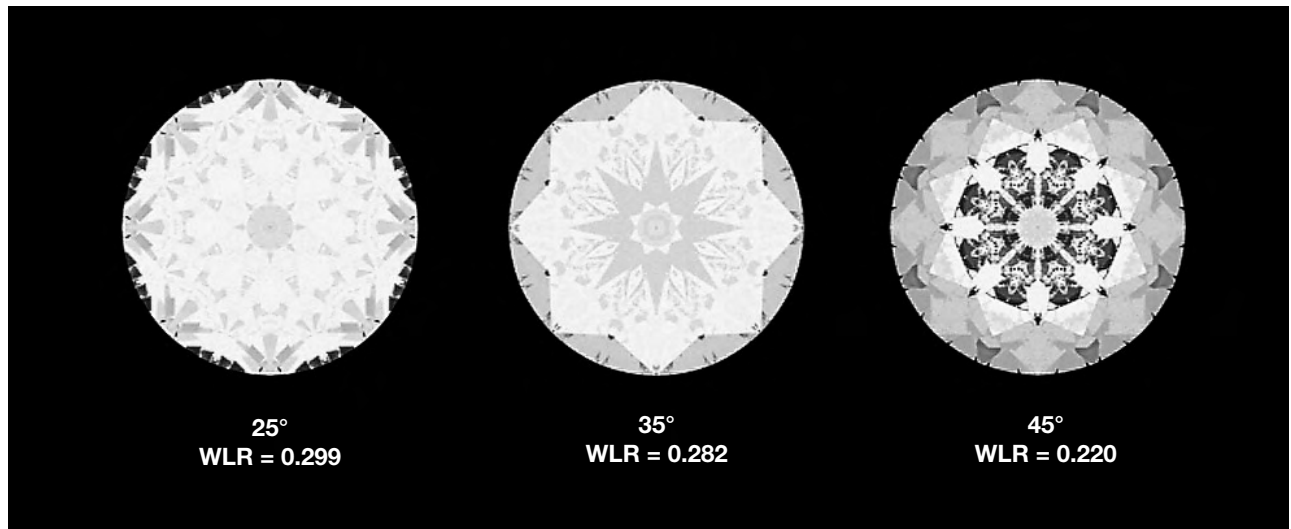


Figure 4. These digital images show how variations in the crown angle from 25° to 45° affect the appearance of a standard round brilliant diamond. All other proportions are held constant at the “reference proportions” shown in table 4. These digital images confirm what the graph of crown angle and WLR illustrates: WLR is highest at very shallow crown angles. The graph shows local maxima at 13°, 23°, and 34°, it begins to drop sharply at crown angles above 38°.

as crown angle increases, but the pattern of light and dark also changes substantially.

Pavilion Angle. This is often cited by diamond manufacturers as the parameter that matters most in terms of brilliance (e.g., G. Kaplan, pers. comm., 1998). With all other parameters at the reference positions, we see a smooth decrease in WLR away from a maximum at about 40.7° (figure 5). Images of virtual diamonds with low, optimal, and high pavilion angles (again, see figure 5) are consistent with the appearances that we would expect for actual diamonds with these pavilion angles (“fish-eye,” nor-

mal, and “nail head,” respectively; see *GIA Jeweler’s Manual* [1989]). However, note that although the pavilion angle is optimal at 40.7° when the other parameters are at the reference values, this need not be the case in general. For instance, we calculated the WLR values of a diamond with a completely flat crown. As the pavilion angle of this “crownless” virtual diamond increased from 38° to 43°, WLR increased smoothly from 0.270 to 0.340.

Table Size. With other proportions held at the reference parameters (again, see table 4), there is one broad maximum for WLR as a function of table size, as shown in figure 6. This maximum extends from about 53% to 59%; it is followed by a gradual decrease as table size increases to 70%. (A small shoulder is seen between 72% and 73%.) However, WLR as a function of table size behaves quite differently when this parameter is varied together with crown angle and pavilion angle, as discussed below.

Combined Effects. Some of the interactions between crown angle, pavilion angle, and table

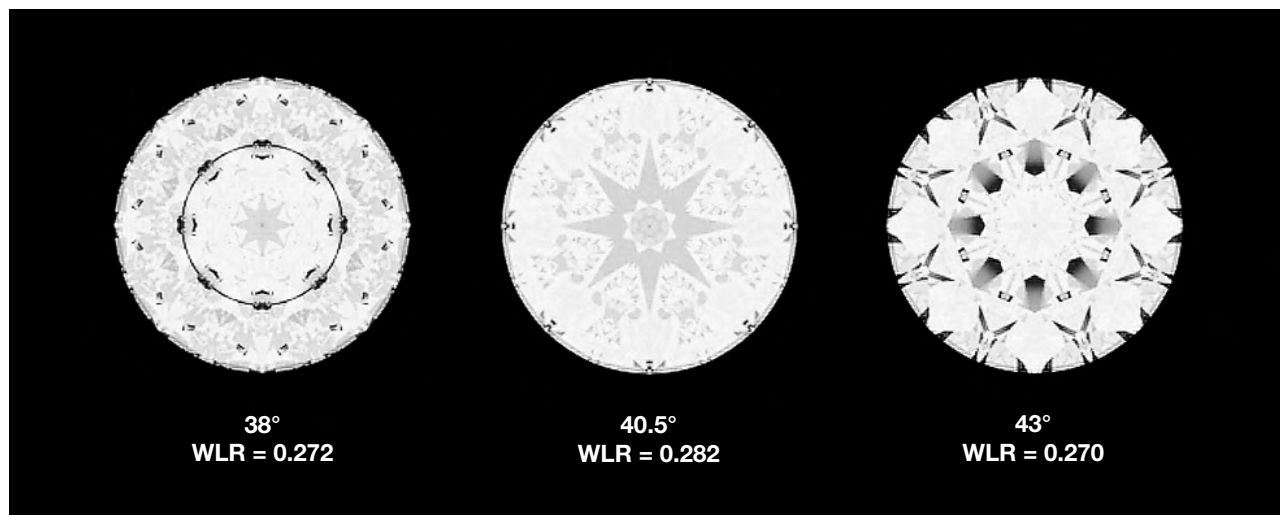
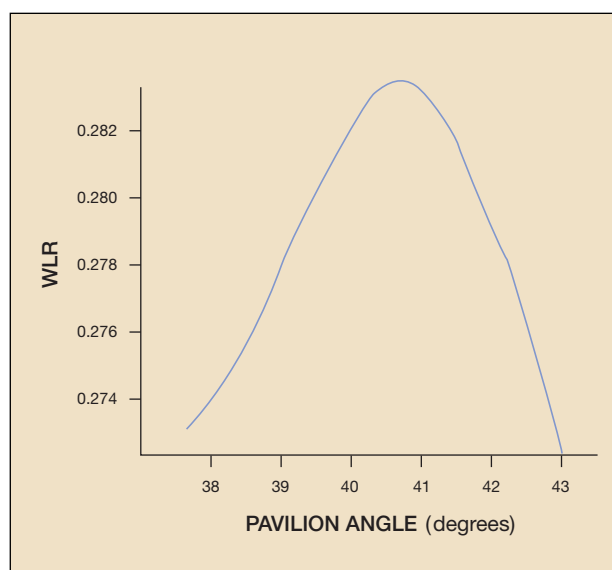


Figure 5. Variations in pavilion angle also affect the appearance of a faceted diamond. These virtual diamonds have pavilion angles of 38°, 40.5°, and 43°; all other parameters are set to the reference proportions (table 4). Although diffuse illumination reduces the contrast in all three images, they do illustrate well-known optical effects, including the “fish-eye” that results from a very shallow pavilion (far left), and the “nail head” caused by a very deep pavilion (far right). The graph of WLR as a function of pavilion angle (with all other parameters at reference proportions) shows a maximum at a pavilion angle of 40.7°.



size—and their joint effects on WLR values—can be seen when these proportion parameters are examined two at a time. One way to visualize these effects is to draw them to look like a topographic map (which shows the differences in elevation of an area of land). We can draw subsets of the data as cross-sections (slices) through the data set with one parameter held constant, and the WLR values can then be expressed as contours. These cross-sections can be read in the same manner as topographic maps; but instead of mountains, these “peaks” show proportion combinations that produce the highest calculated WLR values for diamonds within a small range of proportions.

As illustrated in figure 7, when the crown angle and table size are varied together, the WLR changes in an unexpected fashion. There are “ridges” at

crown angles of 23° and 34°. Along these ridges, round brilliants with large tables show unexpectedly high WLR values: For instance, for a 40.5° pavilion angle, a virtual diamond with a 65% table and a 23° crown angle returns more light (high WLR of 0.288) than one with a 56% table and a 34° crown (moderately high WLR of 0.283; again, see figure 7). Although the first of these stones is not a typical commercial cut, crown angles this low are sometimes seen at GIA GTL. In addition, at crown angles up to 37°, the table size has a significant influence on WLR; in general, WLR increases as table size decreases within this range.

When we attempt to illustrate the effects of all three parameters at the same time, the limitations of graphing on two-dimensional paper are readily apparent. The projection of a “three-dimensional

graph" in figure 8, for example, shows contours of constant WLR against crown angle, pavilion angle, and table size. This figure shows clearly that the higher-value WLR surfaces have a complex dependence on the combination of these three parameters. In particular, the white contour (WLR of 0.275–0.280) is concave as well as convex, and defines a broad range of proportions that have the same WLR values. However, only a limited region of the WLR surfaces can be displayed on such a graph.

To better show this complexity, figures 9–11 illustrate the results for proportion combinations from three perspectives: constant table size, constant pavilion angle, and constant crown angle. Three points representing distinct sets of proportions are plotted on these cross-sections; the point labeled A, for example, shows the position of a virtual diamond with the "reference proportions" (again, see table 4) in each of the three perspectives. Tolokowsky's proportions are shown as point T. Point B represents another high-WLR virtual diamond with a shallower crown angle.

Constant Table Size. Figure 9 shows the "topography" of the WLR values in a series of slices through surfaces of constant table size. It provides data for virtual diamonds with crown angles between 28.5° and 37.5°, and pavilion angles between 38° and 43°, at table sizes ranging from 50% to 66%. Overall, WLR is highest for fairly small tables (53% to 59%), and increases as crown angle decreases. Note the ridge of higher WLR that trends from the lower left corner of each constant-table-size slice to the center of the right side. This ridge becomes broader and shallower (smaller range of WLR values) as table size increases. It is evident that this complexity cannot be accounted for in a model of diamond proportions that treats the optimal set as the center of a three-dimensional "bull's-eye" pattern, surrounded by concentric shells of worsening results.

Constant Pavilion Angle. In figure 10, we show slices through the data at constant pavilion angle. The complex nature of the WLR surfaces is apparent from this view as well. The cross-section for a 39.3° pavilion angle shows a pronounced ridge of higher WLR values starting in the upper left corner (shallow crowns and small tables), and trending toward higher crown angles at table sizes less than 63%. This ridge is seen at all higher pavilion angles

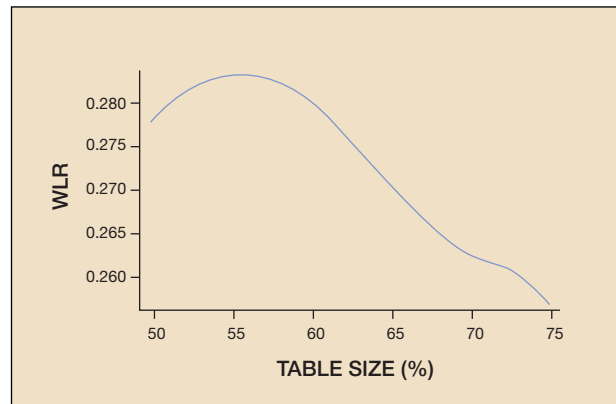
as well; it is the same ridge seen at higher crown angles in figure 7, as viewed from many different pavilion angles.

As the pavilion angle increases, the ridge defined by the WLR values seen in the orange, yellow, and white areas of figure 10 extends first to higher crown angles, and then broadens to include larger tables. From this perspective, it is clear that pavilion angle can interact strongly with the other two proportion parameters to produce similar WLR values across broad ranges of crown angle and table size.

Constant Crown Angle. From the third perspective, constant crown angle (figure 11), the WLR contours look much smoother. They form broad oval curves at shallow crown angles, with oval maximum regions at crown angles between 30.5° and 36.5°, surrounded by relatively smooth contours of decreasing WLR.

For crown angles greater than 30°, the set of optimal parameters appears in this perspective as a "bull's-eye" pattern, where a deviation in any direction worsens the WLR. However, the pavilion and table slices demonstrate that—in terms of WLR—there are many proportion combinations that yield equally bright results.

Figure 6. This graph of WLR versus table size, with all other proportions at the reference values, shows a broad maximum centered at about 56% and a gradual drop-off toward both smaller and larger table sizes. The wide, gently sloping top of this graph suggests that WLR is not strongly affected as table size varies between 50% and 62%, for these properties.



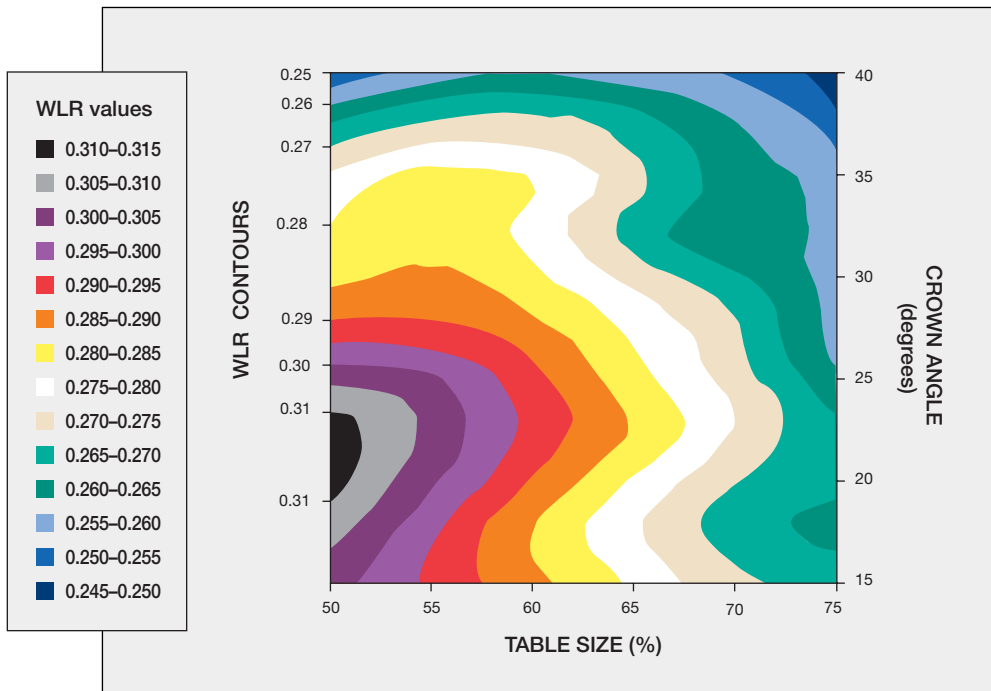
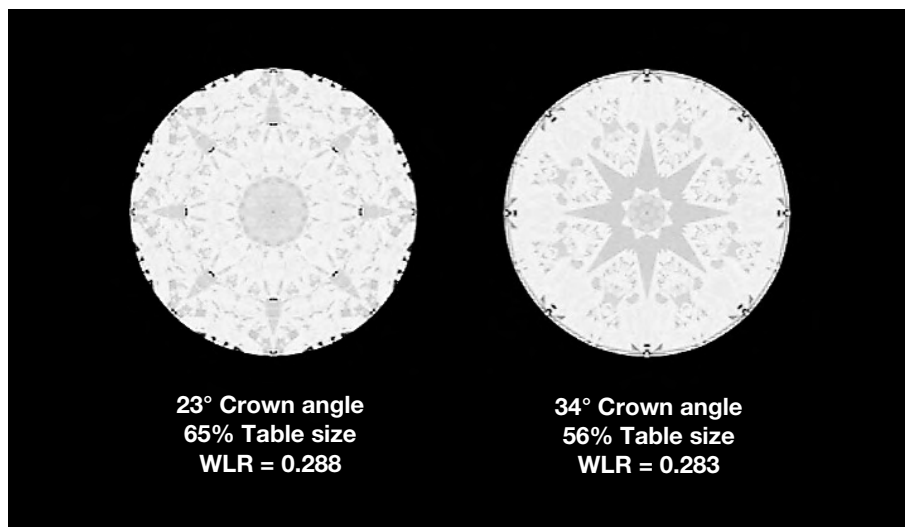


Figure 7. This diagram shows the variation in WLR with changes in both crown angle and table size. The WLR values are contoured, like a topographic map; each line is a constant WLR value. Regions with the highest WLR are shown in black, gray, and purple. High WLR values are found at crown angles up to 35°, beyond which WLR decreases rapidly. Note that the highest WLR values are seen at small table sizes. The shape of the 0.280 WLR contour line reflects the variation in WLR due to different crown angles; the local maxima at 23° and 34° in figure 4 become “ridges” in this figure. Note also the prominence of the “ridge” at the 23° crown angle; WLR remains high for much larger tables than at either larger or smaller crown angles. The digital images show how the pattern of light and dark can differ for proportions leading to similar WLR values. The virtual diamond on the left has a 23° crown angle and a 65% table (high WLR of 0.285), and the one on the right has a 34° crown angle and a 56% table (moderately high WLR of 0.283); all other proportions for both virtual diamonds were held constant at the reference proportions in table 4.



Influence of the Other Five Parameters on WLR Results. We explored the contribution to WLR of the remaining five proportion parameters—girdle thickness, number of girdle facets, culet size, lower-girdle length, and star length—by calculating WLR values while varying one parameter and holding the other seven (including crown angle, pavilion angle, and table size) constant at the reference proportions in table 4. We found that WLR decreases slightly as the thickness of the faceted girdle increases, presumably because more light is lost through a thick girdle. In addition, WLR was approximately con-

stant as the number of girdle facets varied from 32 to 144. A smaller WLR value was obtained for the extremely low value of 16 girdle facets.

We expected to see a steady decrease in WLR with culet size, similar to that seen for girdle thickness; instead, we found relatively constant values for culets as large as 12% (which would be described as very large), and then a decrease as the culet size increased further. Although we have not yet examined this result in significant detail, it implies that relatively few light rays escape through the culet.

The graph of WLR versus lower-girdle length shows a smooth curve with one maximum, similar to the curve seen in figure 5. With all other proportions at the reference values, we found the highest WLR when the lower-girdle length was 70%, rather than the commonly cut 75%. The total variation in WLR was small, and optimization of this parameter showed a strong dependence on star length.

The graph of WLR versus star length shows several local maxima (figure 12A). The overall maximum is found for a star length of 57%, rather than the 50% that is commonly cut for round brilliants. However, WLR varies by only 0.010—from 0.274 (typical) to 0.284 (moderately high)—over the range of 25% to 95% star length. With the crown angle fixed at the reference value of 34°, the 57% star length corresponds to a star facet angle of 22.5° and an upper-girdle-facet angle of 41.2° (WLR of 0.284), while the 50% star length yields a star facet angle of 21.5° and an upper-girdle-facet angle of 40.4° (WLR of 0.282; see figure 12B). This change makes a rather subtle difference in the profile of the diamond, producing a slightly steeper profile along these two facets without any change in crown height. Although WLR varies only a little, indicating little change in brilliance, the pattern of light and dark across the crown changes significantly, as shown in the digital images (figure 12C).

DISCUSSION

Verification of the Model. To verify our study, we need to ask whether our model adequately reproduces both the visual appearance of white light return from actual diamonds and the effects of cut that are familiar from observation of actual diamonds. The data indicate several similarities in appearance between the virtual diamonds generated with this model and actual stones. As we saw in figure 5, the virtual diamond images showed characteristics of actual faceted diamonds (e.g., “fish-eye” and “nail head” appearances), as pavilion angle alone was changed. Similarly, we found a sharp decrease in WLR for crown angles above 38°, and actual stones with such steep crown angles may look darker (see, e.g., figure 1).

The most meaningful test of our mathematical model is to compare the calculated WLR values to the appearance of actual diamonds with those same proportions. Figure 1 shows photos of actual diamonds with proportions that correspond to varying WLR values. As table 1 indicates, the stones in fig-

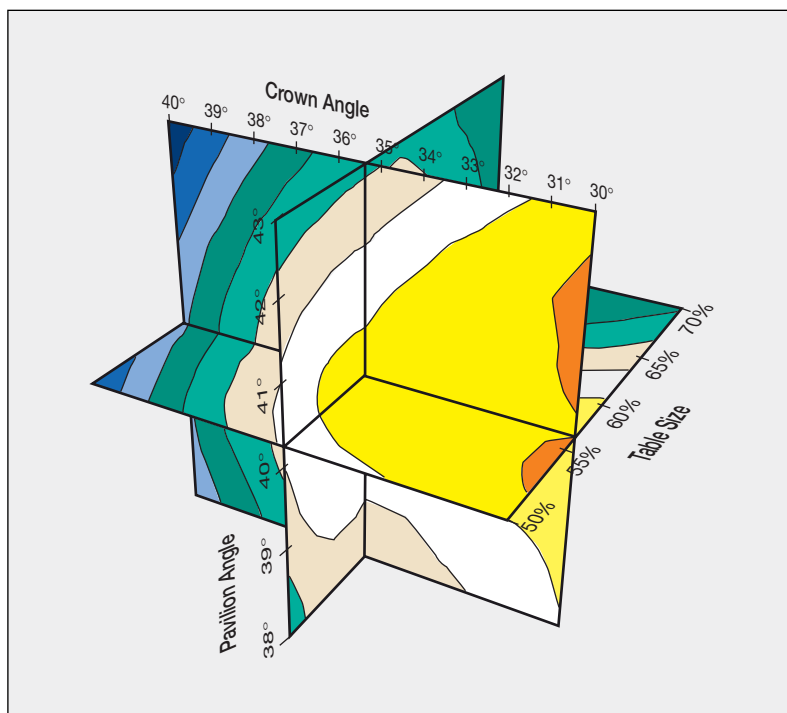


Figure 8. The full complexity of the WLR surfaces becomes apparent when we vary all three parameters—crown angle, pavilion angle, and table size. The contours show constant values of WLR in increments of 0.005, from above 0.285 for the orange area to below 0.250 for the dark blue area. The greatest complexity in the contours is seen at the highest WLR values. However, since this three-dimensional projection is drawn from only one perspective, it cannot show all the variations in the WLR surfaces.

ure 1 have proportions that would fall in four of the five general categories of WLR values: (1) high (calculated WLR greater than 0.285); (2) moderately high, which includes the proportion ranges of many professed “superior” cuts (from Tolokowsky, Eppler, and Eulitz in table 2; WLR range of 0.280–0.285); (3) typical (WLR range of 0.270–0.280); and (4) low (WLR less than 0.265). However, because WLR measures light return from many different perspectives, not just one, no single photograph can demonstrate WLR results exactly.

Using WLR Data to Evaluate Brilliance. The WLR surfaces that we have calculated as a function of crown angle, pavilion angle, and table size are irregular, with a number of maxima, rather than a single maximum. These multiple “peaks” are a principal result of this extensive three-dimensional analysis. Their existence supports a position taken by many

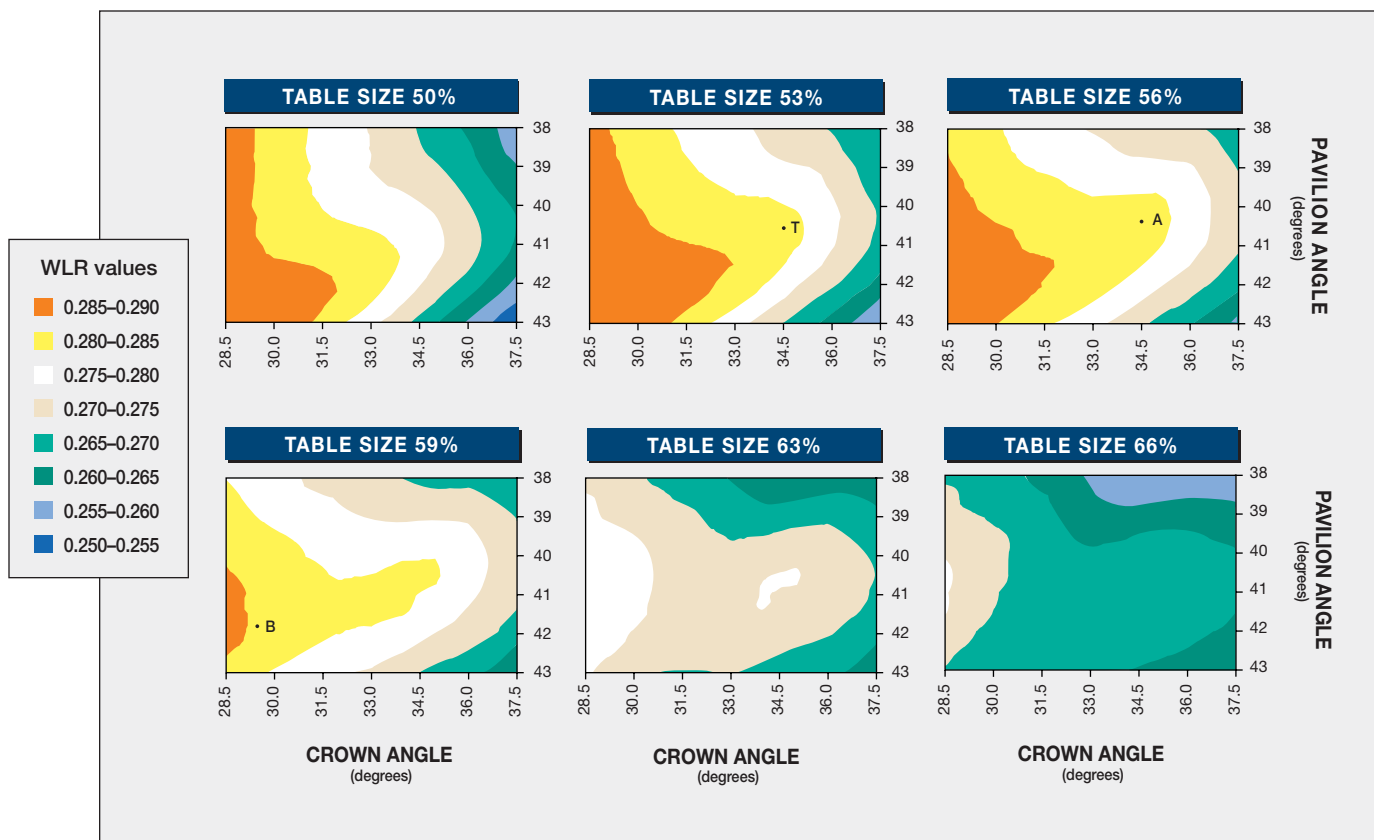


Figure 9. A series of slices through the data plotted in figure 8 makes it easier to see how WLR changes as these three parameters vary. Each plot shows contours of constant WLR for a given table size, as crown angle varies along the horizontal axis and pavilion angle varies along the vertical axis. Note that the contours define irregular surfaces. In general, the WLR values increase as table size decreases, with the highest values at a table size of 53% (for 30° and higher crown angles). The WLR values are also higher at intermediate pavilion angles and at lower crown angles. Three points are marked on these plots: Point A denotes a virtual diamond with a 34.5° crown angle, a 40.7° pavilion angle, and a 56% table (our reference proportions), with a WLR value of 0.282. Point B shows the location of a virtual diamond with a 29.5° crown angle, a 41.7° pavilion angle, and a 59% table, with a WLR value of 0.284, and point T marks a virtual diamond with a 34.5° crown angle, a 40.7° pavilion angle, and a 53% table (Tolkowsky's proportions), which yields a WLR value of 0.281. These same three points are shown in figures 10 and 11 as an orientation aid: Each point marks the same set of proportions.

in the trade (see, e.g., Federman, 1997): At least in terms of light return, or “brilliance,” there are many combinations of parameters that yield equally “attractive” round brilliant diamonds. This interaction between the proportion parameters is not taken into account by existing cut-grading systems, which examine each parameter separately.

It is especially important to note that some proportion combinations that yield high WLR values are separated from one another and not contiguous, as shown in the cross-sections of the WLR surfaces. Thus, for some given values of two proportions, changes in the third proportion in a single direction may first worsen WLR and then improve it again.

This variation in WLR with different proportion combinations makes the characterization of the “best” diamonds, in terms of brightness, a great challenge. Even for one simple shape—the round brilliant cut—and variation of only three proportion parameters, the surfaces of constant WLR are highly complex.

The specific proportion combinations that produce high WLR values have a variety of implications for diamond manufacturing. Because many combinations of proportions yield similarly high WLR values, diamonds can be cut to many choices of proportions with the same light return, which suggests a better utilization of rough (see Box C).

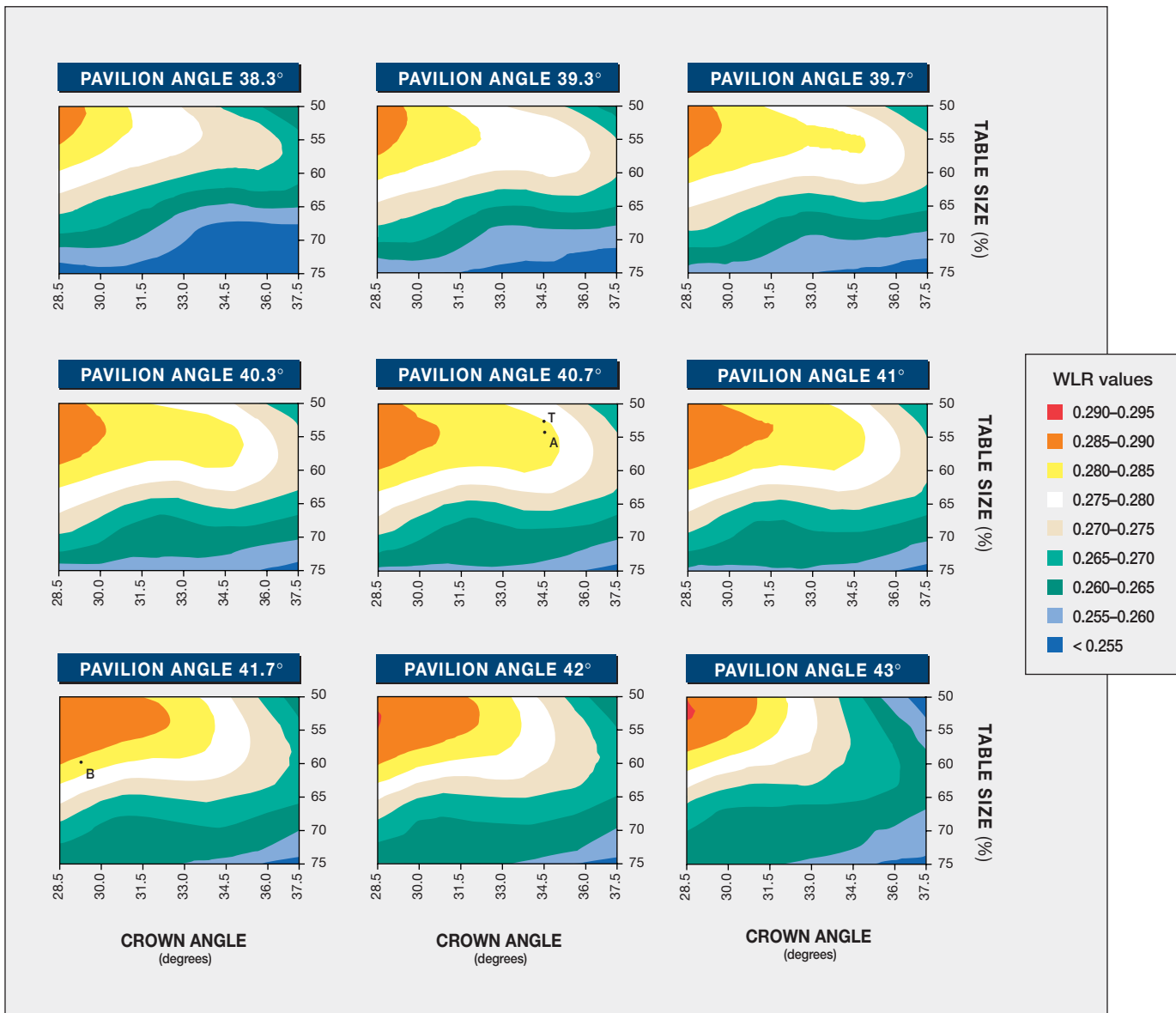


Figure 10. Each plot in this figure shows contours of constant WLR for a given pavilion angle, as crown angle varies along the horizontal axis and table size varies along the vertical axis. Here again, the complex nature of the WLR surfaces is apparent in the patterns shown in these cross-sections. The highest WLR values are seen at higher pavilion angles, for very shallow crown angles and small tables. In general, higher WLR values are found for the widest range of crown angles and tables sizes as the pavilion angle tends toward 41°. Points A, B, and T from figure 9 are shown as orientation aids.

Evaluation of “Superior” Proportions Suggested by Earlier Researchers. Because a gem diamond should display an optimal combination of brilliance, fire, and pleasing scintillation, the best overall appearance might not be found among the brightest round brilliant cuts. According to our WLR calculations, however, some of the “superior” proportions proposed by other researchers (see, e.g., table 2) do not

produce a reasonably bright diamond—for example, those from Stoephasius (1931; especially the one with a 43.8° crown angle, with a calculated WLR of 0.216) and Suzuki’s Dispersion Design (1970; even Suzuki’s Brilliance Design, with a WLR of 0.252, calculates as dark). Tolowsky’s proportions yield a moderately high WLR of 0.281. It is interesting to note that only seven of the 31 sets of superior pro-

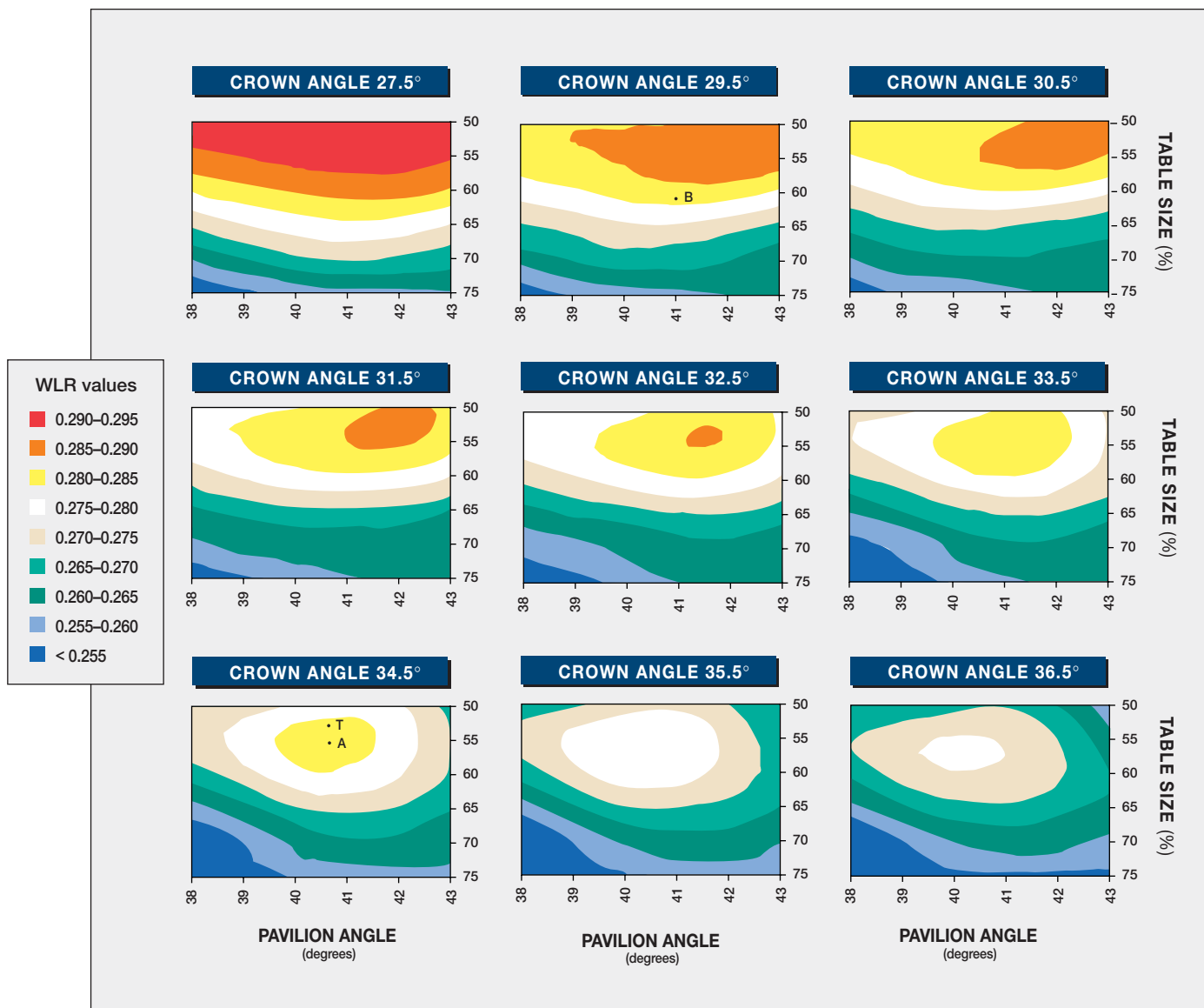


Figure 11. Each of the slices in this set shows contours of constant WLR for a given crown angle, as table size varies along the vertical axis and pavilion angle varies along the horizontal axis. WLR surfaces look much smoother and more concentric from this view, and generally WLR decreases as crown angle increases. Points A, B, and T from figure 9 are shown as orientation aids.

portions proposed since Tolkowsky have better calculated WLR values (Eppler, 1939; Parker, 1951 [cited by Eppler, 1973]; Schlossmacher, 1969; Eulitz, 1972; Scandinavian Diamond Nomenclature Committee, 1979; Dodson “most fire,” 1979; and [one of four] Shannon and Wilson [Shor, 1998]). Relative to Tolkowsky’s proportions, all of these have larger tables (56%–60%) and shallower crowns (25.5°–33.6°); all but one have comparable pavilion angles (40.7°–40.9°; the exception, Dodson’s “most fire,” has a 43° pavilion angle). The highest WLR

(0.297) is calculated for Parker’s (1951) cut, with a 55.9% table, 25.5° crown angle, and 40.9° pavilion angle.

Recent work by Shannon and Wilson, as described in the trade press (Shor, 1998), presented four sets of proportions that they claimed gave “outstanding performance” in terms of their appearance. Yet we calculated typical to moderately high WLR values for these proportions (again, see table 2). In comparison, Dodson’s (1979) proportions for the “most brilliant” diamond yield a WLR value of

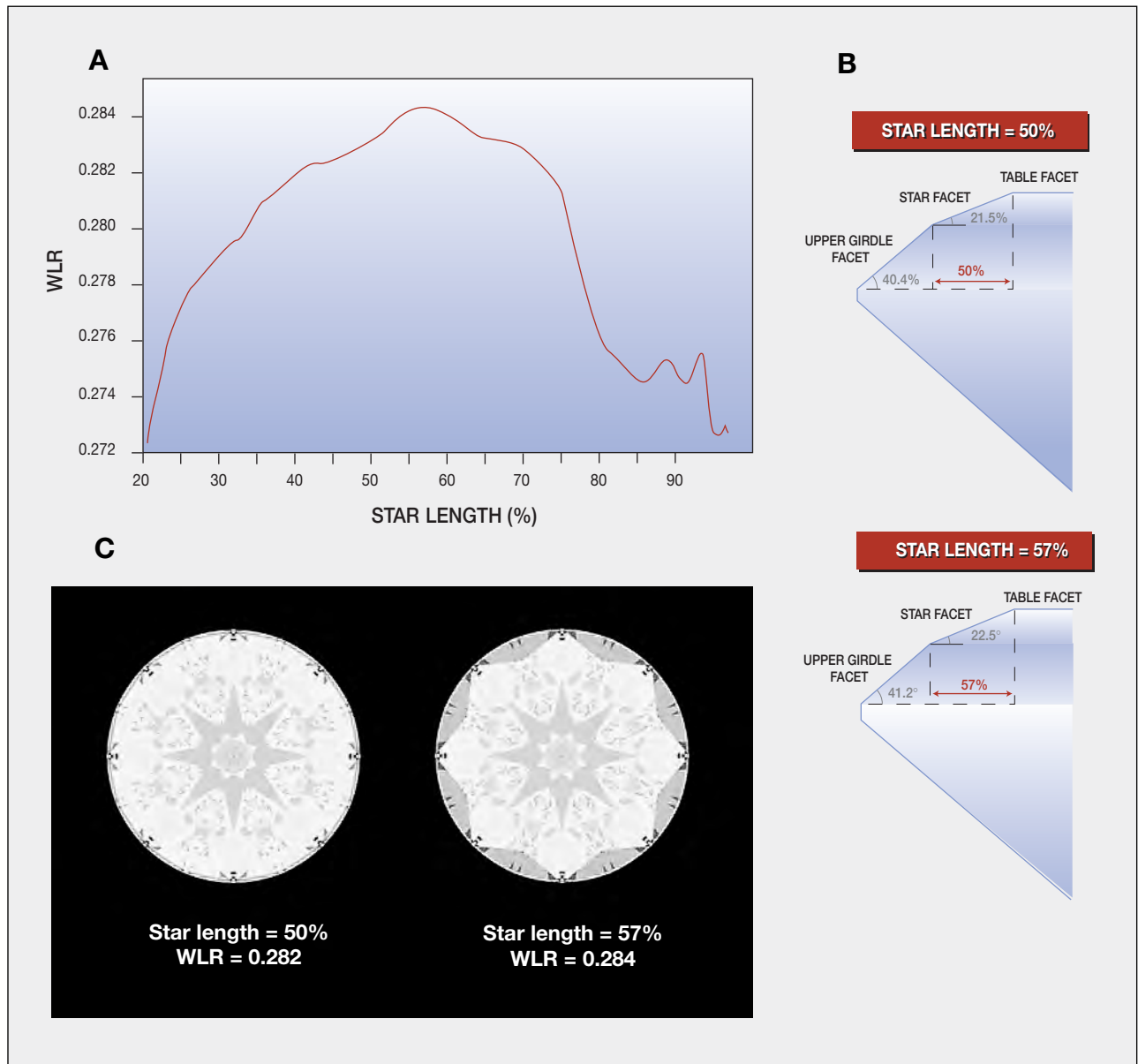


Figure 12. (A) The graph of WLR versus star length (with all other parameters held constant at the reference proportions) shows many local maxima within a relatively small range of WLR. This calculated WLR implies that brilliance can be increased slightly if the star length is increased from the usual to 57%. (B) These diagrams show how longer star length results in slightly steeper angles for both the upper girdle facets and the star facets. The upper diagram, with a star length of 50%, corresponds to the reference proportions in table 4; the lower diagram shows a star length of 57%. (C) The virtual diamond images are of diamonds with a 50% star length (left) and a 57% star length (right). Although the image on the right is darker around the edge, it has a slightly higher WLR value (0.284) than the image on the left (0.282).

0.277 (typical range) for a 40% table size (much smaller than any commercially cut stones), a 26.5° crown angle, and a 43° pavilion angle. However, Dodson also evaluated one metric each for fire and “sparkliness” for four table sizes, three crown heights, and 10 pavilion angles. His “most fire” pro-

portions gave a high WLR of 0.287, which is far brighter by our calculations than his “most brilliant” stone. The differences between our weighting technique and those of Dodson and of Shannon and Wilson are probably responsible for these discrepancies.

Implications for Existing Cut-Grading Systems. Our results disagree with the concepts on which the proportion grading systems currently in use by various laboratories appear to be based. In particular, they do not support the idea that *all* deviations from a narrow range of crown angles and table sizes should be given a lower grade. We have calculated the WLR values for the proportion ranges of each grading system in table 3. The highest grades for most of those systems yield WLR values from 0.275 to 0.284 (typical to moderately high). Clearly, these are attractive stones. However, the maximum WLR achievable increases as the grade worsens in these systems.

For example, diamonds with a 31° to 32° crown angle, a 41° to 41.4° pavilion angle, and a table size between 53% and 57% have WLR values of 0.284–0.285 (moderately high). Although their WLR values are slightly higher than those of the top grades in table 3, these round brilliants would receive lower cut grades in most systems because of the lower crown angle. Similarly, diamonds with crown angles between 31° and 33°, pavilion angles of 42°, and tables between 53% and 59% yield calculated WLR values from 0.281 to 0.286 (moderately high to high). These values may exceed those of diamonds that currently receive the best grades, but such stones earn medium to low grades from the existing systems because of the larger pavilion angle. Last, round brilliants with larger tables (61% to 63%) are much more common than those with small tables (again, see Box B). Such diamonds can show moderately high WLR values when combined with crown angles between 30° and 33°, and pavilion angles from 40° to 42°, but diamonds with large tables are penalized heavily in most of the existing cut grading systems, regardless of their brightness.

Although arguments can be made for downgrading diamonds with lower crown angles or larger tables (on the basis, for example, that they do not yield enough fire), there is little documented evidence at present to support—or refute—such claims. However, at least according to Dodson (1979), both fire and scintillation depend on combinations of proportions, rather than on any single parameter.

Although our results for brilliance do not support current cut grading systems, we do not expect them to surprise most diamond manufacturers. GIA GTL has seen significant numbers of diamonds that are cut to various proportion combinations that

would correspond to moderately high to high WLR values. The results of this study support the empirical understanding that cutters have of the relationships between proportions and brilliance.

FUTURE DIRECTIONS

The model presented here can be used readily to explore many aspects of how diamond cut affects appearance. The greatest challenge in this research is the derivation of metrics for appearance concepts, including selection of the best lighting and observation conditions for each metric. Currently, we are exploring metrics for fire, which has many possible variables, such as: the size, extent, placement, and exit angle of colored light rays; the distribution of colors observed; and how the observation and lighting geometries govern the recombination of colored light rays into white light. We plan to devise a metric for scintillation as well, and to compare these results over the same proportion ranges to the metrics for brilliance and fire. We also intend to explore other lighting conditions, as we develop metrics for the other appearance concepts.

In addition, we plan to explore two important considerations that have been neglected thus far: symmetry and color. From our efforts and observations of actual diamonds for this study, we suspect that symmetry deviations may produce significant variation in brilliance (this was also suggested by A. Gilbertson, pers. comm., 1998). Incorporation of symmetry deviations requires adding more parameters to describe the shape of the round brilliant, and devising a method of tracking multiple symmetry faults. Once this is done, the model can be used to calculate both images and metric values that show how symmetry deviations, both singly and in combination, change diamond appearance.

Incorporating color, whether letter grades (e.g., from J to Z) or fancy colors, requires giving the virtual diamond a set of dimensions, applying a specific absorption spectrum, and specifying the color distribution (even or zoned). Then the model can keep track of the energy a ray loses by absorption (in addition to leakage) as it travels through the virtual diamond. Fluorescence effects can be included by similar techniques (applying a fluorescence spectrum), and the claim that fluorescent diamonds look better at different proportions than those that are inert (G. Tolkowsky, 1996) can be directly evaluated.

This model can also be used to explore the many

BOX C: AN EXAMPLE ILLUSTRATING CUTTING CHOICES

Fully symmetrical octahedral rough lends itself quite nicely to the higher crown and smaller table typical of the "Ideal" cut, as shown in figure C-1. However, several diamond manufacturers have estimated that only about one fourth of the rough they cut is fully symmetrical. (A. D. Klein, pers. comm., 1998). Other rough shows some irregularity in shape: shorter along one point-to-point distance than the other two; one or more flattened edges with minor development of cube or dodecahedral faces; or some relative tilt or twist between the two pyramids that comprise the octahedron. These variations in the shape of the rough can be accommodated during cutting either by accepting a lower weight yield or by modifying the cutting proportions.

If we consider a typical slightly asymmetric octahedron (see, e.g., figure C-2), one could still work toward an "Ideal" cut despite the limitations of the rough. Choosing to saw such a piece just slightly off center separates the top from the bottom of the octahedron, yielding two symmetrical square pyramids; for the purposes of this example, let us assume that the larger of these two pieces weighs about 1.75 ct. Aiming for a crown height of 16% or 17% (which allows for a crown angle of 34°–35°, at a range of table sizes) pushes the girdle down below the widest part of the rough, forcing a lower yield. After exploring the possibilities for this example with a DiaExpert system (see, e.g., Caspi, 1997), the best yield we found for top-graded

proportions as defined by most of the cut-grading systems (see table 3), was 0.93 ct, with a 35.5° crown angle, a 40.8° pavilion angle, and a 57% table, giving a calculated WLR value of 0.279.

However, the shape of this rough suggests a different sawing position; it promotes cutting a shallower crown and a larger table. From the same sawn bottom piece of about 1.75 ct, one could plan a round brilliant with a 60% table and about a 60% total depth, with a 32.7° crown angle and a 41.5° pavilion angle, which would achieve a calculated WLR value of 0.279 and a final weight of 1.02 ct. In this example, striving for a high cut grade (table 3) results in a substantially lower weight yield while achieving the same brightness, as expressed by WLR.

There is broad agreement throughout the diamond trade that cutting a diamond for maximum weight yield without consideration of the final appearance constitutes unacceptably poor manufacturing. Nevertheless, the disagreement over which proportions yield the best-looking diamonds fuels the debate as to how to maximize both weight yield and appearance. Although brilliance is only one aspect of overall diamond appearance, our results indicate that for the same piece of rough, it is possible to attain greater yield with the same WLR.

Figure C-1. Starting with a rough diamond that is a highly symmetric octahedron, one can manufacture a stone with the high crown typical of the "Ideal" and obtain a good yield.

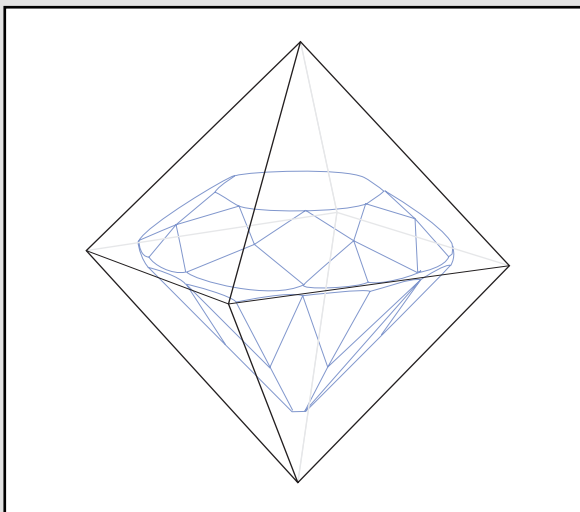
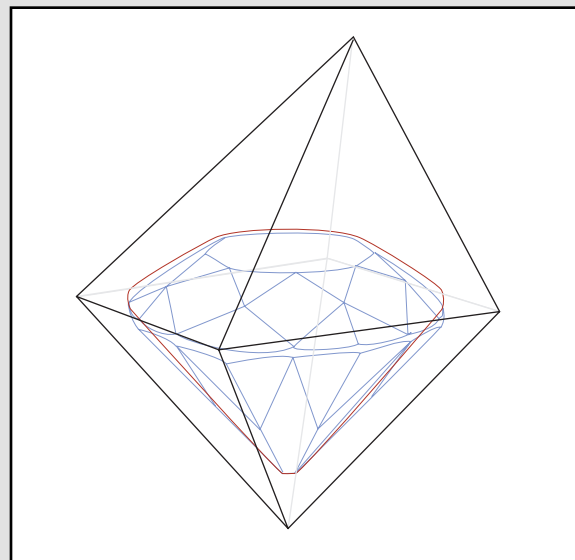


Figure C-2. Other sets of proportions, particularly slightly lower crown angles, often give the best yield from commonly encountered asymmetric octahedral diamond rough, with equivalent brightness. This yield can be significantly lower when such rough is fashioned to "Ideal" proportions.



ways that faceted shape and proportions affect the face-up appearance of fancy-colored diamonds. In addition, we hope to address the effects that different kinds of inclusions can have on the paths of light rays in a diamond (e.g., reflection from the surface of a “feather,” or scattering from a cloud of pin-points), and the additional light loss that results from poor surface finish.

CONCLUSION

In this first report of the results of our research on cut proportions, we have presented a mathematical model of the round brilliant diamond that describes this shape in terms of eight proportion parameters. It also incorporates the physical factors that affect how light interacts with a faceted diamond. At present, the “virtual” diamonds we have examined are all colorless, flawless round brilliants with mathematically perfect symmetry and polish; they vary only in their proportions. We created digital images of some of these virtual diamonds that reproduce the key features of actual diamonds (again, see figures 2, 4, 5, 7, and 12).

In this report, we have focused on brilliance, which was considered the main factor of diamond appearance in most previous analyses of the round brilliant diamond—from Tolkowsky in 1919 to Shannon and Wilson in 1998. We have quantified brilliance on the basis of weighted light return (WLR). After calculating WLR values for more than 20,000 proportion combinations, we found that the relationship between brilliance and the three primary proportion parameters (crown angle, pavilion angle, and table size) is complex, and that there are a number of proportion combinations that yield high WLR values. We also discovered that there are some commercial proportion combinations that produce rather low WLR values (again, see figure 1 and Box B). Comparisons to actual diamonds support our premise that WLR captures the essence of brilliance.

Our model differs from its predecessors in one or more of three ways: (1) it is three-dimensional; (2) it uses the most detailed existing data on the properties of a colorless diamond; and (3) it uses an averaged observer condition that takes into account the likeliest ways in which a diamond dealer or consumer looks at the stone. (The last is unique to this model.) Nevertheless, we do not consider the WLR metric we have devised to be the whole story with regard to diamond appearance.

Brilliance is only one part of the puzzle; fire and scintillation, and probably symmetry deviations and color, will also have to be analyzed before the effects of cutting on diamond appearance can be fully understood. Yet, no fashioned diamond can be considered beautiful if it lacks brilliance. We can infer from the WLR data that certain combinations of proportions will produce low light return. This is important since a round brilliant that is severely deficient in any one appearance aspect cannot be considered well cut, even if it performs well for another aspect. For example, these WLR results could be used to define proportions for which a round brilliant diamond will appear too dark; no amount of fire or pleasing scintillation would balance such darkness to produce beauty.

Ultimately, we hope to use this model to find the various ranges of proportions that clearly fail to bring out the attractive qualities of a round brilliant diamond for each appearance aspect (brilliance, fire, and scintillation). The proportion ranges that remain can be examined for balances between the different appearance aspects, and an intelligent, fact-based discussion can take place regarding which proportions produce diamonds of superior appearance. It is our opinion that any cut grading assessment devised in the absence of this broader picture is premature.

Acknowledgments: Several people provided stimulating discussions and a broader perspective: Glenn Nord and GIA colleagues Bill Boyajian, Brook Ellis, Richard T. Liddicoat, Vince Manson, Tom Moses, and Tom Yonelunas, as well as GIA GTL researchers Peter DeJong, Ronnie Geurts, and Marc Verboven. Dona Dirlam and the staff of the Richard T. Liddicoat Gemological Library and Information Center assisted with literature searches. Himiko Naka (GIA GTL) and Ronnie Geurts translated articles published in Japanese and German, respectively. Sheryl Cashmore, Kim Cino, Alan DeGhionno, and Julie Lahman of GIA GTL located examples of actual diamonds of various proportions, and Richard Von Sternberg of EightStar Diamond Company, Santa Rosa, California, provided a diamond that approximated the symmetry of the model. A number of diamond manufacturers spoke with us about the variables involved in creating a polished round brilliant from diamond rough; we especially thank those at Julius Klein, Inc., New York.

REFERENCES

- Astric B., Merigoux H., Zecchini P. (1992) Etude de la variation de l'aspect de pierres taillées à l'aide d'images de synthèse. *La Gemmologia*, Vol. 17, No. 1, pp. 7–31.
- Bergheimer H. (1938) Die Schleifrichtungen auf den Facetten des Diamantbrillanten. *Neues Jahrbuch für Mineralogie, Geologie, und Paläontologie*, Vol. 75A, pp. 145–158.
- Caspi A. (1997) Modern diamond cutting and polishing. *Gems & Gemology*, Vol. 33, No. 2, pp. 102–121.
- Connellan M., Pozzibon L. (1984) The Australian ideal design for round brilliants. *Australian Gemmologist*, Vol. 24, pp. 219–226, 243–246.
- Crowningshield G.R., Moses T. (1997) Diamond: Damaged from wear. *Gem Trade Lab Notes, Gems & Gemology*, Vol. 33, No. 1, pp. 55–56.
- Dodson J.S. (1979) The statistical brilliance, sparkliness and fire of the round brilliant-cut diamond. *Diamond Research*, pp. 13–17.
- Elbe M.G. (1972) Erstaunliche Schmuckeffekte an Brillanten. *Zeitschrift der Deutschen Gemmologischen Gesellschaft*, Vol. 21, No. 4, pp. 189–212.
- Eppler W.F. (1933) *Der Diamant und seine Bearbeitung*. Wilhelm Diebener GmbH, Leipzig, 68 pp.
- Eppler W.F. (1938) Die Ideal-Schleifformen durchsichtiger Edelsteine. *Zentralblatt für Mineralogie, Geologie, und Paläontologie*, Abteilung A, pp. 1–5.
- Eppler W.F. (1939) Die Brillanz durchsichtiger Edelsteine. *Fortschritte der Mineralogie, Kristallographie, und Petrographie*, Vol. 23, pp. 1–40.
- Eppler W.F. (1940) Beitrag zum Brillanzproblem II. *Zentralblatt für Mineralogie, Geologie, und Paläontologie*, Abteilung A, No. 4, pp. 93–96.
- Eppler W.F. (1973) *Praktische Gemmologie*. Rühle-Diebener Verlag KG, Stuttgart.
- Eppler W.F., Klüppelberg E. (1940) Die praktische Brillantschliff des Diamanten. *Neues Jahrbuch für Mineralogie, Geologie, und Paläontologie*, Vol. 75A, pp. 135–144.
- Eulitz W.R. (1972) Die rechnerische Ermittlung der optimalen Brillanz der Brillanten. *Zeitschrift der Deutschen Gemmologischen Gesellschaft*, Vol. 21, No. 1, pp. 13–43.
- Federman D. (1997) Make believe. *Modern Jeweler*, Vol. 96, No. 9, pp. 23–38, 62–63.
- Foley J.D., Ed. (1996) *Computer Graphics: Principles and Practice*, 2nd ed. in C, Addison-Wesley Publishing Co., Reading, MA.
- GIA Diamond Dictionary*, 3rd ed. (1993) Gemological Institute of America, Santa Monica, CA, 275 pp.
- GIA Jeweler's Manual* (1989) Gemological Institute of America, Santa Monica, CA, 327 pp.
- Gilbertson A. (1998) *Letting Light Speak for Itself*. Diamond Profile Inc., Portland, Oregon, 14 pp. plus appendices.
- Gilbertson A., Walters C. (1997) The measure of beauty. *Rapaport Diamond Report*, Vol. 20, No. 6, pp. 43, 45–46.
- Johnsen A. (1926) Form und Brillanz der Brillanten. *Sitzungsberichte der Preussischen Akademie der Wissenschaften, Physikalische-Mathematische Klasse*, Vol. 23, pp. 322–330.
- Lawrence J. (1998) Just how much sparkle? *Diamond International*, No. 53, pp. 77–78.
- Maier W. (1936) Brillanz geschliffener Edelsteine. *Neues Jahrbuch für Mineralogie, Geologie, und Paläontologie*, Vol. 71A, pp. 458–491.
- Maier W. (1938) Vollreflexbrillanten. *Zentralblatt für Mineralogie, Geologie, und Paläontologie*, Abteilung A, pp. 230–239.
- Nassau K. (1983) *The Physics and Chemistry of Color—The Fifteen Causes of Color*. Wiley Interscience, New York, 454 pp.
- Nestlebaum K. (1996) New AGS lab stakes its claim on cut grade. *Rapaport Diamond Report*, Vol. 19, No. 17, pp. 15–17.
- Nestlebaum K. (1997) Ideals: Worth the trouble to those who cut them. *Rapaport Diamond Report*, Vol. 20, No. 10, pp. 18–19.
- Papadopoulos A.D., Anastassakis E. (1991) Optical properties of diamond. *Physical Review B*, Vol. 43, No. 6, pp. 5090–5097.
- Rösch S. (1926) Die Brillanzwirkung des geschliffenen Diamanten. *Deutsche Goldschmiede Zeitung*, No. 5, pp. 45–48; No. 7, pp. 65–67; No. 9, pp. 88–90.
- Rösch S. (1927) Beitrag zum Brillanzproblem IV. *Zeitschrift für Kristallographie*, Vol. 65, pp. 46–68.
- Scandinavian Diamond Nomenclature Committee (1979) *The Scandinavian Diamond Nomenclature and Grading Standards: Official Version*. Trade Associations of Jewellers in Denmark, Finland, Norway and Sweden, 50 pp.
- Schlossmacher K. (1969) *Edelsteine und Perlen, 5 Auflage*. E. Schweizerbart'sche Verlagsbuchhandlung, Stuttgart.
- Shor R. (1993) Cutting grades—new complications. *Jewelers' Circular-Keystone*, Vol. 164, No. 4, pp. 52–55.
- Shor R. (1997) Consumers who care about cut: A small, but growing group. *Jewelers' Circular-Keystone*, Vol. 168, No. 6, pp. 124–126.
- Shor R. (1998) Computer engineers create proportion grade program. *New York Diamonds*, Vol. 44, pp. 26–28.
- Stoephasius A. (1931) Lässt sich das Gewicht gefasster Brillanten sicher berechnen? *Deutsche Goldschmiede Zeitung*, No. 45, pp. 470–474.
- Suzuki S. (1970) A new design for brilliance plus dispersion. *Australian Gemmologist*, Vol. 10, No. 10, pp. 13–24.
- Tillander H. (1966) Six centuries of diamond design. *Gems & Gemology*, Vol. 12, No. 3, pp. 77–95.
- Tillander H. (1995) *Diamond Cuts in Historical Jewellery: 1381–1910*. Art Books International, London.
- Tognoni C. (1990) An automatic procedure for computing the optimum cut proportions of gems. *La Gemmologia*, Vol. 25, No. 3–4, pp. 23–32.
- Tolkowsky G. (1996) Cutting the Edges. *Diamond Insight*, Vol. 9, No. 2, pp. 9–10.
- Tolkowsky M. (1919) *Diamond Design: A Study of the Reflection and Refraction of Light in a Diamond*. E. & F.N. Spon, London.
- Wade F.B. (1916) *Diamonds: A Study of the Factors that Govern Their Value*. G.P. Putnam's Sons, New York.
- Ware, J.W. (1936) New diamond cuts break more easily. *Gems & Gemology*, Vol. 2, No. 4, p. 68.
- Watermeyer B. (1991) *Diamond Cutting*, 4th ed. Preskor Doornfontein, Johannesburg, 406 pp.
- Wright, W.D. (1969) *The Measurement of Colour*, 4th ed., Van Nostrand, New York.

CULTURED ABALONE BLISTER PEARLS FROM NEW ZEALAND

By Cheryl Y. Wentzell

*The successful culturing of abalone pearls has been known since French scientist Louis Boutan's experimentation in the late 1890s, but commercial production has been achieved only in recent decades. The use of New Zealand's *Haliotis iris*, with its colorful and iridescent nacre, has had the strongest recent impact on this industry. Empress Abalone Ltd. is producing large, attractive cultured blister pearls in *H. iris*. The first commercial harvest in 1997 yielded approximately 6,000 jewelry-quality cultured blister pearls, 9–20 mm in diameter, with vibrant blue, green, purple, and pink hues. Examination of 22 samples of this material by standard gemological and advanced testing methods revealed that the presence and thicknesses of the conchiolin layers had a significant impact on face-up appearance. Empress Abalone Ltd. is also experimenting with producing whole free-formed cultured pearls in this gastropod mollusk.*

Abalone pearls are highly prized for their rarity, dynamic colors, and remarkable iridescence. Their unusual shapes—often conical—and potentially large sizes make these pearls especially well suited for designer jewelry. The beauty of these rare pearls has spawned several attempts at culturing, recorded as far back as the late 19th century. However, these early attempts encountered many obstacles. Only recently have researchers begun to overcome the challenges and difficulties presented by abalone pearl culture. One company, Empress Abalone Ltd. of Christchurch, New Zealand, is successfully culturing brightly colored blister pearls within New Zealand's *Haliotis iris* (figure 1). These assembled cultured blister pearls are marketed under the international trademark, Empress Pearl® (or Empress Abalone Pearl® in the U.S.). The company is also pursuing the commercial production of whole spherical cultured abalone pearls.

This article will focus on the history, production, marketing, and identifying characteristics of cultured and assembled blister pearls produced by Empress Abalone Ltd. Except where referenced otherwise, information was obtained through personal communication with the owners, Liz and Michael McKenzie, from 1996 through 1998.

HISTORY OF ABALONE PEARL CULTURE

The successful culturing of abalone pearls has been elusive because of the difficulty of farming and nucleating abalone. The first cultured abalone blister and spherical pearls were experimentally produced in the late 1890s, by French scientist Louis Boutan using the European ormer abalone *Haliotis tuberculata* (Fankboner, 1991, 1995). Four decades later, La Place Bostwick claimed to have cultured both blister and whole free-formed pearls in abalone from California (Bostwick, 1936). Bostwick's work was succeeded by that of Japanese scientist Dr. Kan Uno during the mid-1950s. Uno

ABOUT THE AUTHOR

Ms. Wentzell (cwentzell@giaatl.org) is a senior staff gemologist in Identification Services at the GIA Gem Trade Laboratory in Carlsbad, California.

Please see acknowledgments at the end of the article.

Gems & Gemology, Vol. 34, No. 3, pp. 184–200

© 1998 Gemological Institute of America

Figure 1. Since they were first introduced to the international gem market in 1996, cultured abalone blister pearls from New Zealand have appeared in many pieces of fine jewelry. This 18K gold and palladium pendant (actually a hidden clasp) is set with a 15 mm "Gem" grade Empress Pearl®. The Tahitian black pearls in the necklace are graduated from 11.5 mm to 15.25 mm. Designed and manufactured by Richard Kimball, Denver, Colorado; photo © Azad.



made some remarkable advances in culturing abalone pearls by drilling a hole through the shell to secure the nucleus (Fankboner, 1995; McKenzie, 1996). He has since reported growing blister pearls up to 22 mm in diameter in *Haliotis discus* in Japan. However, his attempts at producing whole round pearls were not as successful (Fankboner, 1991). Subsequently, Cho Won-Ho, president of Korea Abalone Pearls in South Korea, began cultivating abalone pearls; in 1991, he projected the successful production of large whole spherical abalone pearls ("Bigger abalone . . .," 1991). However, this pioneering effort has been halted, as the company has discontinued operations.

In the mid-1980s, Dr. Peter V. Fankboner, a professor at Simon Fraser University in Burnaby, British Columbia, was the first to produce jewelry-quality cultured abalone blister pearls in North America, using the pinto abalone *Haliotis kamtschatkana* (Fankboner, 1995). Dr. Fankboner has since produced perhaps the world's largest blister pearl, which measures 27 mm (just over one inch) across the base ("SFU marine biologist claims world record . . .," 1996). He has experimented with producing spherical bead-nucleated pearls,

and claims to have cultured a few whole free-formed tissue-nucleated pearls as large as 8 mm (P. Fankboner, pers. comm., 1998).

Dr. Fankboner also reports that, in addition to his own company (Pacific Pearl Culture Ltd., Burnaby, B.C., Canada), there are three other producers of cultured abalone blister pearls on the west coast of North America, all in California: Jack Joyner of California Abalone Pearls, Santa Barbara; Joe Cavanaugh and Art Seavey of Monterey Abalone Co, Monterey; and Tim Ross of North Coast Sea Farm, Crescent City. Dr. Fankboner and GIA Gem Trade Laboratory (GIA GTL) staff members believe that there is also a producer on the west coast of Baja California, in Mexico, but the name could not be obtained.

Abalone pearl culture has been attempted in many other countries, including Australia, New Zealand, China, South Africa, Mexico, Chile, and Ireland (Fankboner, 1995). According to a 1997 article by Cropp, recent experiments for producing three-quarter blister to round pearls in Hawaii were encouraging. Tasmania entered the field in the early 1990s, when Abalone Pearls Pty. Ltd. first successfully produced blister pearls, and began targeting



Figure 2. Empress Pearls are cultured primarily on New Zealand's Stewart Island, with a research facility at Kaikoura on the main south island. The inset shows the Stewart Island production facility, which is located at Halfmoon Bay. Photo courtesy of Empress Abalone Ltd.

spherical pearls, in the greenlip abalone *Haliotis laevigata* (Cropp, 1997). The latter trials, which are nearing completion, have confirmed the formation of a pearl sac, the first stage in the development of these cultured spherical pearls.

Since 1995, Empress Abalone Ltd. of New Zealand has successfully cultured commercial quantities of pearls in the brightly colored *H. iris*, or paua, abalone. Their research and production activities are described below. Another company that uses *H. iris* is Rainbow Pearls, located in New Plymouth, Taranaki, on the west coast of New Zealand's north island. This facility, once solely a commercial abalone hatchery, now produces assembled cultured blister pearls.

BACKGROUND OF THE "EMPRESS PEARL"

Location and Access. New Zealand is a topographically and climatically diverse country that consists of two main islands and several smaller ones (figure

2). Abalone blister pearls are cultured by Empress Abalone Ltd. at Halfmoon Bay on the northeast side of Stewart Island—a third, smaller island southernmost in New Zealand. This facility (figure 2, inset), which is open for visitors, is accessible from Invercargill, on the main south island, via an approximately one hour ferry ride or a 20 minute flight. Empress Abalone also has a research facility at Kaikoura, a small town on the northeast coast of the main south island, about 180 km (112 miles) north of Christchurch (McKenzie, 1996).

New Zealand is surrounded by three major bodies of water: the Pacific Ocean to the north and east, the Tasman Sea to the west, and the Great Southern Ocean to the south. The subtropical and subantarctic currents converge at Stewart Island, creating an influx of nutrients and producing a rich and diverse marine environment. At Kaikoura, the continental shelf comes very close to shore, creating another diverse marine environment that benefits from the upwelling of rich nutrients.

Company Structure and Facilities. In 1995, Liz and Michael McKenzie of Goldrush Gem Co., a New Zealand jewelry firm, teamed up with a group of abalone divers from Abalone Producers and Partners to form a new company, Abalone Partners Ltd., on Stewart Island's Halfmoon Bay. This operation is managed by partner Ron Dennis. The McKenzie family also holds 55% interest in Empress Abalone Ltd., of Christchurch, which has sole marketing rights for the product. The remaining interest is held by 20 shareholders. Recently, Empress Abalone Ltd. has taken over Abalone Partners Ltd., so it is now responsible for both the production and marketing of the cultured blister pearls. They have contracted with Goldrush Gem Co. for all of the post-harvest processing.

The abalone are housed onshore in 150 one-cubic-meter rubber tanks, each capable of holding 1,000 liters of water and 70–80 abalone (figure 3). There are three full-time employees and up to seven seasonal staff members. During the next three years, the McKenzies plan to build a much larger facility, with a projected capacity of 100,000 abalone, 16 km (10 miles) north of Kaikoura, in the small town of Maungamanu.

For its research activities, Empress Abalone Ltd. leases space at the George Knox Research Laboratory at Kaikoura (owned by the University of Canterbury in Christchurch). Currently this facility has 25 tanks and two full-time researchers. With

the help of a government grant, research on all aspects of abalone and pearl cultivation is being conducted in conjunction with the university. This research includes the triggers for nacre production, the effects of feed changes on pearl color, and abalone breeding.

ABALONE BIOLOGY

Abalone mollusks are a primitive group of marine snails of the class Gastropoda, subclass Prosobranchia, order Archaeogastropoda, family Haliotidae (Howorth, 1978). The largest of all gastropods (Nieson, 1994), they are a type of limpet prized for their delicately flavored meat, iridescent mother-of-pearl, and pearls. There are about 90–100 species worldwide (Haldane, 1992; Fankboner, 1995), but according to Fankboner, less than two dozen reach a size practical for pearl culture.

Abalone have separate sexes and breed by external fertilization. Millions of eggs and clouds of sperm are released into the water and drift about until they unite. Because fertilization is so random, a given animal may successfully breed in nature only once every six or seven years (Haldane, 1992). The fertilized eggs grow into larvae, and then into free-swimming veligers which settle on a hard substrate. The veligers develop into abalone, which grow at a rate of about 15–20 mm/year. This growth rate is slower than that of other mollusks used for pearl culture, but with farming it increases to about 25 mm/year. An oval adult shell reaches about 12–14 cm in length.

Abalone live in clusters from the low tide mark to a depth of about 36 m (McGraw-Hill, 1987). They feed nocturnally, by scraping algae (i.e., coralline algae as juveniles, and kelp and other seaweed as adults) with their radula, a file-like tongue with rows of chitinous projections (McLean, 1969; Howorth, 1978). A row of open pores along one side of the shell is used for respiration, excretion, and breeding (figure 4). Although abalone are generally hardy, they have no mechanism to coagulate their blood. If an animal sustains a significant cut, it will probably bleed to death (Cox, 1962), or it may die from the lost mobility that results when it muscularly clamps the wound closed (M. McKenzie, pers. comm., 1998). The average life span is about 10 years, but under ideal conditions, abalone can live as long as 40 to 50 years (Howorth, 1978).

H. iris, which is found exclusively off the coast of New Zealand, is considered by many to boast the most vividly colored mother-of-pearl of all the

abalone species (see, e.g., figure 4). The cause of the rainbow-like hues is discussed by Brown (1985, 1997). According to Liz McKenzie, colder waters, such as those off the south island, favor the formation of highly iridescent and colorful pearl nacre.

GATHERING ABALONE STOCK

Abalone diving in New Zealand is quota-based with a limited entry; the total quota does not exceed 908 tonne/year. (There are approximately 2,000 adult abalone, each at least 12.5 cm long, in a tonne.) Empress Abalone Ltd. leased 4.5 tonne in quotas from other divers last year; they prefer to use their own divers to assure care and quality.

The abalone are collected offshore from the Kaikoura and Stewart Island facilities. The divers choose predominantly rocky locations to avoid sand contamination, which can cause problems during cultured pearl growth. Each quota season begins October 1 and continues all year. However, diving conditions are most favorable from October through March, after which most activity ends. Because the use of compressed-air diving tanks is prohibited by law, snorkelers collect the abalone (figure 5) from

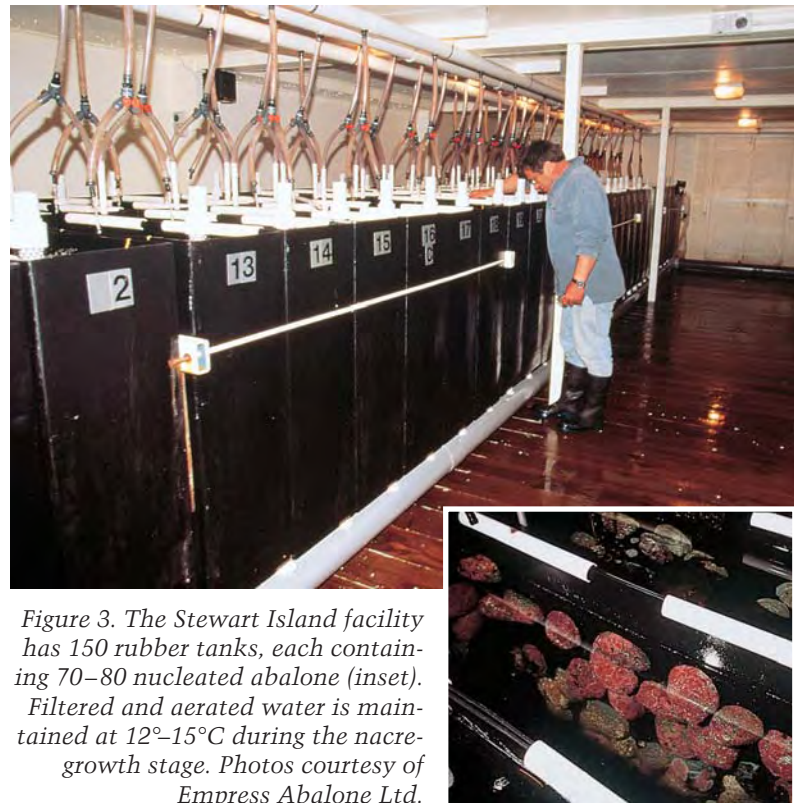


Figure 3. The Stewart Island facility has 150 rubber tanks, each containing 70–80 nucleated abalone (inset).

Filtered and aerated water is maintained at 12°–15°C during the nacre-growth stage. Photos courtesy of Empress Abalone Ltd.



Figure 4. *Haliotis iris*, also known as paua abalone, creates what may be the most iridescent and vividly colored mother-of-pearl and pearl nacre of its genus. Colorful patterns are seen on the exterior of this shell, which has been polished and lacquered. The interior (inset, also lacquered) shows vibrant colors as well; the abalone uses the row of holes for respiration, excretion, and breeding. The nucleus is inserted into an area near the apex of the shell (on the right side of the inset photo), where it is most difficult for the abalone to dislodge it. The cultured and assembled abalone blister pearls in the rings and pendant range from 12.5 mm to 15.8 mm. The rings were designed and manufactured by Ian Henderson, Dunedin, New Zealand; the pendant was designed and manufactured by Goldrush Gem Co., Christchurch, New Zealand; photos by Maha DeMaggio.

the low-tide mark down to about 9 m (30 feet). About 100–200 kg of abalone are gathered during a typical diving excursion (about two hours).

Because of their “hemophilic” nature, abalone must be collected with care. Traditionally, a type of pry bar called an abalone iron has been used; however, Empress Abalone’s divers have found that a triangular masonry trowel presents less risk of injury to the animals. The abalone are gathered by inserting this tool between the animal’s muscular foot and the rocky substrate. The abalone collected are at least five years old; much older abalone, which have thicker shells and grow more slowly than the young ones, are not as desirable for cultured pearl production. The abalone are assessed by eye before they are removed from their environment, and any unsuitable specimens are returned unharmed if possible.

Presently, Empress Abalone is using only wild stock for pearl culturing, but an additional three tonne of abalone are being grown at the Kaikoura facility as the company strives to shift to cultivated stock by late 1999. Natural abalone stocks in New Zealand were once in danger of depletion, but the government quota system has prevented this.

Although the population is sustained only by natural breeding, the New Zealand marine environment is free of the diseases and pests that deplete abalone populations in other locations. The withering-foot disease that infests the American abalone is absent, as are parasitic nematodes, polychetes, boring clams, snails, and sponges that are prevalent in other locations. There are a few predators such as seals, but their impact is minimal.

CULTURING ABALONE BLISTER PEARLS

Nuclei Implantation. Hemispherical plastic forms, used in the culture of traditional blister pearls (Ward, 1998), are also used in abalone. The McKenzies use economical material formed with casein, a by-product from a milk factory. The abalone are very sensitive to the shape of these nuclei. Because of the highly concave shape of their shell, they resist depositing nacre on a convex surface such as a high-domed bead. Better nacre deposition is achieved with flatter nuclei profiles. Also, pointed outlines such as pear shapes and hearts are generally uneconomical because the points often pierce the flesh of the abalone and cause it to bleed to death. Although 8–16 mm hemispherical nuclei

are the most favorable for producing cultured blister pearls, oval profiles often work, and pear-shaped profiles are being modified to achieve greater success.

With their strong musculature, abalone can easily eject any foreign body that comes between the mantle and the shell. To combat this, the nucleus is inserted (along with a piece of mantle tissue to generate nacre deposition) into an area near the apex or whorl of the shell (again, see figure 4), where it is most difficult for the abalone to dislodge it. The McKenzies report that their implantation technique is completely different from that used by Peter Fankboner on the North American coast (see, e.g., Fankboner, 1994). Although the exact methods are proprietary, the McKenzies indicate that they use tools that are specially designed and manufactured for the purpose, and that their technique is less invasive than some methods used by other culturers, as it does not involve cutting.

Nuclei implantation, or "seeding," takes approximately three minutes for each abalone. Although the nuclei can be implanted throughout the year, seeding is typically done from October to the beginning of December (middle to late spring in New Zealand), after the spawning season, when the gonad is smallest and access is easiest. A single nucleus is usually implanted into each animal. If two nuclei are used, the nacre commonly forms a bridge between them.

Cultured Blister Pearl Growth. Although abalone are hardy in their environment, they do not tolerate chemicals and do not like to be handled. If picked up, they will refuse to eat or produce nacre. To get over the shock of nucleation, the abalone are placed in recovery tanks for two weeks before they are transferred to permanent tanks (again, see figure 3). They remain there undisturbed until harvest.

Three basic complications can prevent successful cultured pearl growth: (1) the abalone dies, usually due to bleeding; (2) the nacre is deposited unevenly or incompletely; and (3) the nucleus causes a cyst to form. The mortality rate from abalone collection and blister pearl nucleation is relatively low (5%), but this increases (to 30%) when "free" nuclei (to produce whole pearls) are implanted. If the abalone survives the culturing process, the blister nucleus may be "ignored" rather than expelled; instead of being covered with nacre, all or part may be covered with conchiolin only. Sometimes during nucleation, sand irritation will cause the implanted bead to induce an infection instead of stimulating



Figure 5. Divers collect wild abalone from rocky locations at depths reaching 9 m (30 feet). During each approximately two-hour excursion, the divers typically retrieve 100–200 kg of abalone. Photo courtesy of Empress Abalone Ltd.

nacre growth. The result is a festering cyst rather than a cultured pearl.

H. iris need a minimum water temperature of 12°–15°C (54°–59°F) to stimulate nacre growth. However, if the water becomes too warm (e.g., approaching 18°C or 64°F), the abalone will stop producing nacre and may even seek lower temperatures by crawling out of the tanks. In the wild, nacre is deposited rapidly in the summer and specifically to the irritant site. As the temperature drops, nacre deposition slows. Conchiolin is laid in the winter, in waters as cold as 9°C (48°F). Conchiolin and other organic compounds (the mixture of which will be referred to here as conchiolin) are important, as they provide the dark background against which the colors in the overlying nacre reflect.

Cultured blister pearls up to 12 mm in diameter (starting with 10.5–11 mm nuclei) are formed in two seasons (18 months). Larger blister pearls, 12–18 mm, take three seasons (approximately 24 to 30 months) to form.

Growth Environment. The onshore holding tanks contain clear natural saltwater that is continuously replenished by water piped in from 100 m offshore. The water is filtered to minimize contamination by sand, and is maintained at a temperature of 12°–15°C (54°–59°F) during the nacre-growth phase. The water is aerated to discourage the growth of undesirable algae. The environment in the tanks is

strictly monitored to ensure the health of the abalone, as well as maximize the growth rate and nacre thickness of the cultured pearls. By maintaining specific water temperatures that are varied throughout the growing process, the operators can simulate optimal growth seasons. They also keep the facility in darkness, so that feeding is always stimulated.

Feeding. Abalone require very little care. Once the environment is established and the nuclei implanted, they need only to be fed while the cultured blister pearls grow. No nutrients or artificial feeds are added to the water; the captive abalone feed exclusively on kelp and other algae collected from the Great Southern Ocean (figure 6). The McKenzies have discovered that the brilliant colors of the cultured pearls are somewhat dependent on the type of feed available to the abalone. The alga species *Gracilaria chilensis* has been linked to production of the most desirable purple, blue, and green hues. For this reason, the abalone are fed approximately 50% *G. chilensis* and a 50% combination of three other native algae—*Durvillea sp.*, *Macrocystis sp.*, and *Laminaria sp.*—that varies seasonally. Approximately 300 kg of algae per day are required for two tonne of abalone.

HARVESTING AND PRODUCTION

Although the cultured blister pearls were first harvested twice annually, they are now harvested con-

Figure 6. Kelp is collected from the Great Southern Ocean every three to four days to replenish the abalone diet. The *H. iris* eat an average of 7% of their body weight daily; approximately 300 kg of algae per day are required to feed two tonne of abalone. Photo courtesy of Empress Abalone Ltd.



tinuously from the end of July through March. The later harvest allows thicker nacre deposition on larger nuclei. Whereas some other mollusks are implanted three or four times, *H. iris* are shucked (the shells removed; figure 7) at the first harvest because the cultured blister pearls must be cut from the shell. Both shells and meat are important by-products of the pearl harvest. Most of the meat is exported to Hong Kong. The shell is sought in jewelry and craft manufacturing for its iridescence and vibrant colors.

The results of cultured pearl seeding and growth are unpredictable. Only 25% of the animals nucleated for the pilot harvest (in 1995) yielded marketable cultured blister pearls. One year later, the success rate was up to 50% as a result of greater knowledge and improved techniques. Currently, there is an approximately 60%–70% average success rate for obtaining commercially marketable cultured blister pearls from the implanted abalone.

In addition to research harvests, there has been one small pilot harvest and two larger commercial harvests to date. A third was under way at the time of this writing. The first seeding was conducted in the spring of 1993 by Abalone Producers and Partners. This led to the pilot harvest in 1995, when Empress Abalone Ltd. merged with the divers. That harvest yielded approximately 1,100 jewelry-quality cultured blister pearls. The first commercial harvest of 10,000 implanted abalone took place during October and November of 1997, yielding approximately 6,000 cultured blister pearls of good to excellent quality. Another 2,000 abalone were harvested from March through April of 1998, yielding about 1,800 marketable pearls; the high success of this harvest was attributed to the smaller sizes of the nuclei. The third commercial harvest produced 2,000 marketable cultured blister pearls during September 1998, and another 2,000 were expected by mid-October. By the end of March 1999, the McKenzies expect to have harvested a total of 15,000 jewelry-quality cultured blister pearls for this growth period.

Rarely, either a natural pearl or a “keshi” is found during the harvest. Natural pearls may form due to suspended solids, the invasion of a flatworm, or other irritant that is brought in on the seaweed. A by-product of the culturing process, a keshi may form around the implanted tissue that has separated from the nucleus, or as a result of the introduction of another irritant during nucleation (Farn, 1986).

PROCESSING THE CULTURED BLISTER PEARLS

Once the abalone are harvested, the cultured blister pearls are cut from the shell with a diamond saw (figure 8), and the rough shell is parted from the blister with a scalpel; the nucleus is then removed, and the dome washed out. The McKenzies report that the interior surface of the dome is not worked or treated in any way. With the shell flange still in place, a blue polymer is poured into the inverted dome. The colored polymer camouflages any cracks that may form in the dome if damaged during wear, as well as any thin or transparent areas. A backing is fashioned from the mother-of-pearl of *H. iris*. If the surface of this backing is uneven, an opaque medium-gray polymer is applied to level it before it is attached to the dome. A transparent colorless glue is used to bind the backing to the dome. In all, an assembled cultured blister pearl contains a total of three or four layers, in addition to the nacre (figure 9). The assembly process may be compared to that described by Crowningshield (1982) and Taburiaux (1985) for mabé pearls, where a bead insert is used.

After the layers are assembled, the outline is rounded with a grinder. An attempt is made to bring the outline as close as possible to a calibrated size for ease of setting in jewelry. The dome is then polished with a soft cotton buffing wheel and jeweler's rouge to remove organic compounds. Polishing also imparts a high luster to the surface and optimizes the color. Once assembly and buffing are complete, the cultured blister pearls are cleaned for 20–30 seconds in a warm ammonia solution in an ultrasonic cleaner. This also reveals any cracks that formed during processing. Pearls with significant cracks are rejected.

The McKenzies claim that no coating, wax, or oil is applied to the outer nacre surface, that the ability to achieve a high luster and the transparency of the surface are inherent to the nacre.

IDENTIFYING CHARACTERISTICS

Materials. Twenty-two cultured blister pearl samples were obtained for examination. All of the blisters were round in outline, and four samples were sawn in half. Eighteen specimens ranged in size from 9.82–9.98 × 3.35 mm to 19.02–19.39 × 7.25 mm. (According to the McKenzies, the cultured abalone blister pearls range from 9 to 20 mm in diameter; they average 9–13 mm.) The other four



Figure 7. During the harvest, the abalone meat is removed from the shell by hand, or “shucked.” This abalone contains a 14 mm cultured blister pearl. Courtesy of Empress Abalone Ltd.

samples could not be similarly measured since they were still attached to part of the shell.

The McKenzies provided 15 of the specimens. Although they stated that most of the samples had flaws that would preclude their use in jewelry, they were valuable for observing the ranges of color, luster, surface blemishes, and nacre characteristics. Seven came from their first commercial harvest (figure 10). The McKenzies advised that since these samples were removed approximately nine months

Figure 8. The cultured blister pearls are sawn from the shell with a diamond blade. After trimming (inset), the blisters are ready to be processed. Photos courtesy of Empress Abalone Ltd.



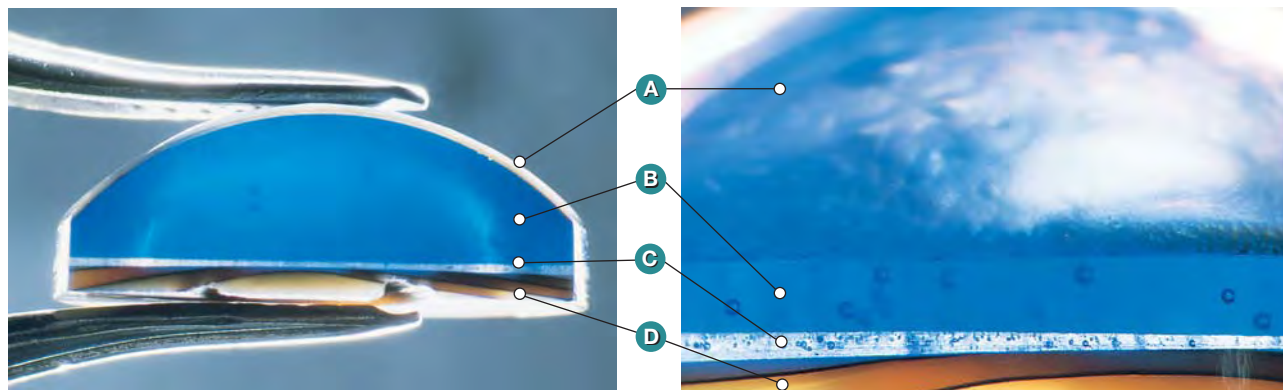


Figure 9. These are two views of one half of an assembled cultured abalone blister pearl. On the left is a cross-section, and on the right is a close-up view along the edge. There are four layers: (A) blister pearl dome (nacre—0.20 mm thick at the crown and 0.10–0.15 mm thick at the base), (B) blue polymer layer, (C) colorless glue, and (D) shell backing. An assemblage with an exaggerated thickness of blue polymer was chosen for purposes of illustration; note the bubbles in the polymer and glue layers. Sample courtesy of Empress Abalone Ltd.; photomicrographs by Shane F. McClure, magnified 10× (left) and 20× (right).

early, as test samples for the harvest, the nacre was thinner than the full-term product. They also noted that four of the seven would be considered rejects by Empress Abalone Ltd., since two had significant cracks and two had noticeably transparent areas.

Figure 10. These seven study samples were from Empress Abalone Ltd.'s first commercial harvest.

They ranged from 14.24–14.57 × 4.74 mm to 19.02–19.39 × 7.25 mm. As test samples, they were removed about nine months before the rest of the harvest, and were considered rejects (i.e., not commercial quality) by Empress Abalone Ltd. Conchiolin blemishes appear as dark brown or black spots, patches of speckles, or bands. (Note that the dark area on the front of each sample is a reflection of the photographic equipment.) Several of the samples have an “orange-peel” effect. Photo by Maha DeMaggio.



In addition to these seven samples, the McKenzies provided two unpolished samples that were still attached to the shell, with the hemispherical bead nuclei intact (figure 11). They also supplied two samples that had been cut from the shell and partially polished, but were left open in the back with the shell flange still attached. They filled one of these, their lowest-quality product, with their standard blue polymer (again, see figure 11). At the author's request, they filled the second blister with blue polymer on one side of the dome and colorless polymer on the other; this sample was then sawn in half so effects of the polymers on the color of the cultured blister pearl could be compared (figure 12). Also supplied—for cross-section observation and measurement of nacre thickness—were three half-samples that had been processed and assembled before they were sawn (again, see figure 9a).

Three unmounted samples were provided by U.S. distributor Betty Sue King of King's Ransom, Sausalito California, as products representative of those on the market in 1998 (figure 13). Five samples set in jewelry were also examined, four of which were provided by designer/jeweler Ian Henderson of Dunedin, New Zealand (see the photo on the cover of this issue) and one that was supplied by the McKenzies (again, see figure 4).

Methods. The colors were observed using a Gretag MacBeth Judge II light box with a neutral gray background and two 20-watt 6,500K color temperature bulbs that simulate average daylight. Refractive indices were determined on all samples by the spot method using a standard GIA GEM Instruments

gemological refractometer. No weights or densities were measured because of the assembled nature of the pieces. Ultraviolet fluorescence was observed in a dark room using a viewing box equipped with a GIA GEM Instruments long-wave (366 nm) and short-wave (254 nm) UV lamp. All samples were examined with a Gemolite Mark VII Stereo Star Zoom binocular microscope. A Cuda Products variable-intensity pinpoint fiber-optic light source was used for observations both with and without magnification. A GIA GEM Instruments table gauge was used to measure nacre thickness on three sawn samples.

Qualitative chemical analysis of three samples was performed with a Tracor X-ray Spectrace 5000 energy-dispersive X-ray fluorescence (EDXRF) spectrometer. One analysis was performed on the nacre dome of a cultured blister pearl assemblage, one was performed on a piece of unprocessed abalone shell, and one spectrum was taken of the blue polymer filler. An X-ray powder diffraction pattern was obtained with a Debye-Scherrer camera mounted on a Siemens Kristalloflex diffractometer, to determine the composition of a shallow surface scraping of the nacre on one assemblage. An Edsyn 951SX Loner soldering station was used at the maximum setting (427°C, or 800°F) as a thermal reaction tester for polymer coating on one lustrous sample with transparent nacre. Attempts to detect polymer coatings were also made using a Nicolet Magna-IR 550 Fourier-transform infrared (FTIR) spectrometer; a

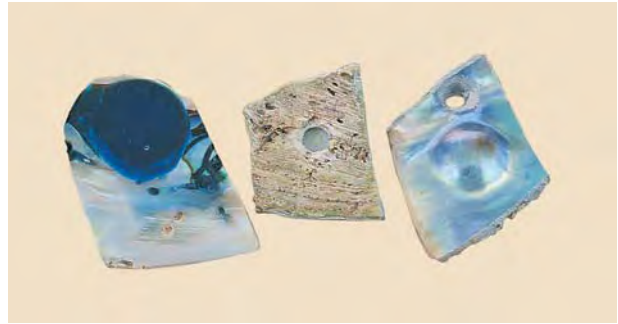


Figure 11. The two unprocessed, unpolished samples on the right were still in the shell with the hemispherical bead nuclei intact (note that the intensity of the colors is similar to the assembled product). The center sample is positioned face-down, to show the rough surface of the outer shell. The sample on the left (also face-down) had been separated from the outer shell, filled with blue polymer, and partially polished. Courtesy of Empress Abalone Ltd.; photo by Maha DeMaggio.

spectrum was obtained of a pelletized shallow surface scraping from the nacre of one sample using the transmission mode. An FTIR attachment for obtaining diffuse reflectance spectra and a Renishaw system 2000 Raman microspectrometer were also used to examine the surface of one sample for polymer coatings.

Some recent coatings are the result of polishing with compounds that leave a very thin film on the surface. Detection of these films, which may be only fractions to a few microns thick, requires equipment such as the scanning electron micro-

Figure 12. One side of this cultured abalone blister pearl was filled with blue polymer, and the other side was filled with colorless polymer (left). The sawn surface allowed observation of two thin conchiolin layers beneath the nacre (which gave a brownish appearance to the colorless polymer). These layers were sufficient to minimize the effect of the blue polymer on the color of the pearl: When the two sides were viewed face-up (right), there was no discernible color difference between them. Sample courtesy of Empress Abalone Ltd.; photos by Maha DeMaggio.

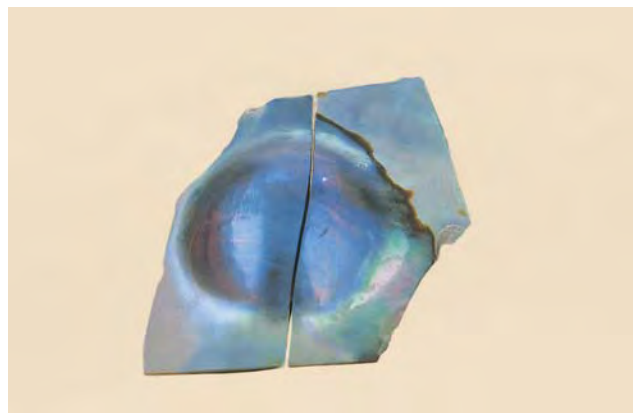
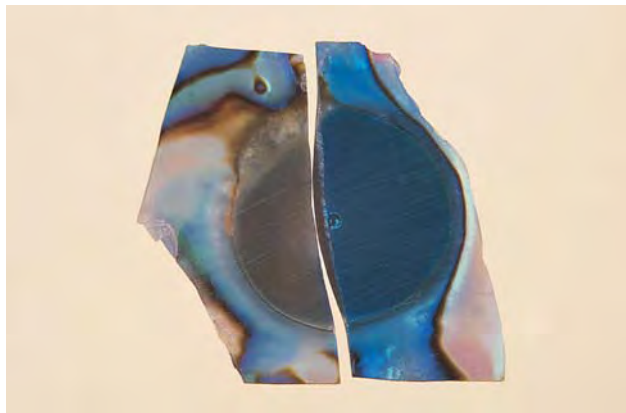




Figure 13. These three cultured and assembled abalone blister pearls are representative of those commercially marketed in 1998. The samples measured from 9.82–9.98 × 3.35 mm to 15.30–15.46 × 5.33 mm. Empress Abalone Ltd. had graded them (from left to right) as “Gem,” “A,” and “B.” Notice the “orange-peel” effect on the “B” grade product. Samples courtesy of Betty Sue King, King’s Ransom; photo by Maha DeMaggio.

scope. Seven cross-section images were taken from freshly broken edges of a cultured blister pearl assemblage using an ElectroScan Model E3 environmental scanning electron microscope (ESEM). For comparison, three images were taken of a fresh abalone shell fracture. The images ranged in magnification from approximately 600× to 6000×.

Durability testing included the use of standard Moh’s hardness points to determine the resistance of the surface of one sample to scratching. A fade test was conducted with an Oriel model 81150 solar simulator with a 300-watt xenon light source; the output emission approximates the daylight spectrum at approximately two times normal intensity. One half of a cultured blister pearl was subjected to 4.5 hours in the simulator, while the other half was kept in a darkened room to be used for comparison.

RESULTS

Color. The McKenzies state that the main bodycolors of their samples range from green through “peacock” green-blue to deep “azure” blue, and rarely, a deep violetish blue. Secondary colors and overtones include pink, purplish pink, purple, yellow, and orange. They report that the colors are typically more intense in the smaller cultured blister pearls than the larger ones. The colors in the study samples were vivid, and strong iridescence caused them to appear to shift or roll across the surface. The main bodycolors of these samples were combinations of blue, green, purple, and pink. Blue and then green were the most prevalent hues and dominated the coloration of most samples. Two samples were

predominantly deep “azure” blue; one sample was dominated by purple. Others showed purple or purplish pink to pink areas. Two samples were a combination of blue and gray. Purple, pink, yellow, blue, and green overtones were observed. Although some of the smaller samples were more blue and some larger samples contained more green, no relationship could be drawn between color and size. All samples appeared equal in intensity.

Luster. The McKenzies report that the luster of their product ranges from satiny to vitreous; the reflections appear diffuse to almost mirror-like. The lusters of the polished study samples ranged from high to extremely high, as compared to other kinds of pearls, and the luster and reflection descriptions concurred with those of the McKenzies. The light reflecting off the conchiolin layers imparted an almost metallic appearance to the pieces. The surfaces of the unpolished samples had very thin layers of organic material and whitish deposits that dulled the luster; these are removed during polishing.

Surface Characteristics. Examination of the surfaces with 10× magnification revealed several features. One sample had a large dark brown spot of conchiolin but otherwise was smooth and highly lustrous. Six other samples had smaller isolated conchiolin spots or several dark speckles; another three each had a dark brown to black band of conchiolin (figure 10).

Observation with 10× magnification also revealed cracks in nine samples. These were usually quite thin and not apparent with the unaided eye: One cultured blister pearl had a small patch of crazing near the edge of the base, one had a network of cracks in an isolated patch, and six had single hair-line fractures. Two of the thin cracks in the lower-quality materials had microscopic evidence of polymer, which typically seeps through pre-existing cracks and exposes them during processing, a benefit for quality control. One sample, a reject from the early harvest, had a large crack across the crown and a large gap at the edge of the base.

Features with the appearance of small bumps and welts gave several samples an “orange-peel” effect (figures 10, 13, and 14). These characteristics were most often seen under the surface of the nacre at the interface with the conchiolin layer, and are typical of abalone pearls. Also seen with magnification (and typical of abalone pearls) was the cellular structure of the nacre (see photo in Kammerling and

Fryer, 1994) and nacre structures that appeared somewhat botryoidal. On four samples, the nacre displayed a milky haziness, and two partially polished samples had polishing marks; both of these characteristics were only visible with 10× magnification. The surfaces of two unpolished domes that were still attached to the shell had thin layers of organic material.

Refractive Indices. Observation of refractive indices revealed a birefringence blink on all samples, and indistinct to fair spot readings. Alpha varied from 1.50 to 1.52 for the 22 samples; this was close to the value for aragonite, 1.530. Gamma was more difficult to see, and only two samples, which had high polish, gave clear readings of 1.68—close to the corresponding aragonite value of 1.685. The other samples gave indistinct gamma readings that were not reliable.

UV Fluorescence. When exposed to long-wave UV radiation, 13 samples showed a mottled and chalky medium greenish yellow fluorescence, eight samples had weak fluorescence, and one had very weak fluorescence. The same, although weaker, reaction was seen with short-wave UV. These characteristics are consistent with those reported for abalone pearls by Brown (1985).

Assemblage Characteristics. The individual layers of each assemblage could be discerned with magnification (again, see figure 9). The layers observed were consistent with those described in the processing section. Only two of the samples examined by the author had the extra layer of gray polymer that was used to level the surface of the backing before it was applied.

Nacre and Conchiolin. The McKenzies report that the nacre thickness of Empress Pearls typically ranges from 0.15 to 0.25 mm on the crown of a blister dome, and up to 2 mm around the base where it attaches to the shell. The nacre thicknesses of the three sawn assemblages ranged from 0.13 mm to 0.40 mm at the apex of the crowns. The dome bases were measured on each side of the sawn face and ranged from 0.10–0.15 mm (again, see figure 9) to 0.30–0.50 mm. The thickest nacre at the point of attachment to the shells had been ground away during fashioning. The blister that had one half of the dome filled with blue polymer and the other half filled with colorless polymer still had the shell

flange; the nacre measured 0.20–0.25 mm at the apex of the crown and 0.80–0.90 mm at the point of attachment to the shell.

When the nacre was examined with an intense fiber-optic light, and without magnification, five of the 22 samples showed noticeably thin or translucent areas that easily transmitted light. Two of these five were early-harvest test samples (both rejects); one, also a reject, had been sawn in half; and two were jewelry-quality samples. One of these latter samples had a transparent patch near the girdle through which the dark polymer could be seen with transmitted and reflected light (figure 14), although it would probably not detract from the face-up appearance if bezel-set in a mounting.

Seven additional samples showed translucent areas of varying size and intensity. Also with the fiber-optic light, numerous gas bubbles in the polymer were eye-visible through the nacre of five samples (figure 15). Except for the one jewelry-quality pearl mentioned above, none of the marketable samples had nacre deficiencies that could be discerned with the unaided eye in reflected light (the normal situation in which pearls are viewed).

The three samples that had been sawn in half were examined without magnification and with an intense fiber-optic light directed at the domes. The visibility through the nacre of both the colored polymer and the associated gas bubbles was dependent on the presence and thickness of conchiolin layer(s) rather than on the thickness of the nacre. A

Figure 14. This assembled cultured abalone blister pearl has a transparent patch of nacre near the edge of the base, through which the dark polymer can be seen. Notice, too, the “orange-peel” effect visible with magnification. Sample courtesy of Betty Sue King, King’s Ransom; photomicrograph by Shane F. McClure, magnified 12×.



single thick conchiolin layer or two thinner conchiolin layers effectively blocked the passage of light from the nacre into the polymer. The dark tone of the polymer also helped block the transmission of light. This was evident in the cultured blister pearl that had been half-filled with blue polymer and half-filled with colorless polymer. This sample contained two thin layers of conchiolin, and strong fiber-optic light did not pass through the half with the blue polymer, but it internally illuminated the half with the colorless polymer. Samples that had no conchiolin layer, or only a single thin conchiolin layer, allowed the transmission of light into the colored polymer, which then glowed through the nacre. This illuminated polymer was visible only with intense fiber-optic light. Although bright overhead lighting caused subtle illumination of the colored polymer in samples with very thin or no conchiolin, moderate overhead lighting did not cause such reactions. The gas bubbles were not visible under normal viewing conditions. It is interesting to note that the polymer appeared green when viewed through the nacre of some assemblages, even though the same type of blue polymer appeared to have been used for all the samples (again, see figure 15).

Testing for Coatings and Dyes. The surfaces of all the domes were examined with magnification for evidence of coatings and dyes, and four were subjected to different advanced testing methods. No coatings or dyes were detected, although some extremely thin polymer films (a few microns or less) and organic dyes cannot be detected by these techniques. The physical properties inherent to abalone nacre, combined with the high luster from polishing, gave a transparent appearance to the surfaces of these samples that mimicked a colorless coating. With 10× magnification, the structure of the nacre was consistent with that of natural abalone pearls seen in GIA GTL, and there was no evidence of dye concentrations.

Heating with a thermal reaction tester did not produce any odors or melting characteristic of polymer coatings. In fact, when heated to the point of burning, the surface sloughed off in platy flakes, a reaction that, in the experience of staff members at GIA GTL, is typical of nacre. When a drop of 37% HCl solution was placed on the surface of a nacre dome and studied with magnification, it was observed to effervesce strongly and immediately. A noticeably thick polymer coating would be expected to block this immediate reaction.



Figure 15. When the nacre was examined with an intense fiber-optic light transmitted through the crown, numerous gas bubbles in the polymer were visible through the nacre of five samples. Note that the blue polymer, illuminated through the nacre, appeared green in some. Sample courtesy of Empress Abalone Ltd.; photomicrograph by John I. Koivula, magnified 40×.

An X-ray powder diffraction pattern of a shallow surface scraping disclosed aragonite. An FTIR spectrum of a pelletized sample of a shallow surface scraping did not reveal any polymers (again, extremely thin microfilms cannot be detected by this method). IR diffuse reflectance was of limited value for detecting polymers, since the laboratory has yet to establish a significant database for pearls; however, there were no perceptible differences in the spectra for a fashioned abalone blister assemblage and an unprocessed piece of abalone shell; no polymers were indicated. The Raman spectra and ESEM images also did not reveal the presence of any recognized polymers, and the ESEM images of nacre cross-sections did not show any discernible differences in the surface structures of the blister assemblage and the unprocessed abalone shell.

EDXRF analysis revealed, in addition to the calcium (Ca) and strontium (Sr) expected for pearls, bromine (Br), iodine (I), copper (Cu), zinc (Zn), iron (Fe), and sulfur (S). Given that the nacre on this sample was relatively thin, the composition of the underlying polymer and its pigments apparently contributed to the results. To confirm this, a piece of unprocessed *H. iris* abalone shell and some blue polymer exposed on one of the samples were tested separately. Ca, Sr, Br, and I were present in the shell. Cu and Zn were confined to the polymer. Small amounts of Fe were present in both the polymer and the shell. (Analyses for S were not conducted in these latter samples.) The EDXRF spectrum of a cultured blister pearl did not reveal any of the heavy elements (e.g., silver or tellurium) that indi-

cate color treatments in some pearls; organic dyes cannot be detected by this method.

Durability. The McKenzies claim that the toughness and durability of their product are very good, although, as with any cultured pearl, care should be exercised in cleaning and handling. They caution against immersing the cultured blister pearl assemblages in hot water, because this may cause cracking and separation of the assembled layers. Eye-visible cracks, transparent areas revealing the colored polymer, and areas of very thin nacre affect not only the appearance, but also the durability, of the assembled cultured blister pearl. Attempts to scratch the dome surface of one sample showed it to be moderately resistant, but it yielded to a Mohs value 4 hardness point. Although some types of shell products may fade in sunlight, the McKenzies have not observed any color fading of their product. No short-term fading was observed in the half of an assembled cultured blister pearl that was left in the solar simulator for 4.5 hours (approximating nine hours of direct sunlight).

MARKETING AND DISTRIBUTION

The McKenzies debuted the Empress Pearl at the Tucson gem shows in February 1996 (figure 16). At the wholesale level, Empress Pearls are sold as “mabés,” “hemispherical pearls,” or “half-pearls.” They are priced according to their size and their color, luster, and surface characteristics. These three attributes are the basis for the Empress Pearl “point matrix” grading system, a 100-point system that was developed in 1995 by the McKenzies specifically for their product. Points are assigned to each attribute according to its rarity and desirability. Color value is based solely on rarity.

The quality grades presently used by the company are “Gem,” “A,” “B,” and “C.” The McKenzies report that only the highest grades—“Gem,” “A,” and upper “B”—are sold as Empress Pearls. Approximately 4% of the material marketable under the Empress name is considered “Gem” grade, 40% is “A” grade, and 56% is “B” grade. Cultured blister pearls with lower “B” grades and those that fall below the “B” classification, termed “semi-perfect,” are sold in sterling silver jewelry under the name Ocean Rainbow®, a product of Ocean Rainbow Ltd., Christchurch.

Empress Pearls are distributed directly to wholesalers in New Zealand, Australia, the U.S., Taiwan, England, Italy, and the Middle East. The largest



Figure 16. Empress Pearls® were debuted at the 1996 Tucson Gem and Mineral Show. The 18K gold rings, each of which contains a “Gem”-grade abalone “mabé” (the largest of which is about 13.5 mm in diameter) were designed and manufactured by A & S Wholesale Jewelers, Union City, New York. Samples courtesy of Empress Abalone Ltd.; photo by Robert Weldon.

market is currently the U.S., followed by New Zealand. High-quality Empress Pearls have been set in fine jewelry that incorporates high-karat gold or platinum, diamonds, and colored gems (see, e.g., cover photo, figure 1, and figure 17).

WHOLE FREE-FORMED CULTURED PEARLS

An exciting aspect of current research involves the cultivation of whole free-formed, especially spherical, cultured pearls within the body of the abalone. Over the past three and a half years, Empress Abalone Ltd. has spent approximately US\$350,000 on this research, and 2,000 abalone have been implanted with “free” spherical bead nuclei, in an attempt to produce these elusive cultured pearls.

The McKenzies have been experimenting with spherical nuclei fashioned from the shell of a species of Mississippi mussel and *Pinctada maxima*, the large golden-lipped oyster used to produce South Sea cultured pearls, with similar results. The optimum nucleus is 6 mm, which is projected to yield an 8 mm cultured pearl. The nuclei are currently being fashioned from *P. maxima*. The McKenzies predict that 6–8 mm nuclei will eventu-



Figure 17. This 18K yellow and white gold necklace contains five “A”-grade round (15–18 mm) Empress Pearls and one 22 × 15 mm pear shape. The necklace is accented by diamonds, rubies, and sapphires. It was designed and manufactured by Hugh Power Designs, Anchorage, Alaska. Photo © TKO studio, New York; courtesy of Empress Abalone Ltd.

ally be used to obtain 8–10 mm whole spherical cultured pearls. Larger nuclei result in a high rejection rate. One nucleus per abalone is inserted in a process that takes four to five minutes. The tools, technique, and exact location within the animal are proprietary and were developed through original research.

If an abalone’s strong muscular force does not expel the loose bead nucleus, the exertion on the bead is usually enough to hinder satisfactory nacre coverage, quality, and shape. The whole free-formed cultured pearls produced to date have nacreous areas up to 2–3 mm thick. This nacre is thicker than that of the cultured blister pearls because the bead nucleus is a greater irritant.

According to the McKenzies, the whole free-formed cultured pearls have evolved from completely baroque shapes, most with a somewhat conical outline, to products that are more spherical. Although

results are preliminary, there have been promising indications of success; the author had the opportunity to see seven of the whole free-formed bead-nucleated cultured pearls at the February 1998 Tucson gem shows (figure 18).

Empress Abalone Ltd. has also been experimenting with whole free-formed tissue-nucleated cultured pearls. The tissue is implanted into the same visceral region where the free-formed bead-nucleated pearls are grown. The McKenzies describe the resulting cultured pearls as thin and curved, somewhat like a fingernail, and partially hollow; they cannot be distinguished from a natural abalone pearl on the basis of their outside appearance. To date, there is no commercial production.

DISCUSSION

Mabés. Blister pearls were the first type of cultured pearls; as early as the 13th century, various types of nuclei were implanted in oysters to be covered with mother-of-pearl, including small lead or tin forms resembling religious idols (Kammerling et al., 1990; Fankboner, 1991; Webster, 1994). More recently, hemispherical shell beads were implanted into the large *Pteria penguin* (Japan) and *Pinctada maxima* (Australia) to produce sizable blister pearls that could be assembled for use in jewelry (Crowningshield, 1982; Taburiaux, 1985; Farn, 1986). These were called mabé pearls. Typically, the blister dome would be coated from the inside with a translucent material, and a mother-of-pearl bead inserted; then any remaining voids would be filled with a colorless glue and a mother-of-pearl backing would be applied (see, e.g., Crowningshield, 1982; Taburiaux, 1985).

Today, an assembled cultured blister pearl from any type of nacreous mollusk is often referred to as a mabé, and usually only epoxy or another polymer fills the dome. Empress Pearls resemble these contemporary mabés in their assembled nature, and Empress Abalone Ltd. often refers to their products as “mabés.” Although the Empress process uses a colored polymer to fill the dome, the inside surface of the nacre is not coated, as is typical of traditional mabés. In general, assembled cultured abalone blister pearls may be separated from other types by their intense coloration, high iridescence, and greenish yellow ultraviolet luminescence; the transparent nacre has unique botryoidal features and a cellular structure (visible at high magnification).

Cultured blister pearls are being or have been produced in other species of abalone, including *H.*

rufescens, *H. fulgens*, *H. kamtschatkana*, *H. discus*, *H. gigantea*, and *H. seiboldii*. These, too, have been fashioned into "mabés." The author had the opportunity to examine a "mabé" from *H. rufescens* (red abalone from the west coast of North America) that was donated to GIA by Dr. Peter Fankboner. In this sample, the nacre dome was attached directly to the mother-of-pearl and shell base with a very thin layer of transparent glue. No other layers or the dome filler were visible. The colors were pleasing, with more silver and pink hues (again, see photos in Kammerling and Fryer, 1994) compared to the more prevalent blue hue of the blisters from *H. iris*. The luster was high, with a slight satin quality.

Effects of Conchiolin on Appearance. The presence and thickness of the underlying conchiolin layer(s) determine the quality of light and color reflected back to the observer. The blue polymer did not affect the face-up appearance of those assemblages that have conchiolin layers sufficiently thick to block the passage of light. The conchiolin acted as a mirror, reflecting normal overhead light back through the nacre toward the observer for maximum light return, color, and iridescence. The face-up color of samples that contained thinner conchiolin layers could possibly be slightly affected by the blue polymer; however, even moderately thin layers of conchiolin acted as a mirror, and the colored polymer in these pearls could only be discerned with intense light. Examination of the sawn blister dome that was half-filled with blue polymer and half-filled with colorless polymer confirmed this conclusion. Face-up examination of both halves revealed no discernible color difference (figure 12).

Conversely, absence of this conchiolin layer diminishes the potentially strong and appealing visual effects; assemblages without a conchiolin layer, or with a very thin conchiolin layer, allowed light to enter the polymer filling. These pearls not only showed less intense color and brilliance, but the light passing into the colored polymer affected the face-up color of the pearl. On careful examination in reflected light and with the unaided eye, this was evident on a sawn reject sample and on the lowest-quality commercial product; they both showed a bluish background color that was at least partially due to the polymer, but the extent of impact could not be determined.

Examination for Surface Treatments. The high luster combined with the transparent nacre have led



Figure 18. The first attempts at culturing whole free-formed bead-nucleated abalone pearls produced these irregular shapes in February 1998. Pressure exerted by the abalone on the bead commonly prevents the nacre from covering the entire nucleus. Samples courtesy of Empress Abalone Ltd.; photo by Maha DeMaggio.

some people to suspect a polymer coating on these "mabés." Also, the vivid colors can mislead one to believe they are dyed (and some dyed traditional mabés resemble this abalone product [R. Kane, pers. comm., 1998]). No coatings or dyes were detected in the course of this study. Not all samples were tested by advanced techniques, and the possibility exists that an extremely thin polymer microfilm or an organic dye could defy detection by all the testing techniques available to the author; however, the vibrant colors, transparency, and ability to achieve a high luster are properties that are inherent to abalone nacre.

Durability. Although comprehensive durability testing was not performed on the Empress product, mabés in general are relatively soft (hardness 3.5-4), and their domes have moderately thin nacre. Care must be taken during wear, as a sharp blow could crack them. It is the author's opinion that the product lends itself best for use in pendants, enhancers, necklace clasps, brooches, and earrings, where the threat of damage is reduced. Rings are only recommended for occasional wear.

CONCLUSION

Empress Abalone Ltd. is commercially producing cultured blister pearls with vibrant colors and a

rainbow-like iridescence that are unique to New Zealand's *H. iris* abalone. In 1997, 6,000 commercial-quality cultured blister pearls were harvested, in sizes up to 12 mm in diameter, and a similar quantity is expected for 1998. In an assemblage process similar to that used for mabés from traditional pearl oysters, the cultured blister pearls are cut from the shell, filled with a blue polymer, backed with mother-of-pearl, and buffed to a high luster. Examination of 22 of these "mabés" revealed the various components that are used to assemble the product, as well as the character of the nacre. Conchiolin plays an important role in the face-up appearance of the "mabés." Where the conchiolin layer is very thin or absent, the blue polymer used to fill the dome can affect the color appearance of the nacre; whereas the presence of thicker layers of conchiolin optimizes the naturally vivid colors and iridescence. Examination with magnification of all samples, and advanced testing of some, revealed no evidence of any surface treatment.

These abalone "mabés" are priced according to their size, color, luster, and surface blemishes. Empress Abalone Ltd. markets the finer quality material as Empress Pearls worldwide (Empress Abalone Pearls in the U.S.). The lower quality mate-

rial is marketed under the name Ocean Rainbow. The abalone product, like other mabés, should be worn and treated with care.

Research is ongoing, and the prospects for decreased mortality rates, increased production yields, and greater control over nacre deposition appear good. Methods for the commercial production of whole free-formed bead- and tissue-nucleated cultured abalone pearls are being explored.

Acknowledgments: The author thanks Liz and Michael McKenzie, of Empress Abalone Ltd., Christchurch, New Zealand, for providing information, samples, and photos; Betty Sue King of King's Ransom, Sausalito California, for providing samples; Shane McClure of GIA GTL for photomicrography, suggestions, and support; Dino DeGhionno of GIA GTL for X-ray powder diffraction analysis; Sam Muhlmeister of GIA Research for EDXRF analysis; Shane Elen of GIA Research for producing FTIR diffuse reflectance and Raman spectra; Claus Hedegaard for producing ESEM images; Dr. Peter V. Fankboner for information; and staff members at the Richard T. Liddicoat Library and Information Center, and Leila Dooley of the Carlsbad City Library, for assistance with the literature search.

REFERENCES

- Bigger abalone pearls in 1992. (1991) *Hong Kong Jewellery*, Vol. 2, No. 50, p. 90.
- Bostwick L.P. (1936) Growing pearls in the laboratory. *The Gemmologist*, Vol. 5, No. 54, pp. 143-149.
- Brown G. (1985) The abalone and its pearls. *Australian Gemmologist*, Vol. 15, No. 11, pp. 400-403.
- Brown G. (1997) New Zealand's Empress Pearl®—An abalone pearl par excellence. *Jewellery World*, Vol. 16, No. 2, pp. 36-38.
- Cox K.W. (1962) California abalones, family *Haliotidae*. *California Department of Fish and Game Fish Bulletin*, No. 118, 133 pp.
- Cropp D. (1997) Abalone pearls from Bass Strait. *Australian Gemmologist*, Vol. 19, No. 9, pp. 375-379.
- Crowningshield G.R. (1982) Cultured 3/4 blister pearls. *Gems & Gemology*, Vol. 18, No. 1, pp. 36-38.
- Fankboner P.V. (1991) Pearl culture in abalone. *Infofish International*, No. 4/91, July/August, pp. 52-55.
- Fankboner P.V. (1994) *Process for Producing Pearls in Abalone and Other Shell-Bearing Molluska and Nucleus Used Therewith*. U.S. Patent Number 5,347,951, Sept. 20, 33 pp.
- Fankboner P.V. (1995) Abalone pearls: Natural and cultured. *Canadian Gemmologist*, Vol. 16, No. 1, pp. 3-8.
- Farn A.E. (1986) *Pearls: Natural, Cultured and Imitation*. Butterworth-Heinemann Ltd., Oxford, England, 150 pp.
- Haldane D. (1992) The mystery of the missing mollusks. *Los Angeles Times Magazine*, January 5, pp. 23-26.
- Howorth P.C. (1978) *The Abalone Book*. Naturegraph Publishers, Happy Camp, CA, 80 pp.
- Kammerling R.C., Koivula J.I., Kane R.E. (1990) Examination of an interesting cultured blister pearl. *Australian Gemmologist*, Vol. 17, No. 5, pp. 174-175.
- Kammerling R.C., Fryer C.W. (1994) Lab notes: Abalone "mabé" pearl. *Gems & Gemology*, Vol. 30, No. 4, p. 268.
- McGraw-Hill (1987) *Encyclopedia of Science and Technology*. 6th ed. McGraw-Hill Book Co., New York, pp. 4, 22-23, 587-588.
- McKenzie L. (1996) The Empress Pearl®—A New Zealand cultured half-pearl. *Australian Gemmologist*, Vol. 19, No. 8, pp. 336-338.
- McLean J.H. (1969) *Marine Shells of California*. Los Angeles County Museum of Natural History Science Series 24, Zoology No. 11, 104 pp.
- Nieson T.M. (1994) *Beachcomber's Guide to Southern California Marine Life*. Gulf Publishing Co., Houston, TX, 192 pp.
- SFU marine biologist claims world record for culturing mother-of-all (abalone)-pearls (1996) *Simon Fraser University News*, Jan. 18, pp. 1-2.
- Taburiaux J. (1985) *Pearls: Their Origin, Treatment & Identification*. Chilton Book Co., Radnor, PA, 247 pp.
- Ward F. (1998) *Pearls*. Gem Book Publishers, Bethesda, MD, 64 pp.
- Webster R. (1994) *Gems: Their Sources, Descriptions and Identification*, 5th ed. Rev. by Peter Read, Butterworth-Heinemann Ltd., Oxford, England, pp. 500-558.

ESTIMATING WEIGHTS OF MOUNTED COLORED GEMSTONES

By Charles I. Carmona

Updated formulas are presented for estimating the weights of mounted colored gemstones. These formulas are derived from measurements and weights of thousands of German-cut calibrated amethysts and citrines, representing most commercially available shapes and sizes. As with the formulas taught by GIA, the dimensions of a stone are multiplied by its specific gravity and by a "shape factor" that is determined by the stone's face-up outline. This article also illustrates how the shape factor changes over a continuum of common face-up outlines. As in previous formulas, a separate weight correction factor is applied to stones that show proportion variations in profile view.

Estimating weights of mounted gemstones has become a common routine for many of today's jewelry tradespeople. Weight estimation is necessary when the stone cannot be removed from its mounting, either because the client will not allow it or because the piece might be damaged. This is typically the case with estate jewelry (i.e., jewelry that has been previously owned). Estimating weight might be done when performing an appraisal, calculating an offer to purchase jewelry with unknown

gemstone weights, or negotiating the sale or pawn of jewelry.

Over the past two decades, estate jewelry has become increasingly important in the market (figure 1). No longer is all second-hand jewelry simply melted down and the stones recut for remounting. In fact, more jewelers are entering this market, at both wholesale and retail levels, as witnessed by regular estate jewelry sections in the trade press (see, e.g., *Jewelers' Circular-Keystone* and *Professional Jeweler*), the growth of estate jewelry sections at trade shows (such as the Las Vegas JCK Show), and the prevalence of this jewelry in on-line bulletin boards (e.g., <http://www.diamonds.net>, <http://www.polygon.net>) and Web sites (e.g., <http://www.antique-estate-jewelry.com>, <http://www.estatejeweler.com>). For appraisers, estate jewelry dealers, and pawnbrokers in particular, the ability to accurately estimate the weight of mounted gemstones is critical to the success of their operations.

Tables of diamond weights according to mil-

ABOUT THE AUTHOR

Mr. Carmona, G.G., is an Accredited Senior Appraiser (ASA) and president of Guild Laboratories, Inc., Los Angeles, California [cicarmona@aol.com].

Please see acknowledgments at the end of the article.

Gems & Gemology, Vol. 34, No. 3, pp. 202-211

© 1998 Gemological Institute of America

Figure 1. Estate jewelry is gaining in popularity with today's customers. However, the valuation of such jewelry is not straightforward, as the gems cannot be removed from their mountings for weighing. As a result, weight estimation is very important for colored stones as well as diamonds. This suite of amethyst jewelry was created in France around 1824. The 65 amethysts are cut in oval, pear, and round shapes and set in two-color gold. The largest amethyst (set in the choker brooch) is estimated to weigh about 92 ct. Courtesy of David Humphrey; photo © Harold & Erica Van Pelt.



limeter measurements first appeared in the gemological literature in the mid-18th century (Jeffries, 1750). However, it was not until the mid-20th century that the first formulas for the estimation of diamond weights appeared (Leveridge, 1937), in a booklet that accompanied the Leveridge® gauge, a spring-return measuring device that was introduced that year. Also included in this booklet were the first specific gravity correction factors to convert diamond formulas for use in estimating the weights of colored stones.

The first weight estimation formula specifically for colored stones was developed for cabochons (Small, 1952); it was followed by formulas for common faceted stone shapes (i.e., round, oval, rectangle, square, emerald cut, cushion, marquise, and pear; Ellison, 1957). Also from the late 1950s to early 1960s, formulas developed by GIA were published as supplements to coursework (R. T. Liddicoat,

pers. comm., 1998). Currently, the earliest version extant at GIA of these colored stone formulas is a notebook on the appraisal of jewelry (Gemological Institute of America, circa 1977). These formulas are the same as those listed in other references that have appeared since then, both published (Altobelli, 1986; Miller, 1988; Drucker, 1997) and on-line (<http://www.geogem.com/weightestimate.html>, <http://www.teleport.com/~raylc/gems/estimate.html>).

The formulas developed by GIA for colored stones have served the industry well since their introduction. Over time, however, there has been no published attempt to corroborate these formulas or adjust them to the modern cutting styles that have evolved with new cutting technologies, increased understanding of optics, and continued artistic expression in the lapidary arts. The present author developed his formulas by measuring and weighing thousands of calibrated citrines and

Alphabetical listing of gems commonly encountered in the trade (by species, variety or both) with their SG's and the SG groups into which they are listed.								
GEM	GP	SG	GEM	GP	SG	GEM	GP	SG
Alexandrite	7	3.73	Diopside	4	3.29	Rhodolite	7	3.84
Almandine	8	4.05	Emerald	1	2.72	Ruby	3	4.00
Amethyst	1	2.66	Grossularite	6	3.61	Sapphire	8	4.00
Andalusite	3	3.17	Idioite	1	2.61	Spessartite	8	4.15
Andradite	7	3.84	Jadite	4	3.31	Spinel	6	3.60
Apatite	3	3.18	Kunzite	3	3.18	Sunstone	1	2.65
Aquamarine	1	2.72	Lapis Lazuli	1	2.75	Tanzanite	4	3.30
Beryl	1	2.72	Malachite	8	3.95	Topaz	5	3.53
Chalcedony	1	2.60	Moonstone	1	2.56	Tourmaline	2	3.06
Chrysoberyl	7	3.73	Nephrite	2	2.95	Tsavorite	6	3.61
Citrine	1	2.66	Opal	*1	2.15	Turquoise	1	2.76
Coral	1	2.65	Peridot	4	3.34	Zircon	8	4.00
Diamond	7	3.84	Pyrope	7	3.78			
	5	3.52	Quartz	1	2.66	*(.20%)		

See page 2 for discussion of weight correction factors (WCF).
See page 19 for varieties not listed above.

OVAL SHAPE FACETED STONES

Length X Width X Depth X S.G. X .0021 X WCF = estimated weight
Range of weights on facing page are for depths of 65% - 70% of diameter.

To estimate the weights of shallow or deep stones, or those with bulges, use the formula above and diagrams below to compare profiles. Each layer of bulge may add as much as 15% more weight.

Figure 2. Reproduced here are two representative pages from *The Complete Handbook for Gemstone Weight Estimation* (Carmona, 1998). The upper left side alphabetically lists commonly encountered gemstone varieties or species and their specific gravities and S.G. groups. Profiles of stones with various depths and bulge patterns are illustrated below to aid in estimating weight correction factors. The right side has tables with eight columns of weight ranges by millimeter sizes, into which most colored stones can be grouped by their similar specific gravities.

amethysts, as well as dozens of synthetic sapphires, in a broad variety of shapes and sizes. He then checked and confirmed the formulas on noncalibrated loose stones over the course of several years, through his work as a gemologist and appraiser. He has also developed formulas for a greater number of shapes than are currently covered in GIA's Colored Stone Grading course. In addition, he has explored in depth the process of using both "shape factors" and "weight correction factors" (WCFs) to estimate the weights of mounted colored gemstones.

The full results of the author's work in this area are being published in *The Complete Handbook for Gemstone Weight Estimation* (Carmona, 1998). This book contains formulas for estimating the weights of 24 common shapes of colored gemstones, and tables to look up weights already calculated for average well-cut stones (see, e.g., figure 2). It also contains another 48 formulas for stones with unusual shapes. The weight estimation tables cover all colored gemstones by grouping them into eight categories according to their similar specific gravities (again, see figure 2).

The Complete Handbook also contains separate sections with formulas and weight charts pertaining to diamonds and pearls. Since diamonds generally are cut differently from other gemstones, they have a separate set of weight estimation formulas. It is unusual for colored stones to be cut with the exact facet arrangements and angles as diamonds (so-

called "diamond cut"); such stones are typically small (calibrated up to 3 mm round). Because of their different critical angles, colored stones are usually cut with steeper crowns, as well as with greater pavilion bulges and thicker girdles, adding weight. Formulas for diamond weight estimation are not addressed in this article, and the use of colored stone formulas to estimate diamond weights may lead to inaccurate results.

The present article reviews both the key considerations for weight estimation and the procedure used by the author to provide more accurate estimates for the weights of colored gemstones. Several examples of shape factors and WCFs from *The Complete Handbook* are provided. These factors are used to compensate for variations from basic shapes that are commonly seen in the present jewelry market.

KEY CONSIDERATIONS FOR GEMSTONE WEIGHT ESTIMATION

A gemstone is a three-dimensional object with a specific volume that can be calculated by measuring its length, width, and depth (figure 3). (Height substitutes for length or width for some shapes.) The weight estimation process involves measuring the maximum values for these three dimensions, which are incorporated into the appropriate volumetric formula. (Volumetric refers to the capacity, size, or extent of a three-dimensional object or region of space.)

Besides the Leveridge gauge, various other devices are used to measure gemstones, including screw micrometers and calipers. All measure in millimeter units, since the metric system is standard in the international gemstone business. Generally, micrometers are the most accurate, but they are not as versatile as the Leveridge gauge (which can also estimate to hundredths of a millimeter) for gemstones that are partially enclosed by mountings. The disadvantage of calipers is that they are accurate only to tenths of a millimeter, which will reduce the accuracy of the results obtained from the formulas.

Careful measurements are necessary to obtain accurate weight estimations. Each dimension should be measured several times to find the maximum value. A table gauge can be helpful for determining face-up measurements of smaller stones. When a bezel setting or prong hides the edge of a stone, examination with a loupe or microscope can help determine the extent to which the stone continues into the mounting. When gallery work obscures direct measurement of the depth, an offset measurement is necessary: Hold the measuring instrument to the side of the stone and line up the measuring device by eye with the top and bottom points of measurement.

There are many possible sources of error in the weight estimation process. Besides measurement and mathematical errors, specific gravity variations can affect the estimated weight. For example, air pockets trapped within a heavily included stone will lower its S.G. Conversely, inclusions with a higher S.G. than the host gem (such as rutile nee-

dles in quartz and tourmaline) will raise the S.G. Since samples of flawless quartz were used as the standard for the formulas and tables presented here, included stones may require slight corrections. Potential margins of error also increase proportionate to the size and S.G. of a stone: The larger and heavier the stone, the greater the care needed to estimate its weight accurately.

However, the greatest challenge in estimating weights of mounted gemstones is correcting for proportion variations. This requires judgment and experience. By thinking of gemstone outlines as a continuum of traditional shapes from one to the next, it is easier to correct for such variations. Examples of such continuums are: round to square, round to oval to cushion to rectangle, and pear to heart. The following discussion first explains the development of the new formulas, and then illustrates these shape sequences and provides the corresponding shape factors. Next, it examines profile variations (e.g., pavilion bulge), and how weight correction factors are applied to stones with nonstandard profiles.

DEVELOPING THE FORMULAS

The proposed formulas are based on numerous weights and measurements of actual stones, not on mathematical constructs or computer models. To develop accurate formulas, the author weighed and measured several dozen parcels—totaling over 5,000 stones—of calibrated German-cut amethyst and citrine in common shapes and sizes. The availability of such a large number of precision-cut stones, along with the fact that amethyst and citrine are

Figure 3. Weight estimation requires that the following dimensions be measured: length (L), width (W) [or height (H) for stones with nonparallel sides], and depth (Dp). Round shapes are defined by their diameter (Di) and depth.

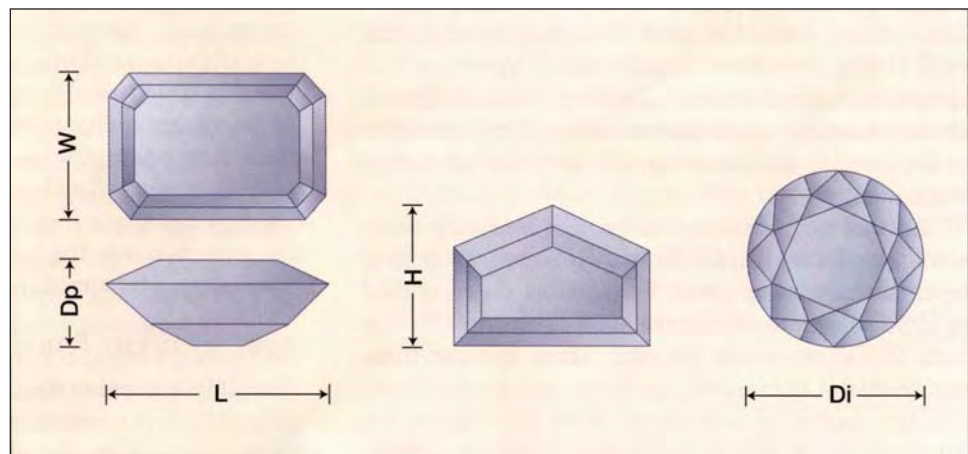




Figure 4. Cabochons are featured by many contemporary jewelry designers. This Bulgari parure consists of a necklace, bracelet, and earrings set with oval sapphire and round ruby cabochons, and accented with diamonds. The sapphire cabochons in the necklace range from 11 × 90 mm to 17 × 24 mm. Jewelry courtesy of Suzanne Tennenbaum. Photo © GIA and Tino Hammid.

two of the most common gem varieties on the market, made them logical standards for this purpose. Since these formulas were first developed in the mid-1990s, hundreds of additional varieties and shapes of colored stones have been checked against them to verify their universality. The formulas proved to be accurate for all the colored stones examined.

Lots of 10 to 50 stones in standard calibrated sizes (e.g., 5 × 3 mm, 6 × 4 mm, 7 × 5 mm, 8 × 6 mm) of each shape were used. Each parcel was weighed to the hundredth of a carat (0.01 ct) using a Scientech SE300 electronic balance. Then, specific measurements of the largest, smallest, and several intermediate stones in each parcel were recorded to the hundredth of a millimeter using a Leveridge gauge.

The average weight of a stone in each parcel was calculated by dividing the total weight of the parcel by the number of stones it contained. The actual weights of the stones in each lot showed minor variations from the average weight, due to slight cutting variations. The average weight, size measurements, and S.G. were used to calculate a shape factor for each calibrated size and shape, as follows:

$$\text{Shape Factor} = \frac{\text{Weight}}{\text{Length} \times \text{Width} \times \text{Depth} \times \text{S.G.}}$$

All of the shape factors (calculated for each size within a given shape) were then averaged to arrive at a single factor for that shape. This process was repeated for each shape, for both faceted stones and cabochon cuts. The shape factor is a critical part of the weight estimation formulas, because it compensates for the fact that *length* × *width* × *depth* is the volume of a rectangular solid, rather than the shape of a faceted gemstone.

Once the shape factor was established, the formula was inverted to solve for weight (and a weight correction added where appropriate), as follows:

$$\text{Weight} = \text{Length} \times \text{Width} \times \text{Depth} \times \text{S.G.} \times \frac{1}{\text{Shape Factor}} (\times \text{WCF})$$

Tables in the *Complete Handbook* present ranges of gemstone weights for many shapes and sizes (up to 20 mm, in half-millimeter increments), in a common range of depths. Weights for intermediate sizes that are not normally calibrated were interpolated by formula. The weights are grouped into eight narrow S.G. ranges (again, see figure 2). The first column, calculated using quartz, also includes other stones with S.G.'s in the 2.55 to 2.75 range (e.g., beryl, chalcedony, and feldspar). A spreadsheet analysis was used to calculate the weights given in the other columns. Formulas for 48 uncommon shapes are also presented, calculated from fewer samples (3–12 for each shape). In addition to quartz, flawless synthetic corundum was used to calculate formulas for uncommon shapes, because this was the only material found in which these shapes occurred.

APPLYING THE FORMULAS

Face-Up Examination. The face-up outline (or “shape”) of the gemstone determines which shape factor is used in the weight estimation formula.

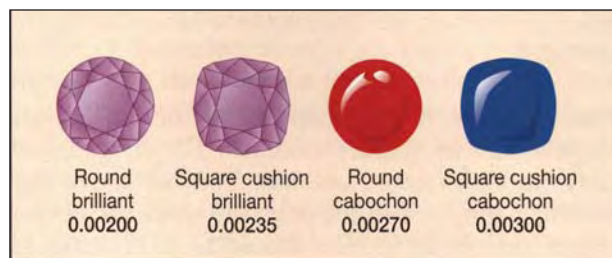


Figure 5. The shape factors (the numbers in boldface type) increase from round to square cushion cuts, for both faceted stones and cabochons.

Many colored stones have mixed cutting styles on the crown and pavilion, but these shape factors can still be applied regardless of minor differences in facet arrangements within similar shapes. These shapes are described by commonly used names, several of which are registered trademarks. (A glossary of names for over 200 gemstone shapes is included in *The Complete Handbook*.)

Following are examples of how the shape factors change according to face-up variations between common shapes. Remember: It will take some practice to learn how to interpolate the shape factors for actual gemstones. In any case, the calculated weight should always be stated as an estimate. Because cabochon cuts (see, e.g., figure 4) are rounded versions of faceted stones, their volumes are greater and their shape factors are always higher than those for the corresponding faceted shapes.

Round to Square. For both faceted and cabochon-cut stones, there is a continuum in the face-up outline from round to square cushion shapes (figure 5). The shape factors for faceted stones increase 17^{1/2}% from the round shape (0.00200) to the average square cushion shape (0.00235). For cabochon cuts, the increase is 11% (from 0.00270 to 0.00300). Shape factors must be interpolated for stones that are intermediate between these two shapes.

In a related continuum, the faceted square cushion shape may show variations toward the cut-corner square (emerald or Radiant*) cut or toward the square step cut or square Princess cut (figure 6). The shape factors for the average square cushion cut and the average square emerald or square Radiant cut show a decrease of only 2% (from 0.00235 to 0.00230, a difference of approximately 0.10 ct for every 5.00 ct). Therefore, the formulas here and the tables and formulas in the *Handbook* can be used

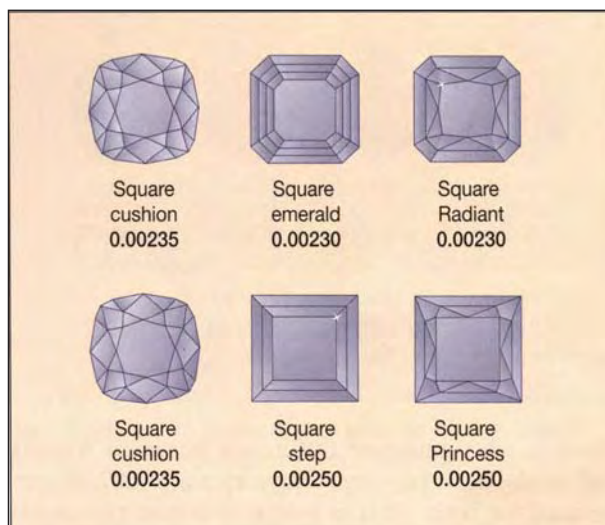


Figure 6. The difference in shape factor between a square cushion and a square emerald (or Radiant) cut is not significant, except in the weight estimation of larger stones. The change in shape factor is more significant (6^{1/2}%) between square cushion and square step cut or square Princess cut stones

interchangeably for both of these shapes, at least for smaller stones. For larger stones (over 3 ct), the difference between these shapes could become significant, so the shape factor should be adjusted appropriately.

The shape factors increase 6^{1/2}% (0.00235 to 0.00250) from the average square cushion cut to the average faceted square step cut or square Princess cut (again, see figure 6). Because this difference is significant, it will be necessary to interpolate the shape factor for all stones that are transitional between these cuts.

Round to Oval to Rectangular Cushion. Another continuum for both faceted and cabochon-cut stones is from round to oval, and also from oval to rectangular cushion shapes. The factors for faceted stones increase 5% from the round shape (0.00200) to the average oval shape (0.00210), as illustrated in figure 7. For cabochon-cut stones, measuring and averaging of hundreds of cabochons revealed that

*Radiant Cut Diamond is a registered trademark of the Radiant Cut Diamond Corp. and is commonly used to describe similarly cut colored stones.

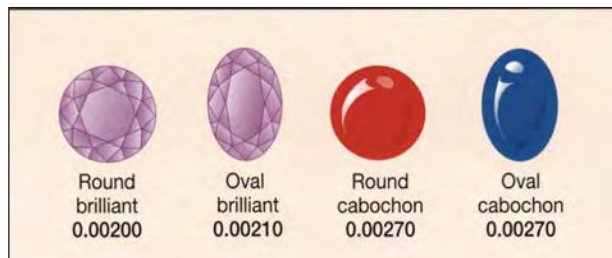


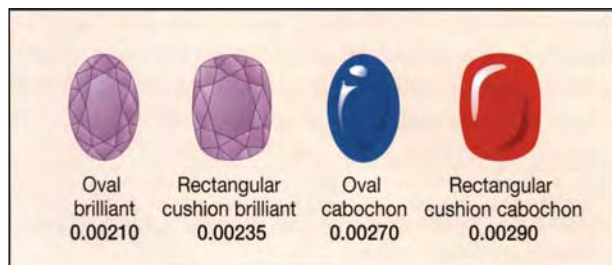
Figure 7. Although the shape factor increases from round to oval shapes in faceted stones, there is no increase for cabochons.

there is no significant difference between rounds and ovals, and the same shape factor (0.00270) can be used for both. This is probably due to the tapering down of the dome along both axes of symmetry as it changes to an oval shape.

As the shoulders of an oval shape bulge, there is a transition toward a rectangular cushion cut (figure 8). The shape factors increase 12% from the average oval cut (0.00210) to the average rectangular cushion cut (0.00235). The increase for cabochons is 7¹/₂% (from 0.00270 to 0.00290). Again, use shape factors somewhere between these numbers for transitional shapes.

Rectangular Cushion to Rectangular Step Cut. Another continuum exists for faceted rectangular gemstone shapes. These range from a rectangular cushion to a rectangular Radiant, through an emerald cut, to a Princess cut (with culet) or a rectangular step cut (with keel; figure 9). Both of these latter cuts have pointed corners. The shape factor increases about 10% from the average rectangular cushion cut (0.00235) to the average rectangular Radiant cut (0.00260). In the shape sequence from the Radiant cut to the emerald, Princess, and step cuts, the

Figure 8. With its bulging shoulders, the rectangular cushion has a larger shape factor than an oval cut, for both faceted stones and cabochons.



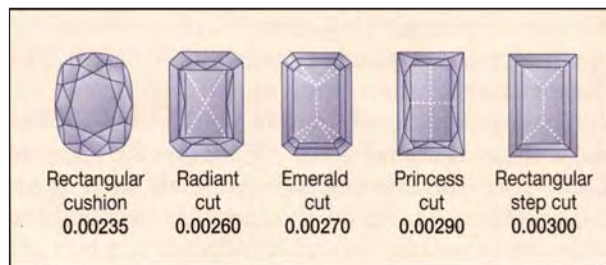
shape factor increases another 15% (from 0.00260 to 0.00300).

Pear to Heart. A pear shape transitions to a heart shape—with its broader shoulders, flatter head, and cleft—in both faceted and cabochon-cut stones (figure 10). Compared to the pear, the shape factors for hearts increase for broader shoulders, or decrease as the cleft deepens.

Profile Examination. Proportion variations seen in the profile view of a gemstone are accommodated by applying a weight correction factor (WCF) to the weight estimation formula. This factor must be selected with utmost care, because profile variations may have a large impact on a stone's weight. Stones that are equidimensional face-up, such as rounds to squares and triangle shapes, will generally show consistent proportion variations in profile, regardless of the viewing direction. Therefore, it is easier to estimate a WCF for these cuts. However, the proportion variations may be greater for oval to rectangular stones, or for pear and marquise shapes. For example, the crown heights and pavilion bulges seen from end views may be different when examined from the side. Also, tables and/or culets in such shapes are commonly off-center, which complicates the weight estimation process. Whereas face-up proportion variations are readily visible from one direction, the profile examination requires a complete rotation of the stone. Therefore, more skill is needed to apply an appropriate WCF to cuts that are not equidimensional face-up.

Brilliant-Cut Stones. The pavilion facets of brilliant-cut stones converge to a point (or culet). Since the weight estimation formulas for brilliant-cut stones were derived from the average weights of

Figure 9. Among rectangular stones, there is a continuous increase in shape factor from a cushion to a rectangular Radiant cut, an emerald cut, a Princess cut, and, ultimately, a step cut.



well-proportioned samples, we use a representative profile of the proportions of an average-cut stone, such as that shown at the far left in figure 11. This profile (viewed from the end) represents a stone with a 30% crown/70% pavilion ratio, a thin to medium girdle, and no culet.

The profiles of the brilliant-cut stones in figure 11 are representative of the profiles for round, square, oval, cushion, pear, marquise, heart, Radiant, and Princess cut stones. Stones with identical length, width, and depth measurements within a given cut style may have significantly different weights, due to variations in girdle thickness, crown height, and pavilion depth, as well as bulges. Using the stone profile at the far left in figure 11 as an example of an average well-cut stone, and assigning it a weight of 1.00 ct, we can see how weights are affected by variations in profile. The other stone profiles in figure 11 represent what a stone with that profile might weigh relative to the profile of the 1.00 ct round brilliant cut. Although the basic measurements are the same, the first of the comparison profiles—with very shallow crown angles—might require a 10% deduction as a WCF. The next profile, with a very steep crown, might require a 10% premium as a WCF; a heavy pavilion could have a 30% WCF; the combination of steep crown angles with a heavy pavilion could have a 40% WCF; a very thick girdle might have a 10% WCF. When a weight correction factor is required, the percentage deduction or premium is then subtracted from or added to the formula at the end of the calculation.

Step-Cut Stones. The pavilion facets of step-cut stones converge to a keel (i.e., an elongated culet). The length of the keel averages about one third the overall length of the stone. Stones with shorter keels will weigh less, and those with longer keels will weigh more (figure 12). Stones that vary in keel length from this average may require a WCF of up to $\pm 10\%$.

Cabochons. The weight of a cabochon is greatly affected by the curvature of its dome. A highly peaked dome with relatively flat sides may require a WCF deduction of as much as 25%, while a dome with a nearly flat top and full shoulders might require a WCF premium of as much as 35% (figure 13).

Examples. For a better understanding of this weight estimation process, the reader is referred to the exercises in Box A.

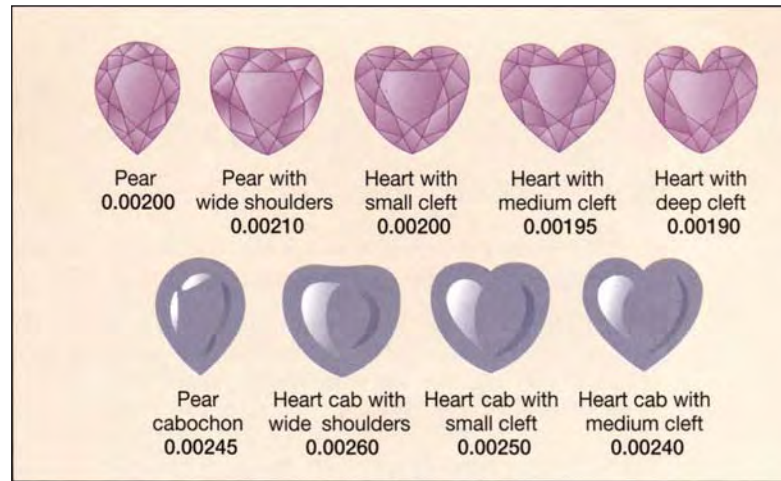


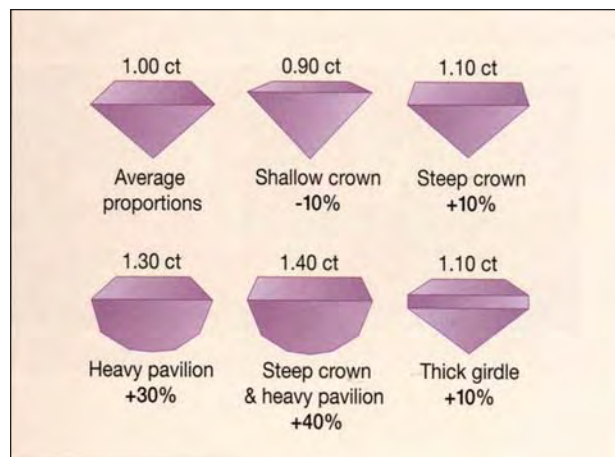
Figure 10. In this sequence of pear- to heart-shaped outlines for faceted stones (top), the shape factors decrease as the clefts become deeper. The same trend is seen in cabochons (bottom).

SUMMARY AND CONCLUSIONS

As the face-up outlines of faceted stones vary from one classic shape to another, the shape factors in their weight-estimation formulas change accordingly. Both precise face-up measurements and profile observations are critical to the accurate estimation of the weight of a mounted colored gemstone.

This task also requires a combination of good references and precise judgments. The formulas and tables developed for this purpose are the basic refer-

Figure 11. Seen in profile view, proportion variations can have a significant impact on a stone's weight, and must be considered carefully in the estimation process. These drawings show how the crown and pavilion proportions, as well as the girdle thickness, can affect the weight correction factors (given as percentages).



BOX A: EXERCISES IN WEIGHT ESTIMATION

The following examples illustrate the weight estimation process for three actual gemstones (figure A-1).

Example 1. This emerald-cut emerald has a slightly asymmetrical face-up outline and a deep pavilion, with an extra bulge on one side. It measures 10.25 × 8.85 × 6.88 mm.

FORMULA FOR EMERALD CUTS:

$$L \times W \times Dp \times S.G. \times 0.00270 = \text{est. wt.} \times \text{WCF} = \text{final estimate}$$

$$(10.25) \times (8.85) \times (6.88) \times (2.72) \times 0.00270 = 4.58 \text{ ct (+10\%)} = 5.04 \text{ ct}$$

Deeper stones tend to have more of a bulge, and this emerald cut is no exception. A WCF of +10% might be appropriate for this stone. Incorporating this factor into the formula results in an estimated weight of 5.04 ct. Although this varies from the actual weight of 4.97 ct by only 1.4%, it is critical to value, as the difference pushes the weight estimate to over 5.00 ct. After more experience, the estimator would apply a WCF between +5% and +10%.

Here is a case where the difference of a percentage point or two in the weight of a gemstone could make a significant difference in its value. It is important at this point to reassess whether the stone can or should be removed from its mounting for actual weighing.

Example 2. This pear-shaped faceted sapphire has a symmetrical face-up outline, a very shallow depth, and a culet closer to the tip (the erratic culet has not created an inordinate bulge in this stone, but such a bulge is

often seen and should be considered, if appropriate). It measures 10.63 × 8.22 × 4.30 mm.

FORMULA FOR PEAR SHAPES:

$$L \times W \times Dp \times S.G. \times 0.00200 = \text{est. wt.} \times \text{WCF} = \text{final estimate}$$

$$10.63 \times 8.22 \times 4.30 \times 4.00 \times 0.00200 = 3.00 \text{ ct (-10\%)} = 2.70 \text{ ct}$$

Because the stone is so shallow, there is not enough pavilion to create a normal bulge. A weight correction factor (WCF) of -10% might be appropriate for this stone. Incorporating this factor into the formula results in an estimated weight of 2.70 ct. This varies from the stone's actual weight of 2.63 ct by 2.7%. After more experience, the estimator would apply a WCF between -10% and -15% to obtain a more accurate weight estimate.

Example 3. This oval cabochon ruby has a symmetrical face-up outline, a medium-height dome, and slightly flattened sides. It measures 10.02 × 7.59 × 5.65 mm.

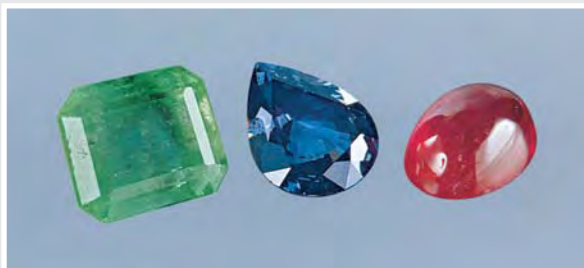
FORMULA FOR OVAL CABOCHONS:

$$L \times W \times Dp \times S.G. \times 0.00270 = \text{est. wt.} \times \text{WCF} = \text{final estimate}$$

$$(10.02) \times (7.59) \times (5.65) \times (4.00) \times 0.00270 = 4.64 \text{ ct (-10\%)} = 4.18 \text{ ct}$$

Because the sides are a little flat, a WCF of -10% might be appropriate for this stone. Incorporating this factor into the formula results in an estimated weight of 4.18 ct, which is 1.9% lower than the stone's actual weight of 4.26 ct. After more experience, the estimator would apply a WCF between -5% and -10%.

Figure A-1. These stones are typical of those that a tradesperson might encounter in jewelry. Left = table up; right = profile view. The weight estimation exercises in this box were developed using these samples. Stones courtesy of Pravin Davé, Los Angeles, (ruby and sapphire) and Ivan Roza, Los Angeles, (emerald). Photos by Maha DeMaggio.



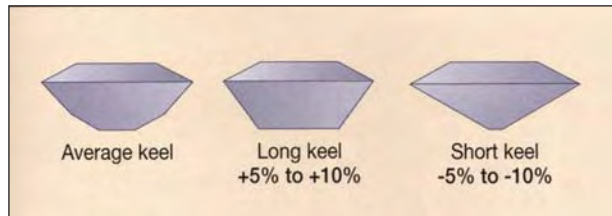


Figure 12. The stone on the left shows an average keel line length. The WCF values vary considerably for short or long keels.

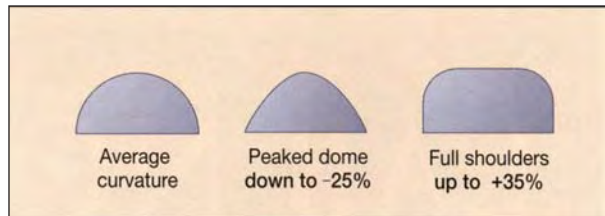


Figure 13. The curvature of a cabochon, as seen in profile, profoundly affects the weight of the stone. As a result, the weight correction formulas may require WCF values that vary from -25% to +35%.

ence tools needed. The formulas described in this article were derived primarily from the average weights of parcels of well-proportioned German-cut calibrated amethysts and citrines. The person responsible for weight estimations must then learn to make the necessary adjustments to the standard formulas. This process requires extensive experience and practice. In fact, the tables and formulas developed by the author were adjusted and refined on the basis of several years of experience with actual colored stones examined in the course of his business.

Most tradespeople who have been estimating weights of colored stones for any length of time are probably using 40-year-old formulas and techniques that carry the disclaimer that “Even for the experienced grader, they are accurate only to within 10 to 15%” (Gemological Institute of America, 1994). With the formulas and estimation procedures developed by the present author, not only is it easier to address contemporary cutting styles, but it is also possible to reduce that potential margin of error to 5% or less.

At all times, however, the person who is using these (or any other) formulas and techniques must

always use qualifying terms such as *approximately*, *estimated*, or *about* in conjunction with the weight estimate. Such disclosure is important, since the value of a piece of jewelry is often greatly affected by the weights of the gemstones it contains.

The updated formulas presented here are meant to set a new standard for weight estimation and to give a fresh look at this important task for many who make their living in the jewelry trade. The weight estimation process may also provide an opportunity for jewelers to improve the accuracy of their gemological skills, while enhancing the profitability of their businesses.

Acknowledgments: The author thanks Renata and Gonen Abrahami of ABC Gem Company, Los Angeles, for making available their vast inventory of calibrated colored gemstones for use in developing the weight estimation formulas. Margot A. McLaren, of GIA's Richard T. Liddicoat Gemological Library and Information Center, is thanked for her help in researching the history of weight estimation formulas for colored stones.

REFERENCES

- Altobelli C. (1986) *Handbook of Jewelry and Gemstone Appraising*, American Gem Society, Los Angeles, CA, pp. 45–46.
- Carmona C. (1998 [projected publication date]) *The Complete Handbook for Gemstone Weight Estimation*, Gemania, Los Angeles, CA.
- Drucker R. (1997) *The GUIDE Reference Manual—Reference Data*, Gemworld International, Chicago, pp. 16–18.
- Ellison J. (1957) Formulas for the weight estimation of colored faceted stones. *Gems & Gemology*, Vol. 9, No. 2, pp. 43–45.
- Gemological Institute of America (circa 1977) *Resident Appraisal Notebook*, GIA, Los Angeles, CA, p. 10.
- Gemological Institute of America (1994) *Colored Stone Grading, Assignment 18*. GIA, Santa Monica, CA, p. 14.
- Jeffries D. (1750) *A Treatise on Diamonds and Pearls*. C. and J. Ackers, London.
- Leveridge A. (1937) *The A. D. Leveridge Weight Estimator*. A. D. Leveridge, Pompton Plains, New Jersey, p. 33.
- Miller A. (1988) *Gems and Jewelry Appraising*. Van Nostrand Reinhold, New York, p. 176.
- Small J. (1952) Weight estimation of cabochons. *Gems & Gemology*, Vol. 7, No. 6, pp. 191–194.

Editors

Thomas Moses ♦ Ilene Reinitz

Shane F. McClure

GIA Gem Trade Laboratory

Contributing Editors

GIA Gem Trade Laboratory, East Coast

G. Robert Crowningshield

GIA Gem Trade Laboratory, West Coast

Karin Hurwit ♦ Mary L. Johnson

Cheryl Y. Wentzell

BERYL, Plastic-Coated Assemblage Imitating Trapiche Emerald

We regularly see various assemblages that imitate emerald (e.g., Winter 1986 Lab Notes, pp. 236–238, and Spring 1990 Gem News, p. 100), and occasionally we see beryl coated with plastic to produce an emerald imitation (see Fall 1995 Lab Notes, p. 199). However, the item shown in figure 1, submitted to the West Coast laboratory for identification, is the first we have examined where both of these methods were used together to imitate a trapiche emerald. The green-and-black oval cabochon measured approximately 14 × 12 × 7 mm and weighed 7.99 ct. When viewed face-up, the item was very believable; but on the back, the sections were misaligned, which proves it is an assemblage (figure 2).

Magnification revealed a green plastic coating over six sections of

near-colorless material and a hexagonal center plug. The various pieces were attached with black glue in some places and colorless glue in others. The shape and curvature of the pieces suggested that an oval cabochon had been drilled through its apex, and then sawn in six sections to form the basis for this assemblage. Gas bubbles were visible in the center of the stone (under the plug) and in the glue planes. We obtained a uniaxial figure from most of the near-colorless sections, but the coating prevented us from getting an accurate refractive index. The piece weakly fluoresced greenish yellow to long-wave ultraviolet radiation and orangy yellow to short-wave UV. Using a desk-model spectroscope, we saw two lines in the red portion of the spectrum, at about 630 and 680 nm, which are not appreciably different from the chromium

lines seen in emerald. The specific gravity was measured by the hydrostatic method at 2.62. This value is somewhat lower than the S.G. of emerald or beryl (usually around 2.72), but it is clearly influenced by the glue that is holding the piece together.

Because we could not get an R.I. and the S.G. was unreliable, we turned to the laser Raman microspectrometer for conclusive identification of the near-colorless sections beneath the coating. The Raman spectra showed these sections to be beryl.

SFM

CHRYSOBERYL, Dark Green

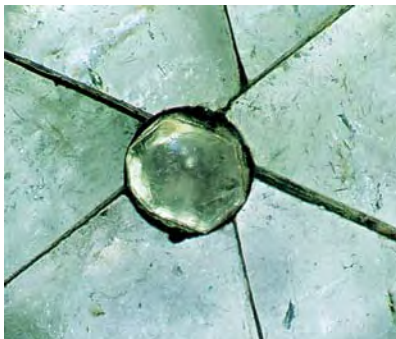
The Tunduru region of Tanzania continues to produce numerous gem minerals in unusual and highly attractive colors (see, e.g., Gem News, Winter 1997, p. 305, and Spring 1997, p. 66). Figure 3 shows yet another example, a 3.65 ct dark green heart-shaped mixed cut, reported to be from Tunduru, that was submitted for identification to the West Coast laboratory.

The refractive indices of 1.741–1.749 and biaxial character indicated chrysoberyl. No inclusions were observed with magnification, but the gemstone did show straight growth bands, which proved that it was natural. With a desk-model spectroscope,

Figure 1. This 7.99 ct cabochon looks like a trapiche emerald, but it is actually a plastic-coated assemblage.



Figure 2. On the back of the cabochon shown in figure 1, the sections were distinctly misaligned, which would not occur in a natural trapiche emerald. Magnified 12×.



Editor's note: The initials at the end of each item identify the editor(s) or contributing editor(s) who provided that item.

Gems & Gemology, Vol. 34, No. 3, pp. 212–217
©1998 Gemological Institute of America



Figure 3. This 3.65 ct dark green chrysoberyl is colored by vanadium. It reportedly came from Tunduru, Tanzania.

we saw a band at 600 nm, which is consistent with the spectrum of light green “mint” chrysoberyl, as reported in the Fall 1996 Gem News section (pp. 215–216). The piece showed no reaction to either long- or short-wave UV radiation.

The 1996 report described both light green and dark green material that was colored by vanadium rather than chromium. Those samples also contained small quantities of Cr, as well as iron, gallium, and tin. We submitted this heart-shaped mixed cut to energy-dispersive X-ray fluorescence (EDXRF) analysis, and found only a few differences in chemistry from the material seen earlier: Traces of V, Fe, and Ga were present, but there was no tin nor any evidence of Cr.

We have seen rare examples of such a saturated green color in vanadium chrysoberyl before, including some material reported to be from Myanmar. This color is also in the same range as synthetic vanadium chrysoberyl grown by the floating-zone method in Russia. Although the natural and synthetic material can show similar fluorescence reactions and spectra, the synthetic chrysoberyl invariably has distinctive inclusions, such as gas bubbles and curved striae.

SFM

DIAMOND

Color Treated from Orangy Yellow to Reddish Purple

Although the East Coast lab receives

many treated-color diamonds for identification, we rarely have the opportunity to examine a diamond and document its properties both before and after treatment. About a year ago, a friend of the laboratory submitted a group of small diamonds for our examination prior to irradiation and heat treatment. We singled out a 0.09 ct orangy yellow round brilliant for thorough documentation. Viewed over diffused light (or immersed in methylene iodide) this diamond showed uneven coloration, with a yellow bodycolor and sparse pale brown graining.

This diamond showed no reaction to long-wave ultraviolet radiation, but it fluoresced greenish yellow with moderate intensity to short-wave UV. With the desk-model spectroscope, we saw increasing absorption from about 500 nm toward the blue. These properties suggested some type Ib component, which infrared spectroscopy confirmed, showing a combination of type Ib and IaA absorption peaks (for an explanation of diamond types, see E. Fritsch and K. Scarratt, “Natural-Color Non-conductive Gray-to-Blue Diamonds,” *Gems & Gemology*, Spring 1992, pp. 35–42). Only a diamond that contains some type Ib component can be treated to produce pink, red, or purple; irradiation and heat treatment of type Ia diamonds produces orange, brown, yellow, or

greenish yellow (see A. Collins et al., “Absorption and Luminescence Spectroscopy,” in J. E. Field, Ed., *Properties of Natural and Synthetic Diamond*, Academic Press, London, 1992, pp. 35–80).

The key to the development of pink to purple colors with treatment is the single substitutional nitrogen that defines type Ib diamond. Vacancies created during irradiation (that is, the holes left in the structure when ionizing radiation displaces a carbon atom) migrate through the diamond during heat treatment and join with the single substitutional nitrogen to create the NV center. The absorptions related to this center—at 637 and 575 nm—combine with the rising absorption in the blue to yield pink, red, and/or purple (K. Scarratt, “Notes from the Laboratory,” *Journal of Gemmology*, Vol. 20, No. 6, 1987, pp. 358–361).

After irradiation with low-energy electrons and subsequent heat treatment, the color of this 0.09 ct orangy yellow diamond changed to a reddish purple (figure 4). It fluoresced a strong bright orange to both long- and short-wave UV radiation (somewhat stronger to short-wave UV), and the hand spectroscope showed strong lines at 637 and 575 nm, with a companion line at 595 nm and both yellow

Figure 4. The strong reddish purple color in this 0.09 ct diamond resulted from irradiation and heat treatment of an orangy yellow diamond known to have some type Ib component.

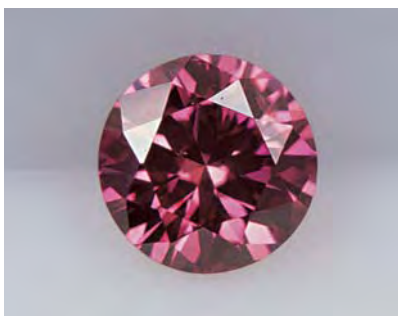


Figure 5. Irradiation with an electron beam created the concentrated purple zone seen at the culet. The combination of this purple zone and the light yellow bodycolor gives rise to the overall “peach” color seen here. Magnified 25x.



low and orange emission lines at 596 and 638 nm, respectively. The brown graining seen before treatment reflected the treated purple color of the culet, and a quick examination might confuse this reflection with the pink to purple graining seen in naturally colored diamonds in this hue range. However, as shown in figure 5, the culet showed a strong concentration of purple, a feature diagnostic of treatment (see, e.g., E. Fritsch and J. Shigley, "Contribution to the Identification of Treated Color Diamonds: Diamonds with Peculiar Color-Zoned Pavilions," *Gems & Gemology*, Summer 1989, pp. 95–101). *IR and TM*

Raman Analysis of Inclusions

Two diamonds recently submitted to the West Coast laboratory for quality analysis contained colorful mineral inclusions, which are relatively unusual in gem-quality diamonds. These gems presented an excellent opportunity to investigate how well such inclusions can be identified by the nondestructive analysis possible with our laser Raman spectrometer. Although sample preparation is not really necessary for Raman analysis, when examining inclusions

we have found that the flatter and better polished the surface of the host is, the less "noisy" the resulting spectrum will be. In addition, the best-quality spectrum is obtained when the surface of the polished diamond is well cleaned of grease and other debris prior to analysis. A plastic film container partially filled with methanol works very well as a means of degreasing a gem for this purpose; it can be agitated in the canister and then air dried.

After cleaning, the next step is to determine the best direction to approach the inclusion from the host's surface. The best results are obtained with an approach perpendicular to the surface and the inclusion less than 1 mm beneath it. Such a geometry, however, is rarely encountered. One must find some compromise between the angle the laser beam makes with the faceted surface and the depth to the inclusion, keeping in mind that the system has decreasing ability to focus on an inclusion with increasing depth in the host crystal. The depth of focus depends on many variables, including the mineral species of both the host and the inclusion.

The first of the two diamonds that we examined using our Raman system was a 2.56 ct oval brilliant cut that contained a cluster of sharp-edged, translucent, dull green crystals

(see figure 6); because of their color, we speculated that they were diopside. Regardless of the angle of approach, however, we could not reach any of these larger inclusions with the Raman system. A much smaller crystal inclusion, which appeared to be very light green (almost colorless), was visible above the main cluster of green crystals and just below the surface of the table (again, see figure 6). When we analyzed this inclusion, we found it to be olivine. While larger inclusions of olivine in diamond may appear pale green, more often they are essentially colorless. Given its small size and proximity to the larger green crystals, we speculate that this smaller crystal might be getting its tinge of green by reflection from the larger crystals, which in all probability are diopside.

The second diamond subjected to Raman analysis was a 1.48 ct round brilliant cut. It contained a purplish red tabular crystal with rounded edges (figure 7) that was visible through both the pavilion and the crown. After we cleaned the stone and selected a direction of approach on the pavilion side, this crystal inclusion proved to be relatively easy to analyze using the Raman system. As expected from its color and habit (considering that it is included in diamond), the result was a match for pyrope garnet.

Close examination of this pyrope inclusion showed that it, too, contained an inclusion. This additional inclusion was a tiny, dark, red-brown transparent crystal (again, see figure 7) that, because of its color, we suspected to be either chromite or rutile. An examination with polarized light microscopy did not show any sign of optical activity (i.e., there was no doubly refractive reaction), so chromite became the prime suspect.

The extremely small size of this "chromite" presented an additional challenge for Raman analysis. Although we could bring it into focus in the targeting microscope, we could not hold the inclusion in the crosshairs long enough to complete the analysis. We currently use a

Figure 6. Although this cluster of green crystals was too deep inside the diamond host to be identified by Raman analysis, we believe that the crystals are probably diopside. The smaller elongate crystal to the upper right of the cluster was closer to the surface, and proved to be olivine. Magnified 10×.

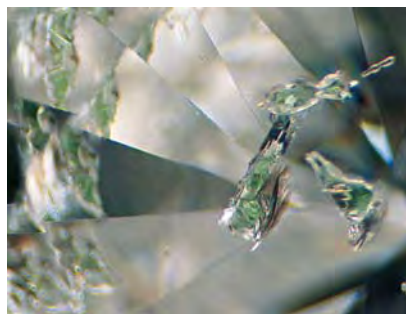
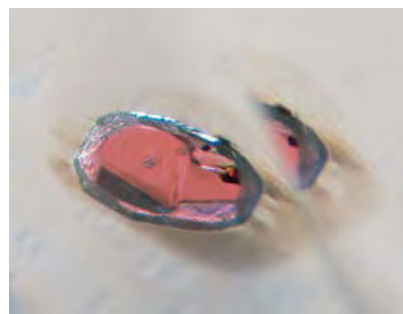


Figure 7. Raman analysis showed that this purplish red crystal in diamond is pyrope, but the red-brown crystal included in the pyrope was too elusive to be analyzed. Magnified 30×.



putty-like substance to hold and position samples for analysis, and this material softens and distorts in shape, causing the sample to move noticeably at high magnifications (e.g., at 500×). The result is what we now call “target drift,” as the analyst can actually watch the subject move away from the crosshairs and out of focus, beginning as soon as the sample is mounted in the microscope and lasting for as long as we have had patience to watch it (about five minutes). Some type of a rigid sample holder, such as a customized stoneholder, will have to be devised and adapted to fit on the moving stage of the targeting microscope in order to handle the smallest samples.

John I. Koivula

Bicolored GLASS

Glass has a long, rich history in jewelry that dates from ancient times. While most glass “gems” that we encounter in the laboratory are not worth mentioning in this section, occasionally we see some that are quite unusual. Such was the case with the 4.28 ct, bicolored (blue and colorless), rectangular scissors cut shown in figure 8.

While glass composed of two or more colors mixed together is relatively common in decorative objects, this particular piece was designed so that the crown portion was colorless and the pavilion was dark blue. This arrangement produced a “stone” that appeared to be a uniform blue when viewed table-up. The crown and pavilion also had radically different refractive indices—1.535 and 1.642, respectively. The specific gravity, determined hydrostatically, was 2.93. Since there are no singly refractive gemstones at either of these refractive indices, and the specific gravity is too high for plastic, glass is the only possible identification. The sample revealed no visible-light absorption spectrum when viewed through a Beck prism spectroscope. There was no reaction to long-wave UV radiation, but the short-wave lamp pro-



Figure 8. Blue and colorless layers are readily apparent in this 4.28 ct faceted piece of manufactured glass when it is viewed along the girdle plane. In this view, the blue color in the pavilion is reflected into a large portion of the crown.



Figure 9. A small droplet of glass encapsulates a fingerprint-like formation of gas bubbles that is sandwiched between the blue and colorless layers in the piece of faceted glass shown in figure 8. Magnified 15×.

duced a very weak chalky yellow reaction over the entire surface.

The most interesting features of this faceted glass were two partially healed fractures—resembling “fingerprint” inclusions—visible in two areas that were spread out along the contact plane between the colorless and blue layers. These “fingerprints” were actually composed of a plane of microscopic gas bubbles arranged in semi-parallel rows; in each case, the whole “fingerprint” was encapsulated in a single glass droplet (figure 9) that had been spattered onto the surface of one of the glass layers prior to its contact with the second layer. We do not know whether these “fingerprints” were intentionally or accidentally formed along the interface between the colored layers in this piece of glass.

John I. Koivula

SYNTHETIC MOISSANITE, Submitted for Diamond Grading

When a practicing gemologist learns about a new synthetic or treatment—through the gemological literature, seminars, or the trade press—this knowledge typically heightens the gemologist’s awareness to the appearance of such a material in his or her daily work. With all of the publicity about synthetic moissanite over the

last 18 months, we were surprised that it took until the summer of this year for the first sample to be submitted to either laboratory.

A client sent several gems to the East Coast laboratory for diamond grading services, but one of them turned out to be something other than diamond. The bodycolor of the 0.90 ct round brilliant was pale gray-green, and there were relatively few inclusions, primarily several long, fine needles. When the round brilliant was tilted and viewed perpendicular to the bezel facets, strong doubling was visible (with the two images of each rear facet junction appearing about twice as far apart as they would in a colorless zircon), which proves a doubly refractive material. However, we could not see doubling of the pavilion facet junctions through the table, which suggests that the round brilliant was oriented with the optic axis perpendicular to the table. Generally, the finish was good and did not show any noticeably rounded facet junctions, but the polish lines smoothly crossed facet junctions without changing direction, which is not possible in diamond. Furthermore, the striated finish of the girdle (figure 10) is unlike anything seen in diamond.

The specific gravity, measured both hydrostatically and with the DiaMension noncontact measuring

system, was 3.22. In combination with the doubling, inclusions, and color, this identified the material as synthetic moissanite. The sample fluoresced a very weak orange to long-wave UV radiation and was inert to short-wave UV. The strong dispersion was also observed as orange and blue flashes that were visible with the microscope when the synthetic moissanite was viewed culet up. A cutoff at 420 nm was seen with a desk-model spectroscope. As expected for synthetic moissanite, the sample showed a high level of thermal conductivity, yielding a reading of "diamond" on the thermal probe. All these properties are consistent with the samples described by K. Nassau et al. in "Synthetic Moissanite: A New Diamond Substitute" (*Gems & Gemology*, Winter 1997, pp. 260–275).

Coincidentally, as we were preparing this note, another round brilliant (1.31 ct) was submitted to the East Coast lab for diamond grading; the properties of this "stone" were very similar to those of the first example. The West Coast lab reported seeing a third synthetic moissanite round brilliant, of 1.25 ct, within a few days of the other two. Note that all three samples were somewhat larger than the synthetic moissanites examined for the *Gems & Gemology* article.

GRC and TM

Figure 10. The subtle striations on the girdle of this 0.90 ct round brilliant are typical of faceted synthetic moissanite, but this texture is unlike the faceted, polished, or bruted finish found on the girdle of a diamond. Magnified 50×.



PEARLS, Freshwater Cultured

In the late 1950s, our laboratories began to encounter the first freshwater tissue-nucleated cultured pearls. One of the editors recalls that these early white and pastel-colored cultured pearls, then exclusively from Lake Biwa in Japan, were sometimes referred to in the trade as natural pearls. The FTC guidelines at that time defined a cultured pearl as "the composite product created when a nucleus (usually a sphere of calcareous mollusk shell) planted by man inside the shell or in the mantle of a mollusk is coated with nacre by the mollusk." This led to some confusion as to how these tissue-nucleated pearls should be described. (Lack of the word *cultured* on export papers for those pearls added to the confusion.) Through the 1960s, the trade and the testing laboratories recognized this product as resulting from the combined efforts of human and mollusk, and for the most part they were represented properly as cultured pearls.

The early production attained a maximum length of about 7.5 mm for the ovals, and diameters of about 6 mm for the rounds (G. R. Crowningshield, "Fresh-Water Cultured Pearls," *Gems & Gemology*, Vol. 10, No. 9, 1962, pp. 259–274). The size range of these cultured pearls varied little for three decades. During the last five years, however, we have reported on somewhat larger sizes and shapes that are rounder (Summer 1994 Lab Notes, p. 118). China now dominates the production of these tissue-nucleated cultured pearls, especially in the larger sizes. G. Bosshart and others have described freshwater pearl culturing in Vietnam ("Freshwater Pearl Cultivation in Vietnam," *Journal of Gemmology*, Vol. 23, No. 6, 1993, pp. 326–332), where the sizes remain smaller.

The necklaces shown in figure 11 were examined recently in the East Coast lab; they represent a dramatic increase in the size of Chinese freshwater tissue-nucleated cultured pearls (D. Federman, Gem Profile, *Modern*

Jeweler, June 1998, pp. 59–60). The lengths of these primarily oval cultured pearls reach up to 15 mm, and their widths reach up to 13 mm. The colors include both white and pastel shades, similar to those we first encountered in the 1950s. In these sizes, this product now provides an interesting and attractive alternative to South Seas cultured pearls.

GRC and TM

QUARTZ: A Large "Crystal Ball"

Rock crystal quartz should be an easy material to separate from other gems; however, synthetic quartz looks very much like the natural material. Recently, the West Coast laboratory received a large sphere, 9.6 cm in diameter (about 3 3/4 inches), for identification. That it was quartz was evident: The sphere had a (spot) refractive index of 1.54 and a very good "bull's-eye" optic figure. In addition, printing viewed through the sphere appeared doubled. It was inert to both long- and short-wave UV radiation. Because synthetic quartz is manufactured hydrothermally, we suspected that it was not available in the size that would have been needed to cut this very clean sphere (without a seed plate being present), but we could not call the piece natural without more conclusive evidence. As is so often the case in such situations, we had to rely on distinctive inclusions.

However, even finding inclusions was a significant challenge in such a large object with a curved surface. The sphere was eye-clean and too large to focus through with the microscope. We tried using diffuse illumination to locate any dark or opaque inclusions, and we used red-filtered fiber-optic illumination in the hope that any inclusions would appear as red sparkles within the stone. The technique that finally prevailed was to set the sphere against the well of the microscope's darkfield illuminator, and then to look from the side for any sign of light bouncing off any features within the sphere. (The round opening of the darkfield illuminator

served as an ideal base for the sphere, making it convenient to rotate the quartz ball to any desired position.) Using this method in conjunction with a 10× loupe, we spotted some very tiny features. By disengaging the rack and pinion on the microscope and elevating the pod by hand, we were able to resolve these tiny features at 63× into several small needles (some showing curvature) and some small dark crystal rods with modified triangular cross-sections (possibly tourmaline), deep within the stone. Since inclusions of these morphologies have only been encountered in natural quartz, this gave us the proof we needed to identify the sphere as natural rock crystal quartz.

*MLJ, SFM, Dino DeGhionno,
John I. Koivula, and Philip Owens*

RUBY, With a True Double Star

Tom Schneider, a colored-stone dealer in San Diego, California, recently shared the unusual phenomenal gem shown in figure 12 with the West Coast lab. The 8.19 ct red cabochon showed a true double star: two six-rayed stars slightly offset from each other (rather than a 12-rayed star).

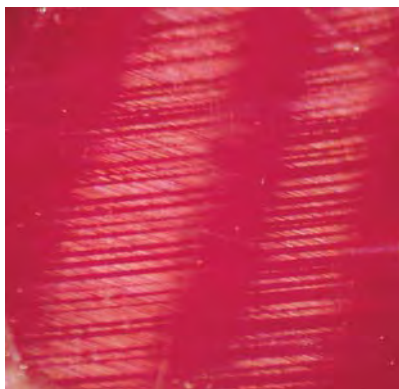
Figure 12. The true double star in this 8.19 ct ruby is caused by differences in the orientation of rutile “silk” across pervasive twin planes.



Figure 11. These lustrous white and fancy-color freshwater tissue-nucleated cultured pearls range up to 15 mm long. Thus, they provide an alternative to some South Seas cultured pearls.

The refractive index of 1.76 and the characteristic absorption spectrum proved that the gem was ruby. The pervasive inclusions of rutile needles (typically referred to as “silk”) indicated a natural stone. However, the double star seemed illogical: The

Figure 13. The closely spaced twin planes throughout the ruby in figure 12 produced two sets of slightly offset silk-like rutile inclusions, aligned in every other plane. Magnified 34×.



normal configuration of silk in a ruby should produce a single star from one viewing direction with one light source.

Further observation with magnification revealed the cause of the double star. The ruby was twinned throughout, with closely spaced lamellar twinning planes. The silk was slightly offset across each of these planes, as shown in figure 13, because of the difference in the orientation of the twins; thus, the twinning produced silk that was aligned in every other plane. This offset led to the appearance of two stars slightly separated from each other. In addition, when the rays were viewed with magnification, they had small gaps (like a dotted line); they looked continuous to the naked eye because the spacing between these many twin sets of planes was so small. *SFM*

PHOTO CREDITS

*Maha DeMaggio took photos 1, 4, 5, and 11.
Shane McClure provided figures 2, 3, 12, and 13.
John Koivula photographed figures 6–9. Nicholas DelRe was the photographer for figure 10.*

Editors • Mary L. Johnson and John I. Koivula

Contributing Editors

Dino DeGhionno and Shane F. McClure,
GIA GTL, Carlsbad, California

Emmanuel Fritsch, IMN, University of Nantes, France

Henry A. Hänni, SSEF, Basel, Switzerland

Karl Schmetzer, Petershausen, Germany

DIAMONDS

Diamonds at the International Mineralogical Association meeting. Every four years, the IMA brings together scientists from around the world to present new data in mineralogy, petrology, and geochemistry. About 700 scientists attended the 17th General Meeting, which was held in Toronto, Ontario, Canada, August 9–14, 1998. The meeting featured several presentations on diamonds, most of which were conducted at a symposium on gems and diamonds in honor of the late Dr. Henry Meyer.

Techniques for identifying and characterizing gem diamonds were reviewed by E. Fritsch (University of Nantes, France) and J. Shigley (GIA Research). Dr. Fritsch

Figure 1. This 8.2 ct diamond, from the Eldorado Lead, Beechworth district, Victoria, Australia, may have been formed by subduction. The 12 mm stone was found in 1977. Photo by Francesco Coffa; courtesy of W. D. Birch, Museum of Victoria.



showed how advances in UV-visible-infrared spectroscopy have helped characterize absorptions related to color centers, which can be used to separate synthetic and treated-colored diamonds from natural, untreated diamonds. Cathodoluminescence (CL) patterns and CL emission spectra can also be used to identify natural versus synthetic diamonds. Dr. Shigley reviewed the challenges of identifying diamond treatments and simulants—including synthetic moissanite—as well as synthetic diamonds, but he stressed that both of these synthetics are currently rare in the gem marketplace.

Another technique for characterizing gem diamonds is X-ray topography. I. Sunagawa (Yamanashi Institute of Gemmology and Jewellery Arts, Japan) used this technique to reveal the growth history of diamond crystals by imaging their structural inhomogeneities and textures. X-ray topography is particularly effective for distinguishing single crystals from polycrystalline morphologies. Dr. Fritsch (in another presentation) reviewed diamond morphology in great detail (see Winter 1997 Gem News, pp. 300–301, for a description of this work), and further noted that synthetic diamond crystals have distinct morphologies that show cube faces.

Several scientists gave presentations on the genesis of diamond. S. E. Haggerty (University of Massachusetts) provided an update on the use of carbon isotopes to study the formation of diamond in diverse environments: microdiamonds in meteorites (presolar and impact origins) and deep crustal rocks (continental collision zones), and macrodiamonds in the Earth's mantle (the only source of gem diamonds). P. J. Wyllie (California Institute of Technology) indicated that the composition of fluid inclusions in diamonds from Botswana is consistent with their formation in upper-mantle peridotite. J. W. Harris (University of Glasgow) and colleagues studied inclusions within alluvial diamonds from São Luiz, Mato Grosso, Brazil, and concluded that these diamonds may have formed at depths exceeding 450 km. This depth corresponds to the transition zone between the upper

and lower mantle, and is almost three times deeper than areas where most gem-quality diamonds are thought to form.

In studies of gem diamonds from Australia, W. D. Birch (Museum of Victoria, Australia) pointed out that the sporadic association of gem-quality diamonds (figure 1) with gem corundum and zircon in Victoria is consistent with a subduction model that has been proposed for the origin of these diamonds. F. L. Sutherland (Australian Museum, Sydney) and colleagues indicated that the source of Copeton diamonds in New South Wales is still an enigma; these diamonds contain such unusual inclusions as coesite and scapolite.

There were many presentations on gem diamonds from Russia. T. V. Possoukhova (Moscow State University) and colleagues examined diamonds from several deposits in the Arkhangelsk region. Morphologic and spectroscopic studies have shown that diamonds from kimberlites in the northern east-European and Siberian platforms are typically rounded rhombododecahedra that are type Ia. The morphology of these diamonds was attributed to resorption during the transportation of diamonds in kimberlite magma. At the Pionerskaya pipe in Yakutia, macrodiamonds from the upper horizons show morphologies that are typical of kimberlitic diamonds, whereas at depth microdiamonds with an unusual skeletal morphology were recovered, resembling diamonds found in metamorphic rocks. At the M. V. Lomonosova deposit, diamonds apparently formed in several stages under oxidizing conditions, as indicated by their morphology, nitrogen aggregation state, isotopic composition, and fluid inclusions. A. B. Makeyev and colleagues (Russian Academy of Sciences, Ukhta) reported that diamonds are found with placer gold at the Ichetju alluvial deposit (Middle Timan platform); a high proportion of the diamonds are gem quality, and many colors have been found (e.g., yellow, green, and brown). A. A. Rogozhin and colleagues (VIMS, Moscow) described the concentration of fluorescent minerals (calcite, apatite, and zircon) around the kimberlite pipes in the Arkhangelsk region, and proposed that such haloes might be useful in prospecting for kimberlite pipes.

In other presentations, J. E. Butler (Naval Research Laboratory, Washington, D.C.) noted that drusy plates of synthetic diamonds grown by chemical vapor deposition (CVD) may reach 300 mm in diameter and 1 mm thick; he showed some interesting jewelry that incorporated CVD druses. Finally, G. Harlow (American Museum of Natural History, New York) pointed out that diamonds are quite seductive learning aids: Visitors stayed at "The Nature of Diamonds" exhibit three times longer (i.e., one hour) than is typical for the museum's other exhibits.

Update on the Ekati project, Northwest Territories, Canada. According to BHP Ltd. press releases, diamonds have been found in two additional small pipes in the Ekati project area at Lac de Gras. The 0.6 hectare Koala



Figure 2. The historic Four Peaks mine in Arizona is again producing amethyst. These brilliant cuts, shown next to a rough crystal, weigh approximately 6 and 4 ct. Photo © Jeff Scovil; courtesy of Commercial Mineral Co.

North pipe (which is under the same lake as the already-studied Koala pipe) yielded 126.5 carats from 201.7 tons of ore, for a grade of 0.63 ct/ton; the 1 hectare Beartooth pipe, 900 m north of the Panda pipe (the first pipe to be mined—others include Misery, Koala, Fox, and Sable), yielded 227 carats from 189.3 tons of ore (grade of 1.20 ct/ton). The stones were evaluated in Antwerp in May; the Beartooth sample was valued conservatively at US\$79/ct, and the Koala North sample was valued at \$200/ct. Much of the value of the Koala North sample came from three gem-quality stones, which weighed 3.26 to 5.41 ct.

Construction at the Ekati diamond mine is nearly complete, and the first production is expected in October 1998 from the Panda open pit. Evaluation of other pipes in the area is proceeding. In late May, the joint-venture partners (BHP Diamonds Inc., Dia Met Minerals Ltd., and individuals Charles E. Fipke and Stewart Blusson) agreed that BHP Diamonds Inc. would be the sales representative for the Ekati venture.

COLORED STONES

Amethyst from Arizona. Faceted amethyst is again being produced at the historic Four Peaks mine in Maricopa County, near Phoenix. The deposit was originally discovered at the turn of the century, and is located in the rugged Mazatzal Mountain Range at an altitude of 2,200 m (7,200 feet). After more than 20 years of inactivity, the mine has been purchased and reopened by a joint venture between Commercial Mineral Co. (the sole distributor of the material) and Four Peaks Mining Co. (mining operations management). According to Mike Romanella of Commercial Mineral Co., Scottsdale, Arizona, about 2,000 carats of calibrated goods in many shapes are available in sizes from 0.5 to 2 ct; very limited quantities of 2–6 ct stones are also being sold (figure 2). The small size of faceted stones is due to the nature of the rough, which is color zoned and included. Because the partners are cutting only "high-quality" stones, the yield of faceted

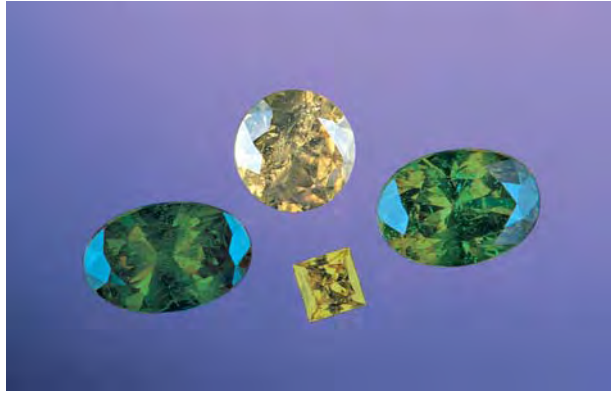


Figure 3. These four fashioned andradite garnets (0.27–2.36 ct) come from northwestern Yemen. Photo by Maha DeMaggio.

goods from cobbled material is about 1%. Mr. Romanella expects that larger sizes will be cut from the latest 1,000-pound (455 kg) shipment of rough. There are plans to increase production through more mechanized mining, and a line of custom jewelry is currently being designed for marketing by Commercial Mineral Co.

Andradite garnet from Yemen. Until recently, agate was the only well-known gem material to come from the small republic of Yemen, on the southwest Arabian subcontinent. However, Ali Jabr Alawi, of Yemen Genius in Brooklyn, New York, recently showed GIA Gem Trade Laboratory vice president Tom Moses four yellowish green to brown faceted stones (figure 3) from the northwestern part of Yemen.

Gemological properties on the four stones were as follows: color—greenish yellow-brown, yellowish green, yellow-green, and greenish yellow; refractive index—greater than 1.81 (the limit of our standard refractometer); optic character—singly refractive, but strained; fluorescence—inert to both long- and short-wave ultraviolet radiation; spectroscopy spectrum—strong absorption band between 437 and 448 nm (viewed with a handheld spectroscope). With magnification, all four stones exhibited high dispersion, growth zoning, partially healed fractures (“fingerprints”), and fluid inclusions. One stone contained tiny needle-like inclusions, and another revealed small clusters of transparent crystals. These properties are those expected for andradite garnet, and the Raman spectra of all four stones also matched that of andradite. Two partial chemical analyses, provided by Mr. Alawi, were also consistent with andradite garnet.

Danburite from San Diego County, California: A potential gem mineral. Dr. John Sinkankas, of San Diego, California, writes that danburite is one of the more recent discoveries at the Little Three mine area near Ramona, California. This mine is famous for its fine gem spessartine garnet; topaz, tourmaline, beryl, and the rare

gem hambergite are also found there. The mineralized area at the Little Three deposit consists of a swarm of dike-like pegmatite-aplite bodies; some are located on private property, and others are covered by mining claims. The danburite was recovered from small pockets in an eastern extension of the main Little Three dike, along with schorl tourmaline, smoky quartz, almandine-spessartine garnet, and potassium feldspar crystals. The largest danburite crystal, “pale straw yellow” in color and measuring $4.1 \times 3.7 \times 3$ cm (figure 4), is now in the collection of the Los Angeles County Museum of Natural History. The crystal is striated parallel to the c-axis and shows small pyramidal faces as well. Although this crystal contains numerous internal fractures, and shows only very small clear areas from which faceted gems of much less than a carat could be cut, some smaller crystals (up to 5 mm long) are entirely transparent.

Application of large-scale mining techniques to Colombian emeralds. During the first World Emerald Congress held last February in Bogotá, Colombia, a session on the geology and mining of emeralds was held concurrently with the session on emerald treatments described in the Spring 1998 Gem News section (pp. 56–57). William Rohtert, manager of gemstones for AZCO Mining Inc., Vancouver, British Columbia, spoke on the application of exploration and production technologies that are now routine in the diamond industry to the mining of other gem minerals. He was kind enough to provide a copy of his notes to the Gem News editors.

Figure 4. Danburite has been recovered for the first time in San Diego County, California, in an extension of the Little Three mine dike. This crystal measures $4.1 \times 3.7 \times 3$ cm. Photo by Anthony R. Kampf; courtesy of the Los Angeles County Museum of Natural History (catalog no. 44050).



In the future, Colombian emerald deposits could be exploited systematically using an integrated approach that combines: (1) remote sensing to locate mineral districts; (2) detailed investigations of the geology, geochemistry, and geophysics of the mine sites; (3) measurement of mineable reserves, with data derived from core drilling; (4) mechanized mining; and (5) automated extraction of the emeralds from their host rocks. This approach, unfortunately, can be expensive: A “pioneer” evaluation of the red beryl deposit in the United States cost Kennecott Exploration Company about \$20 million, or \$4.00 per (polished) carat of the proven reserves. (Mr. Rohrt notes, however, that about half these costs were related to research, administration, and marketing.)

Although satellite-based remote sensing works best in arid terrains, a promising technique for mapping emerald districts in vegetation-rich Colombia is side-scan radar. In addition, the broad haloes of pyrite that surround *cenicero* (the ash-colored altered black shale in Colombian emerald deposits) might be detected using airborne electromagnetic surveys.

Delineation of an emerald deposit on the ground still relies on field geology to map structural and stratigraphic controls on the mineralization. Also, soils overlying productive veins show elevated ratios of sodium relative to potassium; dispersion haloes containing parisite, apatite, and fluorite with elevated contents of rare-earth elements are known to be indicative of mineralization. A type of surface geophysical technique (controlled source audio-frequency magneto-tellurics, or CSAMT) would probably detect the carbonaceous alteration haloes surrounding emerald veins to depths of 610 m (2,000 feet), as well as the diffuse pyrite concentrations that typically surround the ore.

Even the tiniest emeralds recovered from drill cores and bulk samples may be used to determine statistically the likelihood of finding large gems in the deposit. Caustic fusion in high-temperature lye dissolves the host rock and releases the beryl; pulsed-power disaggregation can serve the same purpose. The microcrystals and macrocrystals are collected and measured, and a log-normal plot of stone frequency versus size enables prediction of the grade and extrapolation of the relative abundance of any gem mineral by weight.

Extraction techniques should be appropriate to the material being mined. Large volumes of low-quality material should be mined rapidly using bulk techniques, including mechanized mining, but zones with high-quality material should be mined slowly and carefully. Tools for the select removal of large, high-value gemstones include hydraulic wedges, expansion polymers, abrasion guns, and portable diamond saws. Mechanized mining “robots” could mine rock faces continuously (with no risk of loss by theft).

The large volumes of bulk-mined ore could be processed using a variety of modern techniques. For example, biochemical leaching uses bacteria to break down



Figure 5. This 6.37 ct pear-shaped garnet, reportedly from Mali, was identified as grossular and not grossular-andradite, on the basis of its refractive index. Courtesy of Kaufman Enterprises; photo by Maha DeMaggio.

iron, sulfur, and organic material in the ore, and liberate the emeralds into a concentrate for collection. Automated techniques to remove emeralds from the concentrate could include optic sorters or beryllometers (which induce and detect short-lived radioactivity in beryllium minerals).

Most of these exploration and production techniques are expensive: Geophysical surveys can cost up to \$50,000 per district, and beryllometers cost about \$250,000 each. One major concern is that modern mining and extraction techniques greatly reduce the need for low-skilled labor—that is, the *garimpeiros* who currently form the backbone of the Colombian emerald mining industry. If the modernized emerald mine cannot support the surrounding towns in the district, the social costs must also be considered.

Gem-quality grossular garnet from Mali. When “Gem-Quality Grossular-Andradite: A New Garnet from Mali” (M. L. Johnson et al., *Gems & Gemology*, Fall 1995, pp. 152–166) was written, we had seen garnets from this region in three color types: orange to brown, somewhat desaturated yellow-green, and bright green. All were found to be grossular-andradite. Subsequently, however, Mark Kaufman of Kaufman Enterprises, San Diego, California, loaned one of the editors three pale, slightly yellowish green garnets, also reportedly from Mali (western Africa), that proved to be otherwise. All three stones—one 6.37 ct pear (figure 5) and two oval (4.18 ct and 5.32 ct) modified brilliants—were much paler in tone than the grossular-andradites we had previously examined and, therefore, looked more like greenish yellow grossular garnet from other localities (such as East Africa). Also, all three had refractive indices between 1.739 and 1.750, again in the “typical” grossular range, and outside the range we use as a criterion for grossular-andradite (1.752 and over, but not greater than 1.81).

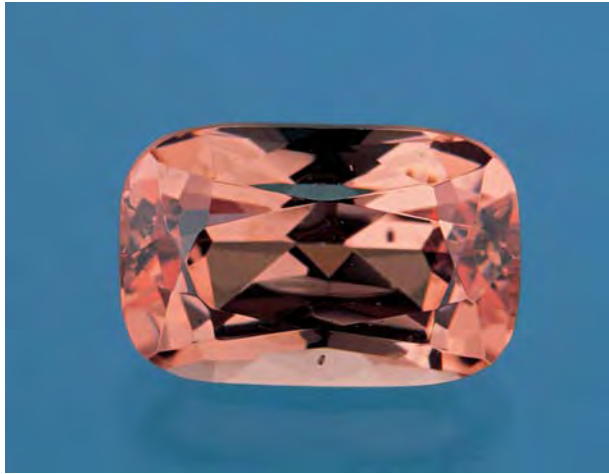


Figure 6. This 1.60 ct brownish pinkish orange pyrope-spessartine garnet from Madagascar is being marketed as "Imperial malaia" garnet. Photo by Maha DeMaggio.

Specific gravity, measured hydrostatically, ranged from 3.61 to 3.63 (versus 3.63–3.70 for grossular-andradite).

However, like grossular-andradite, the stones all showed an absorption band at 435–445 nm when viewed with a desk-model spectroscope; this band was strongest in the stone with the highest refractive index. Also, all three showed strong growth zoning when viewed with magnification between crossed polarizers (also characteristic of grossular-andradite). Energy-dispersive X-ray fluorescence (EDXRF) spectra revealed chemical compositions similar to that of grossular-andradite, that is: major Ca, Al, Si, and Fe; minor Ti; and traces of Cr, Mn, and V. Two of the stones fluoresced faint orange to long-wave UV radiation (the third was inert), and all three were inert to short-wave UV.

Since no other significant amounts of garnet components were present—that is, the garnets consist almost entirely of grossular and andradite components—then the composition of these garnets can be estimated from their refractive indices, as described by Johnson et al. This method gives compositions between $\text{Gr}_{97}\text{And}_{03}$ and $\text{Gr}_{90}\text{And}_{10}$ for the three stones. (In comparison, the yellow-green garnets described by Johnson et al. had compositions between $\text{Gr}_{88}\text{And}_{12}$ and $\text{Gr}_{77}\text{And}_{23}$; the green garnets were between $\text{Gr}_{82}\text{And}_{18}$ and $\text{Gr}_{80}\text{And}_{20}$; and the orange-to-brown garnets were between $\text{Gr}_{75}\text{And}_{25}$ and $\text{Gr}_{71}\text{And}_{29}$). Therefore, on the basis of their refractive indices, we would simply call these stones grossular—despite their absorption spectrum, growth structure, and reported source. In 1996, Bank et al. ("Gemmologie Aktuell," *Zeitschrift der Deutschen Gemmologischen Gesellschaft*, Vol. 45, No. 1, pp. 1–4) also reported on "almost colorless" grossular garnets from Mali, with low andradite contents and refractive indices between 1.742 and 1.751.

These stones illustrate that not all garnets reportedly from Mali are grossular-andradite. Perhaps more impor-

tant, they again illustrate that garnets are a complex classification problem, since their chemical composition is a continuous admixture of "end-member" components, with few (if any) natural breaks that can be used to distinguish among gemologically significant varieties.

Pyrope-spessartine garnet from Madagascar. Several varieties and colors of garnet from Madagascar were described in the Spring 1994 Gem News column (pp. 50–51), including: orange to brownish orange spessartine, medium-dark brownish orange hessonite, red garnets from Maralambo, medium purple-pink and dark red-purple rhodolite, and dark orangy red pyrope-almandine. In March of this year, gemologist L. Allen Brown of All That Glitters, Methuen, Massachusetts, loaned another Madagascar garnet (figure 6), a 1.60 ct pyrope-spessartine of an unusual brownish pinkish orange, to contributing editor Shane McClure. The material came to Mr. Brown's attention in late 1996; he was told only that it comes from the center of the country. The garnet crystals are about the size of a "fist" or "softball," but because of fractures and inclusions, eye-clean faceted stones are typically smaller than 1 ct. Larger fashioned stones are relatively uncommon. Mr. Brown knew of five stones over 3 ct, but none larger than 4 ct. The material is being marketed as "Imperial malaia garnet."

Sometime later, in July of this year, Margit Thorndal of Madagascar Imports, Laurel, Montana, showed us nine of these garnets, with a total weight of 3.65 ct; we examined a 0.95 ct oval in detail. Ms. Thorndal had about 250 carats of finished goods available, mainly in sizes less than 1 ct; she reported that this material is also being marketed as "champagne garnet."

The two stones we studied had the following properties: color—brownish pinkish orange; diaphaneity—transparent; optic character—isotropic, with strong anomalous double refraction; refractive index—1.760; specific gravity (measured hydrostatically)—3.89–3.90; fluorescence—inert to both long- and short-wave ultraviolet radiation; spectroscope spectrum—typical pyrope-spessartine absorption spectrum (as seen through a hand-held spectroscope), with strong 430 and weak 500 nm bands. With magnification, black disks or platelets were visible in the 1.60 ct stone, as is typical for pyrope-spessartine garnet; the 0.95 ct stone contained needles and dark crystals.

Color-change pyrope-spessartine garnet, also from Madagascar. Contributing editor Karl Schmetzer provided the following information about a new source for color-change garnet. Garnets that show a distinct alexandrite-like color change between daylight and incandescent light can be divided into two different groups according to their chemical composition. The less common group consists of Cr-rich pyrope, with greater than 3 wt.% Cr_2O_3 . The more common group is formed by members of the solid-solution series pyrope-spessartine,

which contain traces of chromium and/or vanadium (below 1 wt.% Cr₂O₃ and/or V₂O₃). Color-change pyrope-spessartine with a relatively low iron content appears greenish gray or greenish yellow in daylight, and pink or red in incandescent light; with higher amounts of iron, the colors are greenish blue to almost violet in daylight, and reddish violet in incandescent light. Faceted color-change pyrope-spessartine from Sri Lanka and from Umba, Tanzania, has been seen in the trade since the late 1970s. Recently, samples were also reported from the new Tundur-Songea mining area in southern Tanzania (see, e.g., Spring 1996 Gem News, pp. 58–59).

Three faceted color-change pyrope-spessartine garnets (2.52, 3.25, and 5.23 ct—two of which are shown in figure 7) were submitted by a dealer to Dr. Schmetzer for examination. The samples were purchased several months ago at a gem market in Madagascar, but no exact locality within Madagascar was provided. Their refractive indices (1.765–1.766) and specific gravities were typical for intermediate members of the pyrope-spessartine series.

The color of all three stones can be described as light greenish yellow in daylight (figure 7, left) and intense pink to red in incandescent light (figure 7, right). The UV-visible absorption spectra of all three samples were almost identical and consisted of a group of four strong Mn²⁺ absorption bands at 207, 237, 242, and 245 nm, and two relatively weak Fe²⁺ absorption bands at 199 and 218 nm. This spectrum is superimposed on a dominant, broad V³⁺/Cr³⁺ absorption with a maximum at 571 nm, which is responsible for the two absorption minima in the red and the green regions. This two-minima absorption spectrum is frequently observed in color-change gem materials.

All three garnets revealed a distinct three-dimensional network of fine rutile needles and small mineral inclusions—probably tiny zircon crystals—with associated tension cracks. Some additional small, birefringent mineral inclusions have not yet been identified.

Hackmanite from Myanmar. Hackmanite is the UV-sensitive, luminescent, color-change variety of the sulfur-rich mineral sodalite. Until recently, transparent gem-

quality hackmanite was known only from Mont Saint-Hilaire, Quebec, Canada, in very limited quantity (see, e.g., Summer and Winter 1989 Gem News, pp. 112 and 245–246, respectively). Nearly unknown to jewelers, hackmanite has unusual and distinctive optical characteristics that make it a very desirable collectors' stone: Exposure to long-wave UV radiation produces a strong, bright orange fluorescence and causes a dramatic (if unstable) color change from white to purple. Recently, translucent-to-opaque cabochon-quality hackmanite was found in the course of ruby mining at the Dattawa mine in Mogok, Myanmar. This discovery was reported to the Gem News editors by Mark H. Smith, a gemologist and gem dealer living in Bangkok. At the Tucson gem shows in February of this year, Mr. Smith displayed a few hundred carats of Myanmar hackmanite cabochons, as well as some cutting-quality rough (figure 8, left), at his booth.

As obtained from samples donated to GIA, the gemological properties of this material were similar to those for sodalite (R.I. about 1.48, S.G. about 2.2–2.3). Exposure to long-wave UV radiation produced a strong, bright orange fluorescence and, after a few minutes, resulted in a dramatic color change from grayish white or white to intense, dark purple (figure 8, right). As has been our experience in the past, it was difficult to photograph the full color change because the purple quickly faded back to "normal" under the intense illumination of the flood lamps used in photography.

"Striped" labradorite feldspar. In addition to labradorescence, labradorite can show some other interesting characteristics. One example was the "bicolored" labradorite from Ylmaa, Finland, reported in the Spring 1997 Gem News (pp. 62–63). At the Costa Mesa (California) gem and mineral show this past May, Joseph Lieberz of Jewel Tunnel Imports, Baldwin Park, California, showed us another interesting labradorite, this one striped (figure 9). As the stone is tilted, different bands show the labradorescence, which is due to exsolution of feldspar with two slightly different compositions (see, e.g., J. V. Smith, "Phase Equilibria of Plagioclase," and P. H. Ribbe, "Exsolution Textures in Ternary and Plagioclase Feldspars; Interference Colors," in *Reviews in Mineralogy*,

Figure 7. These 2.52 and 3.25 ct color-change pyrope-spessartine garnets are reportedly from Madagascar. Left, daylight-equivalent fluorescent light; right, incandescent light. Photos © GIA and Tino Hammid.

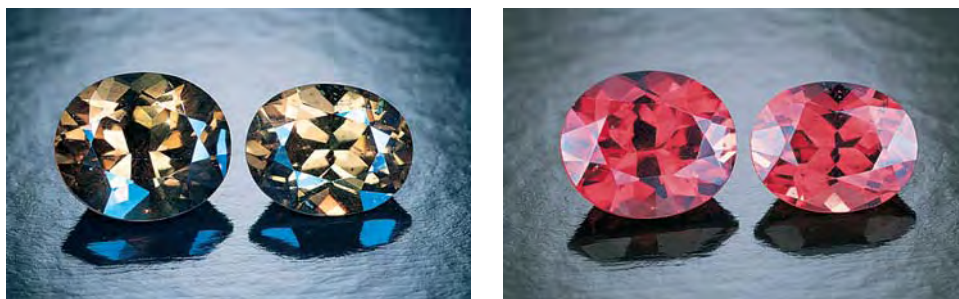


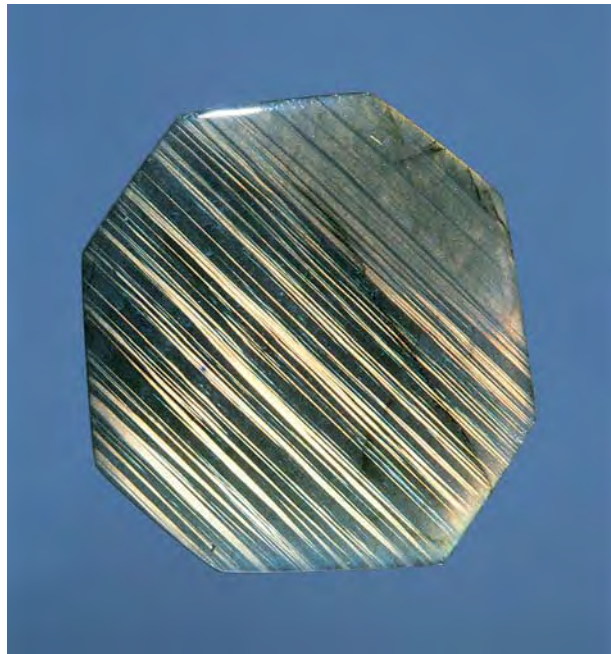


Figure 8. Before exposure to long-wave UV radiation, these hackmanites (rough, 46 mm; largest cabochon, 1.92 ct) from Myanmar were white to light gray (left). After one minute of exposure to a long-wave UV lamp, the hackmanites turned purple to pink (right). The color change, however, is unstable if the stones are exposed to light. Photos by Maha DeMaggio.

2nd ed., Vol. 2, *Feldspar Mineralogy*, Mineralogical Society of America, Washington, DC, 1983, pp. 223–239 and 241–270, respectively). However, this particular sample demonstrates at least two events: the twinning that caused the labradrescent bands to change orientation relative to one another, and the exsolution that caused the labradrescence itself.

The 126.71 ct octagonal cabochon came from the extensive deposits in Madagascar, near the village of

Figure 9. The labradrescence in this $40.70 \times 38.05 \times 8.12$ mm (126.71 ct) labradorite cabochon occurs in two sets of stripes with different orientations. Photo by Maha DeMaggio.



Bekily in Tulear Province. This is one of the most prolific sources in the world for small pieces of labradorite, and tons of material are mined every year. (Jewel Tunnel alone imports about 2 tons of labradorite each year.) The largest pieces are fashioned into gem spheres.

Colorado lapis lazuli. Geologist Gary Christopher of The Prospector's Cache, Gunnison, Colorado, is marketing lapis lazuli from the Blue Wrinkle mine (figure 10), in the north Italian Mountain area about 170 km southwest of Denver. The deposit, known since 1939, was featured in *Gems & Gemology* shortly after its discovery (H. I. Rosencrans, "Colorado Lapis Lazuli," Vol. 3, 1941, pp. 154–156). At the Tucson gem shows last February, Mr. Christopher reported that 2–3 tons of the material (mined over the period 1959 to the present) were available. Of this, an estimated 5% was lapidary quality, with the best material occurring as veinlets within the host rock (figure 11). The deposit has produced some large pieces of good-quality material; Mr. Christopher indicated that a boulder weighing about 18 kg (40 lbs.) is in the collection of the Denver Museum of Natural History.

Pearls highlighted at the 2nd International Jewellery Show in Kobe, Japan. GIA Gem Trade Laboratory vice-president Thomas Moses sent in the following report from this show, which was held at the Kobe Convention Center on June 11–13, 1998. Most of the major Japanese suppliers of cultured pearls were present, with large stocks of all types. The importance of South Seas and Tahitian products continues to grow: These cultured pearls were offered in a large range of sizes, with a particularly good supply of commercial-quality, as well as some high-quality, goods. Mr. Moses also saw a large selection of treated-color Akoya and freshwater cultured pearls that were mainly blue to gray, imitating the colors of the popular Tahitian products. Chinese freshwater cultured pearls were available in a wide range of sizes and



Figure 10. Lapis lazuli is once again being commercially mined from the Italian Mountain area of western Colorado. Photo courtesy of Gary Christopher.



Figure 11. At Colorado's Blue Wrinkle mine, the lapidary-quality lapis lazuli forms veinlets within the host rock. The slab on the left is 4.6 cm wide. Photo by Maha DeMaggio.

colors, including pink, orange, and purple. There was also a good selection of conch pearls.

In an invited lecture, Andy Müller of Golay Buchel, Japan, presented cultured pearl production statistics (in U.S. dollars); these demonstrated the growing importance of South Seas and Tahitian cultured pearls. The estimated production value for these two sources (combined) is about \$350 million annually, versus approximately \$200 million for Japanese Akoya cultured pearls.

Vietnamese “trapiche” rubies. In the Winter 1996 issue of *Gems & Gemology* (pp. 242–250), Dr. Karl Schmetzer and colleagues described trapiche rubies that were obtained in Thailand. These stones were reportedly from Mong Hsu, Myanmar, although the authors also noted that such rubies had been stated to come from Vietnam. One of the authors of that article, contributing editor Dr. Henry Hänni, and his SSEF colleague Dr. Lore Kiefert, have provided additional information about trapiche rubies from Vietnam.

In spring 1997, Drs. Hänni and Kiefert received 29 rough rubies from Carlo Mora of Italy. The stones (2–25 ct) reportedly came from secondary deposits, some eluvial, from Yen Bai Province in Vietnam. The crystals were tabular or barrel-shaped, and some had pyramidal faces. They also showed various degrees of abrasion. The rough pyramidal faces exhibited striations perpendicular to the c-axis, and were commonly partially covered with mica. Figure 12 shows seven ruby crystals that are typical of this occurrence, some with a polished cross-section.

The specific gravities of these stones ranged between 3.92 and 3.97, which is slightly lower than the literature value for ruby; this is probably due to the presence of micas and secondary minerals in the stones and as surface coatings. Refractive indices were $n_e = 1.760$ and $n_o = 1.769$, giving a birefringence of 0.009. Microscopic examination showed hexagonal growth patterns with short rutile needles in three directions parallel to the prism faces. The mica inclusions occur in stringers and patches

and also form the fixed “stars” in these stones. Perpendicular to the prism faces, and parallel to the hexagonal crystal axes a_1 , a_2 , and a_3 , were accumulations of rutile in radiating bands. In addition, fluid inclusions and healing feathers were elongated in these directions, similar to the glide planes in star sapphires.

Mineral inclusions (identified by Raman and SEM) were: rutile (black); apatite, alkali feldspar, zircon, diaspore (all colorless); biotite mica (brown); monazite (yellow); and graphite (black), mainly within three-phase inclusions. Frequently, the mica inclusions were concentrated along the c-axis in the center of the stone, and on planes centered between the hexagonal a-axes, forming a fixed “star.” This pattern resembles the sector growth structures found in trapiche emeralds from Colombia and “trapiche” rubies from Myanmar. (Note that the inclusions in the Mong Hsu rubies were primarily carbonate, rather than micas.)

“Sliders”: Rutile inclusions in quartz. For this gemologist (JK), one of the most unusual internal features ever seen

Figure 12. These “trapiche” rubies from Vietnam show tabular and barrel-shaped habits. The fixed “star” is formed by mica inclusions. Photo by H. A. Hänni.



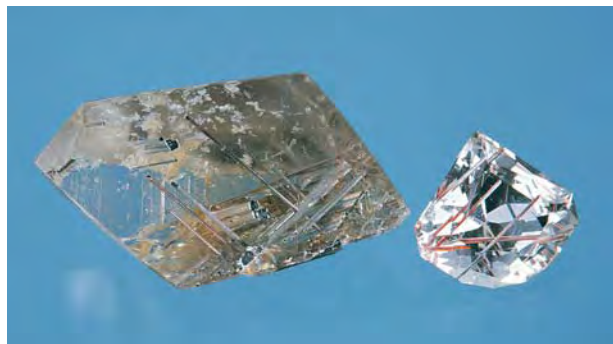
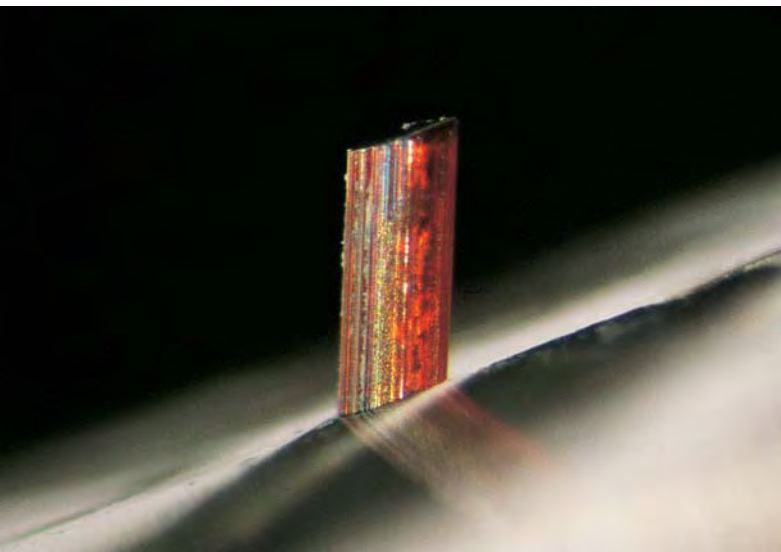


Figure 13. These two polished quartz specimens (64.47 and 12.83 ct) both contain rutile “sliders.” Photo by Maha DeMaggio.

in a gem material is the presence of “sliders”—elongated rod- or needle-shaped inclusions of rutile crystals with high length-to-width ratios that, even at the microscopic level, fit precisely in their quartz hosts. Yet these inclusions are also free to slide back and forth along rail- or track-like grooves in the quartz that precisely parallel the growth striations seen on their surfaces. Sliders would appear to be rare, given the fact that even the slightest growth hillock or similar irregular feature on the surface of any one of these crystals would cause that crystal to bind up, locking it in place in the quartz.

Sliders were first brought to our attention as a result of the rough grinding of a large transparent partial crystal of Brazilian rutilated smoky quartz from Teófilo Otoni. From the pressure exerted during the grinding process, inclusions of rutile needles were pushed out of their host channels and forced into the lapidary’s hand, breaking off like splinters.

Figure 14. This 0.5 mm wide red-brown rutile crystal slides freely within its polished smoky quartz host. It is seen here protruding about 1 mm from the surface of the quartz. Photomicrograph by John I. Koivula.



The quartz containing these “sliders” was subsequently worked by gemologist-lapidary Leon Agee of Liberty Lake, Washington. The intention was to create a demonstration specimen that could display the moving rutile needles. During final grinding and polishing, Mr. Agee intentionally pushed the rutile needles through the surface so they would end up longer than their polished smoky quartz host. The final product of this exercise is a free-form, partially polished crystal section that weighs 64.47 ct and measures 4.0 cm long (figure 13). The longest moving rutile needle in this smoky quartz has a 46:1 length-to-width ratio. Its protrusion from the polished surface is shown in figure 14.

At approximately the same time, gemologist-lapidary Michael Gray of Missoula, Montana, discovered another “slider” while faceting a piece of rutilated rock crystal quartz from Madagascar. When finished, this free-form faceted stone weighed 12.83 ct and measured 17.37 × 16.71 × 10.39 mm (again, see figure 13). During cutting, Mr. Gray observed that two of the longest rutile needles, measuring up to 12.5 mm long and just 0.4 mm wide, were pushed out the back of the stone. As shown in figure 15, bright red rutile crystals protrude from channels in some of the polished facets of this interesting gem.

Sapphire from the Ural Mountains, Russia. According to Nicolai Kuznetsov, of Stone Flower Co. in Moscow, a new deposit of blue sapphires is being mined in the Chelyabinsk region of the Urals, about 3 km from the town of Mias. Although the deposit has been known for two to three years, organized mining did not occur until August 1998, during which time several kilograms of well-formed crystals (see, e.g., figure 16) were recovered. The crystals are embedded in a tough metamorphic matrix that is removed by means of acid dissolution. One stone has been cut so far, a 0.27 ct round brilliant (inset, figure 16). Mr. Kuznetsov believes that the locality has strong potential for producing significant gem-quality material.

Sapphirine: *Gems & Gemology* reader to the rescue. The *G&G* editors offer a big thank you to Murray Burford, of Victoria, British Columbia, who generously donated four samples of sapphirine to GIA after reading (in a Summer 1997 Lab Note about serendibite, pp. 140–141) that the GIA Gem Trade Laboratory reference collection contained no samples of this gem material. According to Mr. Burford, the four stones come from the Kolonne area of Sri Lanka, where such samples have been sporadically (and illegally) mined since 1985. Most of the stones there are fractured, in part because of the harsh manner in which the crystals are removed from the host rock, with explosives as well as hammers and chisels. Most of the sapphirine from Kolonne is a desaturated blue, but some is pinkish brown. The gemological properties of these stones matched the known properties for sapphirine (see, e.g., J. E. Arem, *Color Encyclopedia of Gemstones*, 2nd ed., Van Nostrand Reinhold, New York).

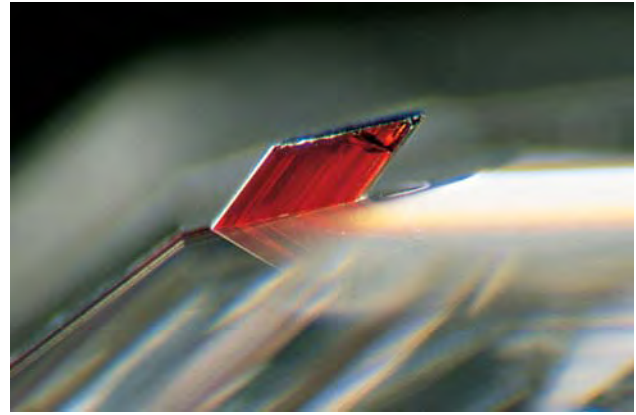
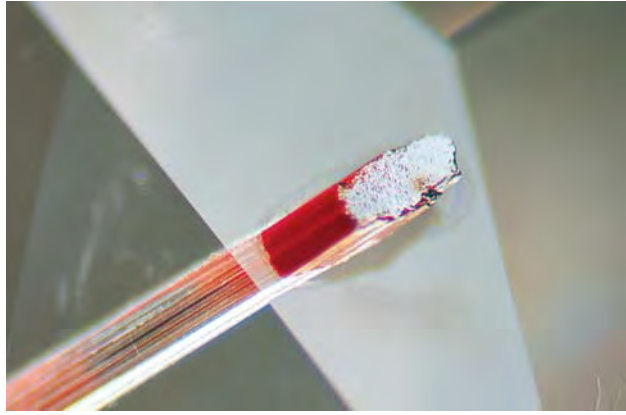


Figure 15. In the view on the left, light reflected from the surface of this faceted quartz shows how perfectly the 0.4 mm wide rutile inclusion fits in its host channel. The bright reflection on the rutile is the ground-off portion of the crystal. In a side view (right), the same inclusion can be seen to protrude from the surface of the faceted stone. If desired, it could be pushed completely through its quartz host in either direction. Photomicrographs by John I. Koivula.

TREATMENTS

Radioactive rubies. Recently, Ken Scarratt of the AGTA lab in New York City received two radioactive rubies for examination. These were provided by Gary Roskin of JCK, who received them from a contact in Indonesia as two examples of the radioactive rubies that have created such alarm in the Asian trade press (e.g., "Irradiated ruby reported in Jakarta," *Asia Precious*, July/August 1998, p. 8).

The two brownish red ovals weighed 2.27 and 2.74 ct, and had the visual appearance of rubies from East Africa (figure 17). They had the following gemological properties (smaller stone first, where different): optic character—uniaxial; refractive indices—1.764–1.775 and 1.763–1.771; specific gravities—4.00 and 4.01; absorption spectrum—typical bands for chromium and iron; fluorescence—inert to both long- and short-wave ultraviolet radiation. With magnification, the 2.27 ct stone was seen to contain two small, somewhat rounded and melted-looking inclusions, each with numerous bubbles (figure 18). The presence of bubble-filled inclusions in corundum has to date been associated with heat treatment. Their presence in one of these stones might indicate that an attempt was made to heat treat the stone first, or that the heat produced during the irradiation process was sufficient to cause the same result. Partially healed "fingerprint" fractures were associated with these inclusions. The smaller stone also contained a large, mirror-like fracture in the pavilion, extending toward the inclusions. The larger stone contained a small nest of "white" needles and particles under the table. Both stones were partially coated with a black crust (figure 19) that looked dark brown along thin edges.

The AGTA lab examined the rubies for any residual radioactivity using a new instrument that was designed by Owen Bordelon of New Orleans specifically for the detection and measurement of radioactivity in gemstones—the AGTA Gemalert. At the time of writing,

Figure 16. Well-formed crystals of blue sapphire were recently found at a new deposit in the Ural Mountains. This crystal measures about 5 cm in diameter; it has been partially removed from the matrix by acid dissolution. The 0.27 ct faceted stone (inset) was cut from a piece of rough that was removed from the back of this specimen. Photos by Maha DeMaggio.

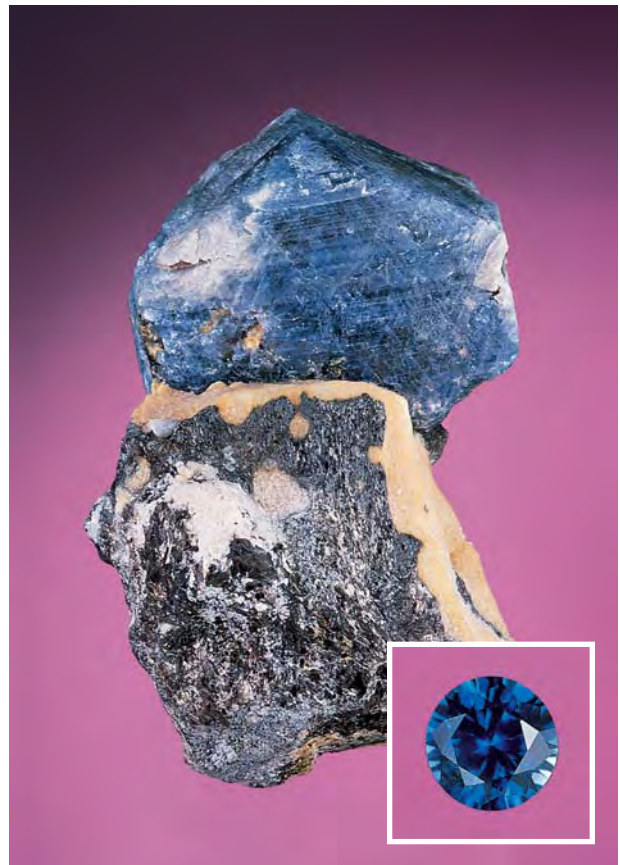




Figure 17. These two rubies (2.27 and 2.74 ct) look like typical East African stones, but they proved to be radioactive. Photo by Maha DeMaggio.

measurements had been recorded for these stones with this instrument at irregular intervals over a period of only one month. Nevertheless, it provided useful indications of the level of radioactivity. The first measurement of the 2.74 ct stone revealed an activity level of 81 micro-Roentgen per hour per carat; for the 2.27 ct stone, the level was 95 micro-Roentgen per hour per carat. (Legal limits for the release of irradiated gemstones depend on the particular isotopes responsible for the radioactivity and their concentrations. This information has not yet been established for these stones.) It is interesting to note that measurements taken on two natural, untreated green zircons during the same period resulted in similar readings; however, the Nuclear Regulatory Commission does not regulate naturally radioactive gems. Further measurements were taken about 10 days and one month later; following calculation, they produced an approximate half-life for each of the two rubies of 300 days, assuming the radioactivity came from only one isotope. Unless future calculations indicate that more than one significant radioisotope is present, this would mean that the radioactivity level for each stone would be reduced to background levels within two years. Thus far, no information is available as to the precise source of these rubies and their original color. Investigations are ongoing into how the material can be identified by standard gemological methods.



Figure 18. The smaller of the two rubies in figure 17 contained two melted-looking inclusions with numerous bubbles. Photomicrograph by John I. Koivula; magnified 20×.

SYNTHETICS AND SIMULANTS

Gallium phosphide, resembling fancy dark orange diamond. This unusual material was called to our attention by graduate gemologist Robert E. La Prad, an appraiser in Santa Barbara, California. A local high-tech company, Digital Instruments, uses the manufactured product gallium phosphide, and an engineer brought a piece to Mr. La Prad for faceting. He noted that during faceting the sample gave off a very pungent (phosphorus) odor.

The 4.11 ct faceted sample (figure 20) had the following properties: diaphaneity—transparent; color—very dark brownish reddish orange; color distribution—even; optic character—singly refractive; refractive index—over the limits of the standard refractometer (greater than 1.81); specific gravity (measured hydrostatically)—4.15; fluorescence—inert to both long- and short-wave UV radiation; spectroscopy spectrum—560 nm cutoff. No inclusions were noted when the sample was viewed through a microscope; however, microscopic examination was difficult because of the somewhat hazy appearance of the facets. According to Mr. La Prad, the Mohs hardness (checked with hardness points) is 5–6.

As this was a new material for us, we ran some additional tests. With energy-dispersive X-ray fluorescence (EDXRF) analysis, Sam Muhlmeister of GIA Research found major gallium and phosphorus. Shane Elen of GIA

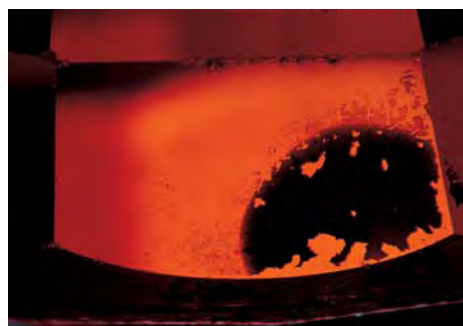
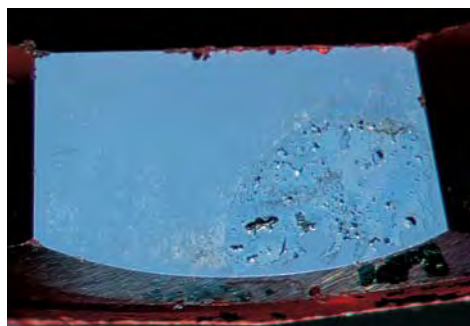


Figure 19. Both rubies were partially coated with a black material (left, 2.74 ct stone in reflected light) that looked brown along thin edges (right, in transmitted light). Photomicrographs by John I. Koivula; magnified 15×.

Research ran laser Raman microspectrometry, which showed a strong peak at 363 cm^{-1} and smaller peaks at 404 , 719 , and 782 cm^{-1} ; and infrared spectroscopy, which showed weak absorption peaks at 1080 and 1105 cm^{-1} , stronger peaks at 785 , 745 , and 700 cm^{-1} , and an absorption minimum at 650 cm^{-1} . An X-ray powder diffraction pattern confirmed that the material was crystalline; it resembled the pattern for sphalerite, but with slightly different lattice spacings.

Gallium phosphide could be mistaken for a fancy-colored diamond. However, the specific gravity and hardness will separate it from diamond. It could also be mistaken for various soft natural stones (e.g., cuprite and proustite; however, these are red, not brown or orange). It would most likely be confused with sphalerite, although orange sphalerite is usually color zoned, and gallium phosphide has a higher luster and is slightly denser.

Unusual jade look-alike. While in Myanmar in 1995, Dr. John Saul, best known to gemologists for the Kenyan ruby mine named after him, purchased an intriguing worn green pebble from a jade dealer and carver (figure 21). The piece measured approximately $8 \times 5 \times 5\text{ cm}$, and reportedly came from the Hpa Kan area in Myanmar. The bright green color was not exactly that of jade, and Dr. Saul asked gemologists at the University of Nantes to identify this stone. Because of the pebble's irregular surface, Dr. Fritsch and colleagues could not measure the refractive index. On close examination, it became clear that the piece was a rock, that is, a mixture of minerals. By removing a small portion of the pebble, they were able to perform X-ray diffraction analysis (XRD) of the bulk material, and prepare a thin section to investigate the nature of the constituents.

The results of XRD revealed that two sodic amphiboles, magnesioarfvedsonite and glaucophane, are the major constituents. Minor quantities of chamosite (a chlorite) and jadeite were also detected. Examination of the thin section confirmed this identification. According to Dr. Fritsch, the bright green coloration of the rock is caused by the magnesioarfvedsonite, and the chamosite is a darker, less-saturated green; the blue glaucophane and the near-colorless jadeite did not affect the rock's color. EDXRF analyses performed on an Oxford ED 2000 spectrometer proved that chromium was the primary chromophore, and examination of the thin section suggested that the Cr was restricted to the magnesioarfvedsonite. This unusual rock is probably the result of high pressure–low temperature metamorphism (to blueschist grade) of a basic rock, such as a gabbro or a basalt.

“Wild Life” assembled gemstone cabochons. Hans Ulrich Pauly, of Idar-Oberstein, introduced the new “Wild Life” line of assembled gemstones at the April 1998 Basel show. These gems display striking designs of wildlife pelts or shells: zebra, giraffe, tiger, leopard, jaguar (figure 22), ocelot, cheetah, and even tortoise shell. Mr.



Figure 20. This 4.11 ct round brilliant was cut from a piece of gallium phosphide by Robert E. La Prad, of Santa Barbara, California, who donated it to GIA. Photo by Maha DeMaggio.

Pauly is marketing the “Wild Life” series as a way to promote endangered species (without further endangering them). The response to this product in Basel was very good, and Mr. Pauly is planning to add more patterns, such as snake and clouded leopard.

These assemblages are constructed from a flat, 1 mm thick mother-of-pearl base and a quartz cabochon top. Depending on the desired bodycolor of the pattern (e.g., white for zebra, yellow for tiger) either rock crystal or citrine (which is sometimes color zoned) is used for the top.

Figure 21. This bright green pebble, which was represented in Myanmar as jade, consists mostly of a mixture of amphiboles with very minor jadeite. Photo by Alain Cossard.





Figure 22. These “Wild Life” assembled cabochons are constructed from an etched and painted quartz top, backed by a thin slice of mother-of-pearl. The zebra cabochon is 16 mm in diameter. Courtesy of Hans Ulrich Pauly; photo by Maha DeMaggio.

Mr. Pauly uses a high cabochon dome to “give more life” to the designs. The flat side of the quartz cabochon is worked with a technique derived from traditional English crystal paintings: The stone is first engraved to make a deep intaglio, then the carved areas are filled with oil-based paint. The base is attached to the cabochon with a glue that contains a special preservative to prevent reaction between the adhesive and the paint over time. The cabochons range from 8 to 50 mm in maximum dimension. A German patent covers the technique and five patterns.

Figure 23. Dr. George R. Rossman (left) joins Richard T. Liddicoat in the distinction of having a variety of tourmaline named after him. Photo by Peggy Wallace.



ANNOUNCEMENTS

Rossmanite, a new variety of tourmaline. Dr. George R. Rossman, Professor of Mineralogy at the California Institute of Technology and a longtime member of the *Gems & Gemology* editorial review board, has had a new variety of tourmaline named in his honor. Rossmanite was recently described by Selway et al. (“Rossmanite, $\square(\text{LiAl}_2)\text{Al}_6(\text{Si}_6\text{O}_{18})(\text{BO}_3)_3(\text{OH})_4$, a New Alkali-Deficient Tourmaline: Description and Crystal Structure,” *American Mineralogist*, Vol. 83, 1998, pp. 896–900) as well-formed pale pink crystals from a granitic pegmatite near Roznà in the Czech Republic. The mineral is characterized by an elemental vacancy in the X site (represented as “ \square ” in the chemical formula); it forms a third member in a family of lithium-aluminum tourmalines that includes elbaite (Na in the X site) and liddicoatite (Ca in the X site, named after *Gems & Gemology* editor-in-chief Richard T. Liddicoat; figure 23).

In addition to the type locality, rossmanite has been found at other pegmatites in the Czech Republic and at Red Cross Lake in northeastern Manitoba, Canada (Selway et al., “Tourmaline from Lepidolite-Subtype Pegmatites,” *Abstracts, Tourmaline 1997—International Symposium on Tourmaline, Czech Republic, 1997*, pp. 91–92). Rossmanite has also been found as colorless zones near the terminations of gem-quality multicolored elbaite crystals from pegmatites on the island of Elba, Italy (Pezzotta et al., “La Rossmanite di Roznà e dell’Elba,” *Revista Mineralogica Italiana*, Vol. 22, No. 1, 1998, pp. 46–50). Pink rossmanite has been documented from the Utå pegmatite in Sweden and the Tanco pegmatite in southeastern Manitoba, in a further study by Selway et al. (“Compositional Evolution of Tourmaline in Petalite-Subtype Pegmatites,” *Abstracts & Programme, 17th General Meeting of the International Mineralogical Association, Toronto, Canada, August 9–14, 1998*, p. A148). Rossmanite is visually indistinguishable from elbaite; it can be identified only by quantitative chemical analysis.

ERRATA: In the article “Benitoite from the New Idria District, San Benito County, California,” (B. Laurs et al., *Gems & Gemology*, Fall 1997, pp. 166–187), Edward Swoboda and Peter Bancroft were described as unauthorized miners. It has come to our attention that Swoboda and Bancroft did indeed have permission to visit the mine, and did so several times in the late 1930s. The authors apologize for this misrepresentation.

The Summer 1998 Gem News item “Of rubies and rubles” (pp. 141–142) reported the location of a new ruby deposit as the Polar Urals of Siberia. Although the ruby deposit was correctly identified as the Rais mine in the Polar Urals, this area is actually west of Siberia.

Challenge Winners 1998

Once again,

over 300 *Gems & Gemology* readers, dedicated to their education and knowledge of the field, participated in the 1998 *Gems & Gemology* Challenge. Entries arrived from all corners of the world, as readers tested their knowledge on the questions in the Spring 1998 issue. Those who earned a score of 75% or better received a GIA Continuing Education Certificate recognizing their achievement. The participants who scored a perfect 100% are listed below.

USA ♦ **Arizona** *Oro Valley*: Geraldine Alex Towns. *Tucson*: Luella Dykhuis, Robert Stewart ♦ **California** *Alamo*: Sam Johnston. *Burlingame*: Sandra MacKenzie-Graham. *Carlsbad*: Marla Belbel, Lori Burdo, Michael T. Evans, Brian Genstel, William Herberts, Jan Luree Lombardi, Roxana Lucas, Wendi Mayerson, Catherine McIntyre, Jana Miyahira, Lynn L. Myers, Shannon O'Rourke, Laura Small, Abba Steinfeld, Paula Straub, Ric Taylor, Melissa Watson-Lafond, Mike Wobby, Phil York. *Chino Hills*: Virgilio M. Garcia, Jr. *Elk Grove*: Michael Pace. *Huntington Beach*: Lyndeth Esgar. *Joshua Tree*: Rebecca Ann Bell. *Los Angeles*: Veronica Clark-Hudson, David Peters. *Redwood City*: Starla Turner. *San Diego*: Tracy Nuzzo. *Ukiah*: Charles "Mike" Morgan

♦ **Colorado** *Colorado Springs*: Molly K. Knox. *Denver*: Alan J. Winterscheidt ♦ **Connecticut** *New Haven*: Matilde Paolini McAfee. *Simsbury*: Jeffrey A. Adams. *Westport*: William A. Jeffery ♦ **Florida** *DeLand*: Sue Angevine Guess. *North Miami Beach*: Fabio S. Pinto. *Palm Harbor*: Tim Schuler. *Plantation*: Garrett Walker. *Surfside*: Pinchas Schechter ♦ **Georgia** *Brunswick*: Thomas R. Hill ♦ **Hawaii** *Mililani*: Abe L. Wilson ♦ **Illinois** *Bloomington*: Anne Blumer. *St. Charles*: Lori M. Mesa ♦ **Iowa** *West Des Moines*: Franklin Herman

♦ **Kansas** *Kingman*: La Shawn Bauer. *Louisburg*: Kathylee Cook ♦ **Maine** *Portland*: Arthur E. Spellissy, Jr. ♦ **Maryland** *Annapolis*: James V. Jolliff ♦ **Massachusetts** *Braintree*: Alan Howarth. *Brookline*: Martin Haske. *Uxbridge*: Bernard M. Stachura ♦ **Nebraska** *Omaha*: Ann Coderko ♦ **Nevada** *Reno*: Terence E. Terras ♦ **New Hampshire** *Merrimack*: Kenneth M. Gatto ♦ **New Jersey** *Carteret*: Bela Dvorcsak. *Fort Lee*: Julia V. Tretyakova. *Union*: Thaïs Anne Lump ♦ **New Mexico** *Albuquerque*: Dr. Susan Gaspar Wilson

♦ **North Carolina** *Manteo*: Eileen Alexanian. *Tryon*: Matthew Randolph. *Winston-Salem*: S. Lee Hall ♦ **Ohio** *Cincinnati*: Jeffrey L. Basse. *North Royalton*: Christine M. Blankenship ♦ **Pennsylvania** *Womelsdorf*: Lori Perchansky. *Yardley*: Peter R. Stadelmeier

South Carolina *Sumter*: James S. Markides ♦ **Texas** *Austin*: Corey Shaughnessy. *Corpus Christi*: Warren A. Rees, Jr. *Houston*: Karen L. Jensen. *San Antonio*: Chris Winbery. *Tomball*: Carroll J. Kiefer ♦ **Virginia** *Hampton*: Edward A. Goodman, Tony Goodman. *Sterling*: Donna B. Rios ♦ **Washington** *Lakebay*: Karen Geiger. *Seattle*: Thomas Estervog ♦ **Wisconsin** *East Troy*: William Bailey

♦ **AUSTRALIA** *Avalon Beach, N.S.W.*: Carol E. Wood. *Coogee, Western Australia*: Helen Judith Haddy. *Melbourne*: Katherine Kovacs. *Slacks Creek, Queensland*: Ken Hunter. *Sydney*: Barbara Wodecki ♦ **BELGIUM** *Diegem*: Guy Lalous. *Diksmuide*: H. Loeters, Leo Loeters. *Hemiksem*: De Maeght Daniël. *Ruiselede*: Lucette Nols ♦ **BRAZIL** *São Paulo*: Alejandro Benjamin Ferreyra, Maria Amelia Franco ♦ **CANADA** *Bobcaygeon, Ontario*: David R. Lindsay. *Calgary, Alberta*: Diane Koke. *Coquitlam, B.C.*: Dominc K.U. Tang. *Cowansville, Québec*: Alain Deschamps. *North Vancouver, B.C.*: Eva B. Nilsson. *St.-Lambert, Québec*: Carmen Rivet. *St.-Hubert, Québec*: Sylvie Careau ♦ **FINLAND** *Kajaani*: Petri Tuovinen ♦ **FRANCE** *Paris*: Marie-France Chateau ♦ **ITALY** *Caltanissetta, Sicily*: Francesco Natale. *Ferrara*: Sonia Franzolin. *Genoa*: Mafalda Pasqui. *Lucca*: Roberto Filippi. *Malnate*: Gabriele Tralli. *Porto Azzurro, Elba*: Diego Giuseppe Trainini. *Rome*: Mauro Papais. *San Remo*: Enrico Cannoletta. *Vicenza*: Francesca Zen ♦ **THE NETHERLANDS** *Rotterdam*: E. van Velzen. *Wassenaar*: Jane Orsak ♦ **NEW ZEALAND** *Lower Hutt*: Dennis Blacklaws. *Wanganui*: Richard Sheppard

♦ **PORTUGAL** *Vila do Bispo*: Johanne C. Jack ♦ **SCOTLAND** *Edinburgh*: James W.M. Heatlie ♦ **SPAIN** *Madrid*: Maria Isabel Cereijo Hierro, José Antonio Gutiérrez Martínez, Shahrazad Krewi De Urquijo ♦ **SWEDEN** *Järfälla*: Thomas Larsson ♦ **SWITZERLAND** *Geneva*: J.M. Duroc-Danner. *Zollikon*: Adrian Meister. *Zürich*: Eva Mettler ♦ **TURKEY** *Istanbul*: F. Oya Borahan

♦ **UNITED KINGDOM** *London*: Jeremy L. Harding

Answers (See page 65 of the Spring 1998 issue for the questions):

(1) a, (2) c, (3) d, (4) d, (5) a, (6) d, (7) b, (8) a, (9) d, (10) a, (11) d, (12) a, (13) c, (14) b, (15) a, (16) b, (17) c, (18) d, (19) b, (20) d, (21) d, (22) a, (23) c, (24) c, (25) c

Book Reviews

Susan B. Johnson & Jana E. Miyahira, Editors



GIA GEM IDENTIFICATION LABORATORY MANUAL

188 pp., illus. plus 2 charts, publ. by GIA, Carlsbad, CA, 1998. US\$59.95*

Earlier editions of this manual were designed to assist students in the GIA Gem Identification course and were structured to be used with the *Gem Reference Guide*, the Colored Stone and Gem Identification course materials, and R. T. Liddicoat's *Handbook of Gem Identification* (12th ed., 1993). The manual is now addressed to "gemologists" as well as gemology students and, for the first time, is available for purchase separate from the course.

First impressions are very good. The substantial cover is attractive, and a quick flick through the spiral-bound pages shows easily readable and well-laid-out text with clear black-and-white diagrams. An initial list of the abbreviations used is important but, at four pages of text, is unnecessarily long; some short words might be better spelled out.

The 40-page section on the use of instruments generally follows a logical order, but it is odd that the paragraphs on the use of the 10× lens

appear in the middle of the Microscope section and not at the beginning of the Magnification section. In the same vein, why is the simple hand spectroscope described after (and not before) the expensive wavelength model? In the section on immersion techniques, the dangers of putting assembled stones into liquids (other than water) are not mentioned, although they may be in the other recommended references. The gem identification worksheets (one is shown) are clearly described, and their use as flow charts is agreeably apparent.

The major part of the manual (114 pages) is devoted to Gem Separations, and is apparently designed to be used with Liddicoat's *Handbook of Gem Identification*. The Separations are divided into seven sections, arranged according to the refractive indices of the species described: (1) Gemstones with R.I.'s over the limits of the refractometer, (2) R.I.'s from 1.70 to 1.80, (3) R.I.'s from 1.60 to 1.70, (4) R.I.'s from 1.50 to 1.60, (5) R.I.'s of 1.50 and below, (6) Glass and Plastics, and (7) Assembled Stones. In each section, an initial page lists the gem materials described along with the species, as appropriate, with which they are commonly confused. As an example, diamond (in section 1) is compared to doubly refracting zircon and synthetic rutile, and to singly refracting strontium titanate, CZ, GGG, and YAG; comparative properties are presented in tabular form. Key separation tests are summarized in a "box" at the foot of each page, with the distinguishing properties of fracture-filled diamonds and assembled diamond simulants shown on following pages.

In citing diamonds as an example, a serious omission becomes apparent—synthetic moissanite is not

mentioned. This is understandable, since this manual would presumably have been prepared and sent for printing during 1997 or even earlier, when synthetic moissanite had not been released. However, the omission ought to be addressed—possibly by the issue of a supplementary sheet for insertion in the manual. The omission of colorless enstatite is less serious.

The accompanying Gem Property Charts A and B for common and less common gem materials, respectively, are very clear and provide a concise summary of the properties and tests for the individual gem materials.

This well-produced manual is admirable for teaching gem identification methods, but a standard gem identification textbook such as Liddicoat (1993) is a desirable adjunct.

ALAN JOBBINS
Caterham, United Kingdom

CAMEOS: CLASSICAL TO COSTUME

By Monica Lynn Clements and Patricia Rosser Clements, 223 pp., illus., publ. by Schiffer Publishing, Atglen, PA, 1998. US\$59.95*

This is a lovely, glossy, picture book with over 1,400 photographs of 19th and 20th century commercial and costume jewelry cameos, carved by hand and machine from stone, shell, glass, plastic, and lava. The book's high production quality is apparent not only in the use of coated paper, but also in the outstanding color photographs. Most of the photos, howev-

*This book is available for purchase through the GIA Bookstore, 5345 Armada Drive, Carlsbad, CA 92008. Telephone: (800) 421-7250, ext. 4200; outside the U.S. (760) 603-4200. Fax: (760) 603-4266.

er, present virtually the *same* carved subject matter—the anonymous female figure—which can become a bit tedious.

Approximate dates and prices are given for all of the cameos pictured. However, the prices appear to be arbitrary and should have been footnoted with the following caveat: “Cameo prices vary widely from one region of the United States to another, as well as globally between countries.” It also would have been fitting to point out that price variances reflect supply and demand and also the personal cameo savvy of the collector/jeweler/dealer. With cameos, *estimated value* is not only subjective, it is also dependent on the scholarship of the viewer.

Although the book contains little text, chapter 1 presents some historical information on cameos. Most of this information is useful, if not new, but there is an error in the following statement on page 7: “The cameo had no apparent purpose other than as an ornament.” In fact, ancient cameos—including Greek and Roman pieces from the days of the earliest Caesars—were more than simple ornaments. These items of miniaturized art were used as magic talismans, religious badges, and, ultimately, as items of political propaganda. It was not until the 19th century that cameos were regarded as pure ornament, with the anonymous female figure as the primary subject. The other six chapters offer a pictorial flood of cameos of various sizes and materials, with the majority set in brooches.

I liked the ambitious format of the book, the quality of the illustrations, and especially the section titled “Plaster Casts of Carved and Engraved Gems.” In the 18th and 19th centuries, plaster casts were used as teaching aids, and they can be a fascinating topic of study themselves. Although plaster casts have been written about and photographed in other books on cameos, this book contains many pages of casts, reminiscent of antiquarian books on cameos. The section on “Lava” cameos is also particularly interest-

ing, with some excellent examples shown.

It is left to the reader to decide how to use the dating and pricing information to aid in subject identification, buying, and selling. Some subjects are mislabeled. For instance, several anonymous female figures from the late 1800s are identified as either the mythological goddess (of agriculture) Demeter or the moon goddess Artemis (a crescent moon in the hair does not always mean the figure is Artemis); the goddess Roma is mislabeled as the goddess Minerva; and a couple of figures labeled as “classical” are mythological gods.

Collecting cameos is an area in which study of mythology, astrology, and art history can be helpful. *Cameos: Classical to Costume* may be useful to collectors who wish to increase their basic knowledge about new (from 1900 forward) cameos. In addition, to the authors’ credit, they have included a useful glossary, bibliography, and index. Unfortunately, there is no historical data or new technical information about cameos in this book, and glyptic art scholars seeking arcane information about the subject will have to look elsewhere.

ANNA M. MILLER, G.G.
*International Director,
Master Valuer Program*

WARMAN’S JEWELRY, 2ND ED.

*By Christie Romero, 293 pp., illus., published by Krause Publications, Iola, WI, 1998, US\$18.95**

This is one of the few times when bigger does mean better! This second edition is billed as “enlarged to include more listings and photos,” and it is absolutely true. There are 600 crisp black-and-white photos and 32 realistic color photos that illustrate the divisions and subdivisions of jewelry eras, from late Georgian (mid-18th century) to the mid-1970s. Each photo has a complete description, “circa” dating, dimensions, and a buyer’s guide price (i.e., those prices a buyer should expect to pay for a piece in excellent to very good condi-

tion). All of the photos are new; none is from the first edition.

Each era has a well-researched Introduction, plus sections on History, References (for further independent study), Reproduction Alert, Museums, and the advisors who assisted Ms. Romero. There are also additional jewelry makers in each era; in particular, the Studio Artists section lists many of the lesser-known artists of the 1950s. The concentration is not just on gemstone and precious-metal jewelry. There are generous sections on Costume Jewelry (circa 1935–1975), Plastic and Other Novelty Jewelry (circa 1920–1970), and Special Collectible Jewelry (Native American, Mexican, Scandinavian silver jewelry).

The most valuable section of all is “Timeline,” where Ms. Romero proves her worth as a jewelry historian. “General History, Discoveries and Inventions” is presented side by side with “Jewelry and Gemstone History, Discoveries and Inventions.” From 1760 to 1974, historical milestones (e.g., the Prussian War of Liberation against Napoleon) are juxtaposed with jewelry history events (e.g., Berlin iron jewelry made in Germany as a patriotic gesture during the War of Liberation: “gold gab isch fur eisen” [“I gave gold for iron”]). This places jewelry movements in the context of real-life occurrences, thereby eliminating the isolation of so many historical treatments.

Unfortunately, the publishers were not attentive in their final review. The Index for Part III (Twentieth Century Jewelry) is not correct; the reader can locate items by subtracting the number 16 from the listed page number, or by contacting the author for an errata sheet. In spite of these inconveniences, the antique jewelry veteran and novice alike will value the enormity of this project, which traces over 200 years of jewelry history.

GAIL BRETT LEVINE, G.G.
*Auction Market Resource
Rego Park, New York*

Gemological



ABSTRACTS

EDITOR

A. A. Levinson
*University of Calgary,
Alberta, Canada*

REVIEW BOARD

Peter R. Buerki
GIA, Carlsbad

Jo Ellen Cole
GIA, Carlsbad

Maha DeMaggio
*GIA Gem Trade Laboratory,
Carlsbad*

Professor R. A. Howie
*Royal Holloway, University of
London*

Mary L. Johnson
*GIA Gem Trade Laboratory,
Carlsbad*

Margot McLaren
GIA, Carlsbad

Elise B. Misorowski
Los Angeles, California

Jana E. Miyahira
GIA, Carlsbad

Carol M. Stockton
Alexandria, Virginia

Rolf Tatje
*Duisburg University,
Duisburg, Germany*

Sharon Wakefield
*Northwest Gem Lab
Boise, Idaho*

COLORED STONES AND ORGANIC MATERIALS

Fluid composition, δD of channel H_2O , and $\delta^{18}O$ of lattice oxygen in beryls: Genetic implications for Brazilian, Colombian, and Afghanistani emerald deposits. G. Giuliani, C. France-Lanord, J. L. Zimmermann, A. Cheilletz, C. Arboleda, B. Charoy, P. Coget, F. Fontan, and D. Giard, *International Geology Review*, Vol. 39, 1997, pp. 400–424.

The authors examined the genetic implications of the composition of fluids, δD of channel H_2O , and $\delta^{18}O$ of structural oxygen in beryl from granitic pegmatites and greisens, and in emeralds from Brazil, Colombia, and Afghanistan. [*Editor's note:* δD and $\delta^{18}O$ refer to the isotopic compositions of hydrogen (deuterium) and oxygen, respectively, and are expressed as per mil (δ) differences relative to the isotopic standard SMOW (standard mean ocean water).] Their study led to the following conclusions. First, fluids in the channels of both beryl and emerald are mainly water and CO_2 , and are independent of the age and tectonic setting of emerald deposits; the Colombian emeralds have the lowest contents of channel H_2O (1.30–1.96 wt.%). Second, the emeralds from all three localities have contrasting and restricted ranges of $\delta^{18}O$ values, which suggests that these values were affected by the local host rock. Relative to emeralds from Brazil, those from Afghanistan and Colombia are strongly enriched in $\delta^{18}O$, indicating extensive isotopic exchange

This section is designed to provide as complete a record as practical of the recent literature on gems and gemology. Articles are selected for abstracting solely at the discretion of the section editor and his reviewers, and space limitations may require that we include only those articles that we feel will be of greatest interest to our readership.

Requests for reprints of articles abstracted must be addressed to the author or publisher of the original material.

The reviewer of each article is identified by his or her initials at the end of each abstract. Guest reviewers are identified by their full names. Opinions expressed in an abstract belong to the abstractor and in no way reflect the position of Gems & Gemology or GIA.

© 1998 Gemological Institute of America

between the emerald-forming fluid and ^{18}O -enriched sedimentary or metamorphic host rocks. Third, in Brazil and Afghanistan the δD compositions of channel H_2O in emerald are compatible with either a magmatic or a metamorphic origin; however, a magmatic origin is demonstrated for Brazil's Carnaiba and Socotó deposits, whereas a metamorphic origin is preferred for those of Santa Terezinha (also Brazil). The authors propose a metamorphic origin for Colombian emeralds. RAH

Imperial topaz. R. B. Drucker, *Jewelers' Circular-Keystone*, Vol. 169, No. 3, March 1998, pp. 112–115.

Many gems are intentionally mislabeled in the hope of capitalizing on a more appealing name or origin to increase their value; "Imperial" topaz is one such example. The term *Imperial* typically refers to topaz that is yellow, yellowish orange, or orangy yellow with overtones of red, orange, or pink. However, because no single group or organization governs the use of gem names, many dealers use *Imperial* for nearly any topaz that falls into a broad range of colors, including brown. Others use terms such as *precious*, *sherry*, and *hyacinth*. "The term imperial . . . is nondescript," said Shane McClure of the GIA Gem Trade Laboratory. "If you ask ten different people what imperial means, you will get ten different answers." As a result, some dealers prefer dropping all descriptive terms for topaz and referring to it by color alone.

The best Imperial topaz, and the world's largest supply, is found in the Ouro Preto area of Minas Gerais, Brazil [see *Gems & Gemology*, Winter 1996, pp. 232–241]. Imperial topaz with red overtones commands the highest prices, with pink topaz priced slightly less; true red or purplish red topaz is extremely rare and expensive. Barry Yampol, owner of a major Imperial topaz mine in the Ouro Preto area, is stockpiling his high-quality material until the year 2000, when he expects it to command considerably higher prices because of pent-up demand. MD

Mineralogical significance of fluids in channels of Colombian emeralds: A mass-spectrometric study. J. L. Zimmermann, G. Giuliani, A. Cheilletz, and C. Arboleda, *International Geology Review*, Vol. 39, 1997, pp. 425–437.

The authors used mass spectrometry to study fluids in emeralds from 10 Colombian deposits. These fluids were trapped in fluid inclusions and in channels within the crystal lattice. The fluids in these two environments have the same qualitative composition, but the fluid inclusions account for only 1%–7% of the total concentration of fluids in any of these emeralds. The bulk composition of the fluids is 80–92 mol% H_2O , 3–10% N_2 , 2.5–5% CO_2 , 1–5% H_2 , 0.1–1.5% CO , <0.5% CH_4 , <0.05% organic compounds, and an unspecified amount of inert gases.

The total amount of fluid in the channels is higher (~20%) in emeralds from the western emerald zone than

in stones from the eastern zone. In addition, the H_2O content of channel fluids is higher in emeralds from the western zone (1.63–2.19 wt.%) than in those from the eastern zone (1.35–1.45 wt.%), the latter being the lowest range of H_2O values worldwide for emeralds. The western zone emeralds are also richer in Na_2O than those from the eastern zone, and a good correlation is found between channel H_2O and Na_2O content. This correlation is taken as evidence for the introduction of channel H_2O in a type II orientation (i.e., associated with alkalis in the channels) in Colombian emeralds. RAH

A new era for opal nomenclature. A. Smallwood, *Australian Gemmologist*, Vol. 19, No. 12, 1997, pp. 486–496.

The play-of-color typical of precious opal is difficult to describe, as it ranges over every color in the rainbow, in every tone from light to dark, and in every degree of transparency. Opal also displays mineralogical differences that reflect the varying geologic environments of its formation. A scheme of opal nomenclature is outlined, based first on whether a specimen is "precious" opal (has play-of-color) or common opal and potch (neither of which exhibits play-of-color). The classification of natural opal takes into account the type of opal (e.g., precious, potch, or common opal), variety (e.g., black, dark, or light), and transparency. Separate criteria are listed for treated opal, composite gemstones (expressed as doublet opal or triplet opal), and synthetic and imitation opal.

The Australian Gemstone Industry Council has accepted this classification, as has the Gemmological Association of Australia, both of which encourage its use. This classification does not establish any method of valuation. RAH

The pearl world's new order. D. Federman, *Modern Jeweler*, Vol. 96, No. 10, October 1997, pp. 46–56 passim.

The production and export of Tahitian cultured black pearls have increased dramatically since 1996, a rise that seems to have corresponded to the launching of Elizabeth Taylor's *Black Pearls* perfume in March of that year. Most of these pearls are sold in the United States. At the same time, exports of white and pink Akoya pearls from Japan have been decreasing. Rather than low demand, this decline may have been caused by decreased production, since about 50% of Japan's nucleated oyster crop was killed off recently by an unknown disease. Japanese dealers reportedly are buying Tahitian pearls and re-exporting them to the U.S., while several individual Tahitian dealers are exporting their material directly to the U.S. West Coast.

The availability and affordability of black pearls (which now cost 25% to 40% less than they did three years ago) has enticed wholesalers into the market, and some are beginning to specialize in specific colors of South Sea pearls. The pearl industry is vibrant, and in 1997 two of Japan's largest pearl companies joined U.S.

companies to gain access to all aspects of American retailing, from large chains and high-volume retailers to small, independent businesses. MD

Rare-earth-element-activated cathodoluminescence in apatite. R. H. Mitchell, J. Xiong, A. N. Mariano, and M. E. Fleet, *Canadian Mineralogist*, Vol. 35, August 1997, pp. 979–998.

Cathodoluminescence (CL), like UV-visible absorption spectroscopy, can help identify the trace elements present in crystals; such a determination can then provide clues to the geologic environment in which a particular crystal grew. For example, apatite from a granite typically displays a yellow CL, whereas that from a carbonatite shows a blue CL because of the different concentrations and proportions of the rare-earth elements in apatite from these different environments. Here, the authors determine the CL spectra for various rare-earth elements—cerium, praseodymium, samarium, europium, dysprosium, and erbium—in synthetic apatite crystals. These CL spectra also resemble the spectra of the same elements in other materials. The authors caution that not all “luminescent” rare-earth elements can be detected in natural materials, since the presence of other elements (i.e., other rare earths, iron, or manganese) can enhance, suppress, or overwhelm an element’s characteristic CL spectrum. In addition, structural defects not related to known luminescent elements may lead to cathodoluminescence. MLJ

Texture and structure of opal-CT and opal-C in volcanic rocks. T. Nagase and M. Akizuki, *Canadian Mineralogist*, Vol. 35, August 1997, pp. 947–958.

Mineralogists differentiate among several varieties of opal on the basis of their X-ray diffraction patterns. These patterns are influenced by the presence of cristobalite and tridymite regions within individual crystals, the size of these regions, and the degree to which these regions are ordered. Cristobalite and tridymite are both polymorphs of SiO₂ (as is quartz) that form at high temperatures and low pressures; their structures are the same except for different stacking sequences of layers of atoms. Opal that is amorphous is called “opal-A.” “Opal-C” has some diffraction spacings that match those of cristobalite, and “opal-CT” has diffraction spacings consistent with both cristobalite and tridymite.

Using high-resolution transmission electron microscopy, the authors investigated the microstructures of opal-CT and opal-C from volcanic rocks in two opal mines in Japan. They found that both materials contained tiny bladed cristobalite crystals; the difference between the opal-CT and the opal-C is the relative amount of disordered and ordered cristobalite. Although some of the cristobalite in the opal-CT showed considerable stacking disorder, there was no evidence of tridymite being present. However, the disordered stacking in the cristobalite probably resulted in the tridymite-like diffraction-line spacing.

These volcanic opal samples probably formed by precipitation from a silica-saturated solution. The opal-CT from volcanic rocks probably formed at higher temperatures than did opal-CT from sedimentary rocks. The studied samples were not gem quality; however, gem opals are found in volcanic environments, as well as in sedimentary environments. [Abstracter’s note: Compare opals from Querétaro, Mexico (high-temperature volcanic), for example, with the Australian opal fields (low-temperature groundwater, similar to a sedimentary environment).] MLJ

Topas. *extraLapis*, No. 13, 1997, 96 pp. [in German]

The German magazine *Lapis* publishes two special issues a year (called “*extraLapis*”) to highlight various minerals or regions. This issue is devoted to topaz, and it is the third recent monograph on this mineral (following D. B. Hoover’s *Topaz*, Butterworth-Heinemann Gem Books, 1992; and a special issue of the *Mineralogical Record* [Vol. 26, No. 1, 1995]).

The first full-length article is a German translation (by Maximilian Glas) of part of the “Historical Perspectives” chapter in Hoover’s book. This chapter explains the etymology of the name *topaz*, and lists other gemstones that have been called topaz, as well as other names that have been used for this mineral. There is also a list of trade names that should no longer be used, such as “Oriental topaz” and “Madeira topaz.” The first section culminates with a paper by Dietmar Schwarz that gives a synopsis of the gemological properties of topaz (together with its simulants) and a summary of its mineralogical properties and crystal structure. Also provided are the geological characteristics of topaz formation and descriptions of selected deposits (Sanarka [Russia], Katlang [Pakistan], and Ouro Preto [Brazil]), and a list of exceptionally large cut topaz gemstones (1,463–36,853 ct; examples taken from Hoover, 1992). This article also provides a valuable discussion of the causes of color in topaz, color treatment by irradiation and heating, and methods of treatment detection. Finally, Dr. Schwarz gives a brief account of inclusions in topaz, illustrated with photomicrographs by Edward Gübelin.

The second part focuses on important topaz mining districts. Heiner Vollstädt and Bernd Lahl describe the history of the Schneckenstein deposit in Saxony, Germany. This was the only major topaz producer in Central Europe and the first deposit to be exploited commercially. Today, however, it is a nature preserve. Next is a reprint of part of the classic paper by Nikolai Ivanovich Koksharov “Über die russischen Topase,” which originally appeared in German in 1855 and described the famous Russian topaz deposits in the Ural mountains and in Transbaikalia. A second article by Dietmar Schwarz on Brazilian topaz focuses mainly on Ouro Preto and the occurrences in eastern Brazil, but it also briefly describes the deposits in Rondonia (western Brazil), where crystals of light blue and colorless topaz are by-products of tin mining. Today, Rondonia is the main source of the topaz

used for color treatment. Andreas Weerth gives a colorful description of traveling and trading in Pakistan (Katlang and the deposits of the Karakorum-Himalaya: Shengus, Dusso, Stak Nala, Niyit-Bruk, Gone) and Afghanistan (Laghman). This account is followed by the German translation (by Christa Behmenburg) of a slightly shortened and updated version of an article by Lanny R. Ream on topaz from the Thomas Range and the Wah Wah Mountains in Utah (*Mineralogical Record*, Vol. 10, No. 5, 1979). Finally, Jan Kanis describes Zimbabwe's St. Anne's mine, which was a major producer of natural blue topaz but is now closed.

The final part of the issue showcases color photographs (most of them previously published) of 14 exquisite topaz specimens, a comprehensive list of the most important and/or interesting topaz sources worldwide, and a short reference list.

[*Abstracter's note*: Back issues of *extraLapis* are available from Christian Weise-Verlag, Orleansstr. 69, D-81667 Munich; phone 89-480-29-33; fax 89-688-61-60; e-mail Lapis.Mineralienmagazin@T-Online.de. Past issues have reported on emerald, gold, rock crystal, fluorite, alpine crystals, tourmaline, petrified wood, native silver, garnet, opal, pyrite and marcasite, and the Ziller Valley in Tyrol, Austria. The most recent issue (No. 14, 1998) focused on calcite.] RT

Tsavorite garnet, king of African gems. R. W. Wise, *Asia Precious*, Vol. 6, No. 3, March 1998, pp. 26–28.

Tsavorite (green grossular garnet) from East Africa is mined in an area northwest of Mombasa, Kenya, within 40 km (25 miles) of the Kenya-Tanzania border. This article primarily discusses the color, clarity, and size considerations that determine the value of this stone.

The finest hues of tsavorite are described as "forest green" and "grass green." As with emeralds, yellow is the bane of tsavorite, and its obvious presence means the gem will not be considered top color. Saturation of color is rarely a factor in evaluating tsavorite.

Tsavorite prices are affected most by the size and location of eye-visible inclusions. Included stones are often cut into cabochons, which typically sell for a quarter of the value of faceted stones of comparable size. Tsavorite is rare in sizes above 3 ct. Approximately 85% of the material mined yields polished stones under 1 ct. Stones over 10 ct make up about 0.1% of total production. MD

DIAMONDS

Angolan progress . . . kimberlites the ultimate goal. *Mining Journal*, London, Vol. 330, No. 8467, February 13, 1998, pp. 121–122.

DiamondWorks is a part owner and the mine operator of two alluvial deposits in Angola—Luo and Yetwene—in the vicinity of Lucapa in Lunda Norte Province. Luo was put into production in July 1997 and yields 6,000 ct/month, valued at US\$238/ct. Yetwene is expected to yield 8,000–9,000 ct/month, valued at \$283/ct.

However, alluvial reserves at Luo are sufficient for only about 18 more months of production (reserves at Yetwene are estimated to last 12 years). Consequently, DiamondWorks is also examining the five known kimberlites on the Luo concession. Two look promising: Camagico and Camatchia. The latter is being explored by a 22-hole vertical drilling program; the deepest hole, at 120 m, was still in kimberlite. "Pre-feasibility" studies have suggested that an open-pit mine is possible, potentially yielding 25,000–40,000 ct/month for 10 years, with an expected value of \$100–\$150/ct, from an ore grading 0.2 ct/ton. This venture would require a serious commitment of capital, however. MLJ

Colorado diamonds: Too little of a good thing. R. Shor, *Jewelers' Circular-Keystone*, Vol. 169, No. 7, July 1998, pp. 100–101.

Redaurum Ltd., majority owner of the Kelsey Lake diamond mine in northern Colorado, closed the mine in September 1997, citing the high cost of additional mining equipment needed to make the mine economic. The mine operated for one year at about half capacity, producing approximately 12,000 carats of rough; stones were sold only in polished form, at six stores in Colorado. [*Editor's note*: For previous entries on this mine, which represented the first attempt to mine diamonds commercially in the U.S. since the mine near Murfreesboro, Arkansas, ceased operations in the early part of this century, see: Winter 1996 Gem News, pp. 282–283, and Spring 1997 Lab Notes, pp. 54–55.] AAL

De Beers faces up to tough times. *Mining Journal*, London, Vol. 330, No. 8470, March 6, 1998, pp. 195, 197.

In March 1998, De Beers Consolidated Mines of South Africa and De Beers Centenary AG of Switzerland reported 1997 aggregate earnings (before investments) of US\$1.04 billion, a 1% increase over 1996. After investments are considered, De Beers earned \$1.23 billion; this was 9% less than its 1996 earnings, and was due primarily to the selling of shares in other mining stocks (JCI and Lonrho) by Anglo American Corp., of which De Beers currently owns 38.5%. Earnings from the "diamond account" rose 6% (to \$849 million), despite poor market conditions toward the end of the year. The Central Selling Organisation is still taking less than 100% of the possible production from member mines. At the end of 1997, De Beers's diamond stockpile was down 6%, to \$4.44 billion.

Diamond sales are vulnerable to overall economic conditions. The worldwide diamond market in 1997, as measured by the wholesale value of polished stones, primarily consisted of the United States (38%), Japan (20%), Asia-Pacific (mainly China and Taiwan, 15%), and Europe (12%). Sales rose 9% in the United States and 1% in Europe, but fell 19% in Japan and 18% in Asia-Pacific, for an overall drop of 4%.

Diamond supplies at the cutting centers were worth

\$5 billion at the start of 1998, and banks were becoming "more wary" of funding continued diamond purchases. There are also signs of polished stones being recycled to cutting centers. *MLJ*

Diadem outlines diamond targets. *Mining Journal*, London, Vol. 330, No. 8470, March 6, 1998, p. 184.

Diadem Resources Ltd. has found three large (up to 20 hectares, or 50 acres) magnetic anomalies at its Leek Springs, California, diamond project. The company interprets these anomalies as diatremes, in part because they occur at the intersections of major structural lineaments. The diatremes are believed to be the main conduits for diamond- and indicator-mineral-bearing volcanic rocks, which outcrop over a widespread area. Exploration will continue in 1998, to identify drilling targets. *MLJ*

Diamond prospecting in the Falklands. *Mazal U'Bracha*, Vol. 15, No. 100, March 1998, p. 63.

British-based Cambridge Mineral Resources has been granted a six-year license to prospect for diamonds in the Falkland Islands. As the Falklands (and South America) were adjacent to Africa in the geologic past, it is hoped that southern African diamonds were deposited on these islands (or their contiguous continental shelf) before the continents drifted apart. The company is encouraged by the reported occurrence of diamond indicator minerals in rivers on one of the islands. *AAL*

A global perspective. C. Pearson, *Mining Journal*, London, *Diamond Supplement*, Vol. 329, No. 8452, October 27, 1997, pp. 11, 13.

Perception is an important factor in the diamond industry. In recent years, there have been great shifts in the relative power of retail buyers and the merchants who sell to them. Middlemen are increasingly being squeezed out. Also, the price of smaller, cheaper diamonds has dropped precipitously compared to the price of larger or finer stones; this may reflect the growing polarization of incomes in the major economies (the rich get richer, the middle classes look for bargains).

On the supply side, De Beers continues to be the major player. The Russian (Gokhran) stockpile has been steadily depleted over the last five years, especially in larger, higher-quality rough. The value of Angola's production is nearly that of Russia's, but political instability makes it hard to predict future supplies. With the promising outlook for Canadian and Russian deposits, the supply of diamonds could grow by 3% per year—if demand grows also. If it does not grow, then De Beers's reorientation of its marketing activities toward "branded" diamonds could cause minor producers still more anguish. The author suggests that diamond miners should consider working together on the issues of supply and demand, competing goods (synthetics, simulants, and treated stones), and marketing. *MLJ*

Growing interest. L. Rombouts, *Mining Journal*, London, *Diamond Supplement*, Vol. 329, No. 8452, October 27, 1997, pp. 1–3.

Diamond exploration continued unabated at the end of 1997, with most activity concentrated on finding primary source rocks, especially in cratons over 2.5 billion years old. Canada has been an attractive target since the Point Lake discoveries (now the Ekati mine) in the Northwest Territories were first announced in 1991. The first pipe at Ekati, called the Panda pipe, is scheduled to produce 3.5 Mct/year, worth about US\$130/ct, by the end of 1998. The nearby Diavik joint venture has also found rich pipes, and production is anticipated to start in 2002. There are newly found kimberlites elsewhere in the Northwest Territories, and at Buffalo Hills in northern Alberta.

In Russia, most of the exploration is centered around the Sakha Republic, where buried kimberlite pipes have been found in the Nyurba district (most notably Botuobinskaya and Nyurbinskaya). In addition, eventual production is expected from diamond pipes in the Lomonosova and Verkhovina project areas, northeast of Arkhangelsk. The nearby Tovskaya and Ust-Pinega regions also are being explored for diamonds, as are Karelia and neighboring Finland.

In Africa, kimberlites are being evaluated in South Africa (for example, the Klipspringer dikes), Zimbabwe, Lesotho (e.g., Liquobong), Botswana (Gope and Martins Drift), and especially Angola. Although political unrest in diamond-rich Angola makes exploitation uncertain, mining companies are showing interest in both kimberlite pipes (e.g., Catoca, Camafuca-Camazambo, and the Alto Kwanza region) and alluvial sources (along the Luo, Chicapa, and Luachimo rivers). Alluvial diamonds are also being sought in Western Kasai and the Kisangani region of the Democratic Republic of the Congo (formerly Zaire). Several groups are pursuing offshore marine alluvial diamonds along the Namibian coast. Exploration is proceeding in several West African countries (Sierra Leone, Guinea, Mali, and Mauritania), but is less advanced.

In Australia, results from further exploration in the Kimberley region (in the general vicinity of the Argyle mine) remain disappointing. Small, potentially economic kimberlites have been found at Merlin, in the Northern Territory, and the exploration focus has now mainly shifted to the Yilgarn craton in southwest Australia.

In China, foreign parties have been invited to improve productivity at the existing diamond mines at Wafangdian (Liaoning Province) and Changma (Shandong Province), and exploration is proceeding in Hebei and Sichuan Provinces. Elsewhere in Asia, alluvial diamonds are being explored both on land (Cempaka) and offshore (the Sunda Shelf) in Kalimantan, Indonesia; and negotiations are underway in India's Madhya Pradesh State for joint ventures to explore and develop known kimberlites in the Raipur district.

Kimberlite pipes have been found in Brazil (near Juina in Mato Grosso State) and Venezuela (Guanamo, west of the alluvial diamond fields). Exploration for alluvial diamonds is proceeding in the Sono and Vermeiho valleys in Brazil's Tocantins State. *MLJ*

Messina's Lesotho diamonds positive. *Mining Journal*, London, Vol. 330, No. 8466, February 6, 1998, p. 105.

Bulk sampling of two kimberlite pipes at Messina Diamond Corporation's Lihobong project in Lesotho has yielded grades of 16.2 carats per 100 tons of ore for the Main Pipe (with average value US\$63.93/ct) and 68.7 ct/100 tons for the Satellite Pipe (with average value \$38.50/ct). Messina is considering an open-pit mine with a projected production of 700,000 ct/year from 2.6 Mton/year of ore for about 11.5 years. *MLJ*

Namibia opens its door to us. G. Charodeyev, *Current Digest of the Post-Soviet Press*, Vol. 50, No. 13, April 29, 1998, p. 23.

Namibian President Sam Nujoma has visited Russia and signed an agreement for a cooperative program to develop his country's diamond industry. Russian companies will carry out geologic exploration and eventually move into mining. The Russians will also help Namibia set up its own polishing industry and will train Namibian cutters. This the first time that Russia has obtained direct access to potential mines in Namibia, and it could use this agreement in forthcoming negotiations with De Beers. *AAL*

River Ranch operations suspended. *Diamond Intelligence Briefs*, Vol. 14, No. 260, March 6, 1998, p. 1628.

Redaurum Ltd. is trying to sell the River Ranch diamond mine in Zimbabwe. Operations have been suspended at the mine, where the January 1998 production of 39,000 carats sold for an average price of US\$15.80/ct. [*Editor's note: This was the only diamond mine in Zimbabwe; in 1997, it produced about 500,000 carats.*] *MLJ*

Russian scene. J. Hill, *Mining Journal*, London, *Diamond Supplement*, Vol. 329, No. 8452, October 24, 1997, pp. 14-15.

Diamond deposits were discovered in Russia in the 1950s. Of the 800-plus kimberlites found since then, about 150 contained diamonds, but only 13 have produced stones in economic grades. In recent years, Russia has produced about 26% (by value) of the world's rough diamond supply. Of the nine major operations since 1959, five are still in production: Mir, Udachnaya, Aykhal, Sytytanskaya, and XXIII Communist Party Congress (CPC). Development is underway at Yubileinaya (Jubilee); and exploration is proceeding at Botuobinskaya, Nyurbinskaya, Festivalnaya, and the Anabar Basin (all these locations are in Sakha). There are plans to increase diamond output by 25% over the next few years if capital

is available.

In the Mirny area, the Mir open pit is depleted at workable levels, but could be deepened if technical problems are overcome. Sputnik is worked out, and CPC is nearly depleted. Internationalnaya could go underground, but it also has major technical difficulties (however, early grades were an amazing 11 ct/ton). In the Udachny area, 480 km north of Mirny, the Udachnaya open pit is nearly depleted, but the mine could go underground; Zarnitza has not been developed due to low diamond grades. In the Aykhal area, 400 km north of Mirny, Aykhal produces 0.5 million carats (Mct) per year, but the stones are of "mediocre" quality. Sytytanskaya produces 0.5 Mct/year, with a "significant percentage" of very large stones; low-grade Komsomolskaya may be mined in the future. Krasnupresnenskaya has not been developed due to geologic problems, while Yubileinaya may replace Udachnaya as Russia's largest diamond mine. The 56 hectare Yubileinaya kimberlite produced 0.5 Mct in 1995, but is not yet in full production; however, buyers report that the stones are not of good quality.

Diamonds have also been found in exploitable primary deposits on the "Winter Coast," 130 km northeast of Arkhangelsk. The main fields are Zolotitsa (where the Lomonosova pipe could produce 3-6 Mct of high-quality diamonds for 30 years or more) and Verkhotina. *MLJ*

Trivalence starts commercial production at Aredor. *Mining Journal*, London, Vol. 330, No. 8475, April 10, 1998, p. 286.

Trivalence Mining Corp. (Canada) has begun commercial operations at its 85%-owned Aredor alluvial diamond mine in Guinea, having upgraded the plant's ore-processing capability to 100 tons/hour. The mining operation produced 16,907 carats of rough diamonds between July 1996 and August 1997. Diamonds sold to date by Trivalence have achieved an average price of US\$624/ct. The largest gem-quality stone, weighing 70.1 ct and recovered from the tailings of a previous processing plant (!), sold for \$2.7 million (over \$38,500/ct). *MLJ*

GEM LOCALITIES

Caratterizzazione mineralogica e gemmologica dei filoni rodingitici di vesuvianite nell'area di Bellecombe (Aosta). [Mineralogical and gemological characteristics of the vesuvianite veins in the Bellecombe area (Aosta Province)]. M. Novaga, *Revista Mineralogica Italiana*, Vol. 21, No. 4, 1997, pp. 360-366. [in Italian with an English abstract]

This article characterizes the vesuvianite found in veins of rodingite within Italy's Bellecombe region. Vesuvianite from Mt. Ros is brown or reddish brown (attributable to its relatively high Ti content), with refractive indices of 1.720-1.730 and a specific gravity of 3.412-3.415. Vesuvianite from the neighboring locality of Banchettes is green or greenish brown, with $\epsilon = 1.717-1.719$ and $\omega =$

1.719–1.720 (for a birefringence of 0.002), and a specific gravity of 3.398–3.415. Gemstones of 1–3 ct have been cut. Chemical analyses are given for vesuvianite from both localities. RAH

Mining and the law: Petrified wood. C. Weller, *International California Mining Journal*, Vol. 67, No. 2, October 1997, pp. 19–20.

In Nevada, collecting of petrified wood from public lands is regulated by both the federal and state governments. Individuals may collect without charge up to “25 pounds [11.3 kg] in weight plus one piece” per day (totaling up to 250 pounds [113 kg] per year) from public lands administered by the U.S. Bureau of Land Management or Bureau of Reclamation; “limited quantities” may be taken from Forest Service lands with the appropriate local permit. Explosives and heavy equipment may not be used, and the material acquired cannot be bartered or sold. Museums, cities, and federal and state agencies may collect pieces weighing more than 250 pounds, provided these samples are publicly displayed.

Petrified wood may be obtained for commercial purposes under federal sales regulations cited in this article. No petrified wood can be taken by anyone, for any purpose, from Petrified Forest National Park in Arizona, or from any land within the jurisdiction of the Nevada Division of State Parks. Nevada’s Board of Museums and History may designate additional protected sites.

Most petrified wood has been silicified—replaced by quartz or chalcedony varieties, or by opal—and most is 225–140 million years old. One species, *Araucarioxylon arizonicum*, is the state fossil of Arizona. MLJ

Opal mining company has “flying start.” *Queensland Government Mining Journal*, Vol. 98, No. 1150, September 1997, p. 49.

An opal mining company could revolutionize “what has traditionally been a cottage industry.” Queensland Opals raised Aus\$2.55 million through the Australian Stock Exchange [becoming the first opal mining company ever listed on the ASX], and used this funding to open Lucky’s mine, at the Kyabra Eromanga site near Quilpie in southwest Queensland. The opal is recovered by systematic strip mining of channel-fill sandstone, which contains boulders. About 10% of the boulders contain gem opal.

A geologic model developed for the mine site performed “exceptionally well.” Advanced exploration techniques (such as satellite imaging) and field work are being used to find additional properties for open-cut mining. Mines are relatively short-lived, but the company hopes to be operating five open-cut mines simultaneously within the next five years. Queensland Opals built a cutting and polishing center in Charleville, and is wholesaling stones (that were purchased from other mines), as well as coordinating marketing endeavors. The ironstone opal matrix is also being marketed. The company will coordinate their efforts to coincide with the year 2000 Olympic Games in Sydney. MLJ

Prospector cuts a colourful figure. T. Winter, *Australia’s Paydirt*, Vol. 1, No. 37, March 1998, p. 64.

Prospector George Swanson owns the only known deposit of blue lace agate, which is located in the district of Karasburg, southern Namibia. This pale blue stone is found in seams about 70 m wide, from which consistent qualities and quantities can be mined. When polished into a sphere, this material resembles the earth as seen from space, which has resulted in its adoption as a symbol of world ecology. Swanson sells rough material for about \$3 per kg. MD

Tanzania consolidating mining. *Advertising Supplement to Mining Journal, London*, Vol. 329, No. 8452, October 24, 1997, 16 pp.

This 16-page supplement begins with an overview of the geography and geology of Tanzania, which has been an important source of diamonds (from the Williamson, or Mwadui, kimberlite) and continues to be a significant source of other gem minerals. In 1996, Tanzania produced 126,670 carats of diamonds, as well as 142,160 kg of other “precious and semiprecious” gems.

Diamondiferous kimberlites are found in the Nyanzian terrain of the Tanzanian craton, in the north-central part of the country. Some of the kimberlites are relatively young, and are thought to have formed less than 50 million years ago. So far, more than 300 kimberlites have been identified, and about 20% of these contain diamonds. (In addition, magnetic surveys have found about 600 potential kimberlite targets.) About half of these occur in clusters in the region between Mwanza and Shinyanga (about 250 km apart), and another cluster is found about 100 km to the south, around Singida. A group of kimberlites east of Lake Nyanza has been barren so far, but alluvial diamonds are found in that area.

The Williamson diamond mine, which was discovered in 1940, reached peak production in the 1960s, with 925,000 carats from 3.5 million tons of ore. By the 1970s, the ore grades had dropped from 25 carats per 100 tons to 8–10 carats per 100 tons, and the processing mill had large power requirements. Recent refurbishment of the mill and changes in mine configuration by 75% owner De Beers resulted in 1996 production of 117,000 carats from 1.1 million tons of ore (with a grade of 10.6 carats per 100 tons), but this is still significantly lower than in the past.

Colored stones are found in a variety of geologic environments in Tanzania. The Proterozoic Usagaran system, part of the Tanzanian craton, hosts high-grade metamorphic gneisses in the Arusha region, including the graphite deposit at Merelani, where tanzanite is found. This mine has an expected life of 40 years at current production rates. Rubies, sapphires, and emeralds are found in high-grade granulite gneisses in the Proterozoic Ubendian and Usagaran systems. Mesozoic and Cenozoic carbonates (such as at Morogoro) locally host ruby and ornamental marble deposits.

The article closes with a discussion of the mining and

investment codes. The Tanzanian government revised its mining laws to encourage investments in 1990, and is working to further encourage foreign investments. Royalties are currently set at 5% for diamonds and 3% for rough colored gems. To encourage the local cutting industry, no royalties are paid on gems that have been cut and polished. MLJ

Team finds tourmaline. *Canadian Jeweller*, Vol. 119, No. 3, June-July 1998, p. 6.

Geologists from the University of British Columbia and the Canadian Museum of Nature (CMN) in Ottawa have recently discovered gem-quality tourmaline in the Canadian Rockies near the Yukon/Northwest Territories border. The colors range from emerald green to red to indigo blue. Colored tourmaline was first found in this area in 1994. Brad Wilson, gem cutter and owner of Alpine Gems in Kingston, Ontario, owns the mineral rights to the site. However, there are no immediate plans to mine the deposit due to the site's remoteness. MM

INSTRUMENTS AND TECHNIQUES

Meiji Technico model GF-252 refractometer-polariscope.

T. Linton, S. Sultman, and G. Peters, *Australian Gemmologist*, Vol. 19, No. 12, 1997, pp. 513–515.

A refractometer and a polariscope are built into this one instrument, which costs substantially less than the two instruments purchased separately. The polariscope is rated as mechanically excellent, as is the quality of its images. The performance of the refractometer is also very good. Only a few limitations of the instrument are mentioned. RAH

A rockhound's guide to UV equipment. *Rock & Gem*, March 1998, Vol. 28, No. 3, pp. 29–32, 34.

Ultraviolet (UV) light assemblies are often used by gem collectors to reveal the hidden fluorescent beauty of their mineral specimens. These lights are now available in a wide range of wavelengths and with more powerful lamps. They come in several models or styles—from large, expensive display lights for museum cases, to handheld, battery-powered models. Short-wave UV lights are most commonly used by collectors, since the majority (80%–90%) of fluorescent minerals will fluoresce brighter to short-wave than to long-wave radiation.

A UV light assembly must have a filter between the bulb and the fluorescent mineral. There are no perfect filters; all will absorb some of the UV they are designed to transmit and, conversely, will transmit some of the visible light that they are designed to absorb. Almost any material that transmits short-wave UV will deteriorate over time when exposed to short-wave UV radiation. This deterioration, called solarization, reduces the amount of short-wave UV transmitted, resulting in weaker fluorescence. High humidity also affects the transmission of short-wave filters, because moisture forms a white

film on them. Even if this coating is removed, it is likely that the glass underlying the filter has been damaged. Thus, short-wave filters should be replaced periodically. Long-wave filters will not solarize and need not be replaced.

Safety is an important factor when using short-wave UV, as even brief exposure can be detrimental to the eyes and skin. Specially designed UV goggles with side protection are recommended. MD

JEWELRY HISTORY

Contributo alla conoscenza dell'amazonite: Studio mineralogico-petrografico e geochimica di elementi di monili neolitici e di esemplari naturali. S. Balzi, S. Vannucci, O. Vaselli, and M. Sozzi, *Mineralogica et Petrographica Acta (Bologna)*, Vol. 40, 1997, pp. 357–371. [in Italian]

A petrographical, mineralogical, and geochemical investigation was carried out on amazonite beads used as jewelry from Neolithic villages in what is now southern Jordan, to determine their geologic provenance. These samples have a uniform mineralogy and chemistry. The study was widened to include various amazonite-bearing deposits (e.g., Colorado, Brazil, Madagascar, Egypt, and Saudi Arabia). Rb, Pb, FeO, and Na₂O data from bulk samples, and Pb isotope ratios of selected amazonite grains, suggest that these Neolithic samples were derived from granite-related pegmatitic bodies found in the Tabuik area of Saudi Arabia. RAH

JEWELRY MANUFACTURING

Angling for pearls. R. Weldon, *Professional Jeweler*, Vol. 1, No. 4, May 1998, p. 70.

Faceting has become a new word in the pearl lexicon. A family in Kofu, Japan, has developed a proprietary technique for faceting pearls that has taken almost a decade to perfect. Pearl's softness (2.5–4 on the Mohs scale) and the propensity of the nacre to flake, present problems for the faceter. Proper faceting requires that the pearls be perfectly spherical and have a thick coat of nacre (with at least two years of growth). Chinese freshwater and Tahitian cultured pearls are considered ideal for faceting because they fulfill these requirements. MM

The renaissance in cabochons. G. L. Wykoff, *Rock & Gem*, Vol. 28, No. 1, January 1998, pp. 64–69.

Cabochon cutting was once assigned "blue-collar status" among lapidaries, but new techniques are reviving interest and respect for this art. Master cabber Bernd Munsteiner and his followers in Germany have delighted the gem world with fabulous geometric gem designs, most of which employ cabochon techniques. This new art of cabochon cutting features dramatic changes in handling gemstones and fashioning both transparent and opaque gem materials. Today's cutters are more creative and must master techniques such as channeling, plateau-

ing, and "running the wheel."

The single wheel is no longer the only device in the innovative cabber's inventory. Many of the modern effects are accomplished with special wheels and customized arbors. Experienced cabbers, for example, have customized their silicon carbide wheels with diamond dressing tools to create dramatic designs. These new concepts merit experimentation since they may offer a whole new approach in design and enhanced optical performance from poorly or deeply colored gems. MD

JEWELRY RETAILING

Beyond the big three: A colorful leap of faith. R. Weldon. *Jewelers' Circular-Keystone*, Vol. 168, No. 5, May 1997, p. 98–102.

Today's consumers are asking for unusual colored stones—even one-of-a-kind gemstones—rather than the traditional rubies, sapphires, and emeralds (the "Big Three") that, in addition to diamonds, are staples in a jeweler's stock. Many of these less traditional stones have been popularized by the television shopping networks. This article suggests the following alternatives to the Big Three: For ruby, there is red spinel, red garnet, rubellite tourmaline, and red beryl; for blue sapphire, there is indicolite tourmaline, blue spinel, blue zircon, and tanzanite; and for emerald, there is peridot, green tourmaline, tsavorite, and green zircon.

Designers have recognized the trend toward other colored stones and are producing exquisite jewelry that both excites and inspires consumers, from stones with unusual inclusions, colors, or patterns. These gem materials, fashioned in repeatable shapes and sizes that are suitable for mass production, are also attracting much attention. Jewelers who offer these alternatives to discriminating clients are learning that there is a better profit margin, since per-carat prices are generally lower than they are for the Big Three. Mai Williams

Diamonds for label junkies. *Mining Journal*, London, Vol. 330, No. 8470, March 6, 1998, pp. 192–193.

De Beers has announced a test-marketing plan for diamonds inscribed with the De Beers brand name and sold through the Central Selling Organisation (CSO). The first market will be in Manchester, United Kingdom. The objective will be to see if consumers will pay a premium for the "extra confidence" inspired by the De Beers name. The De Beers name was chosen because, unlike the CSO, it is already widely recognized by the general diamond-buying public. The marking on the diamond is only visi-

ble with magnification and, according to various grading "agencies," does not affect the grading of the stone. De Beers currently spends \$200 million annually on advertising diamonds, and it hopes to spend its advertising dollars in a way that does not also benefit sellers of diamonds through outside channels. MLJ

SYNTHETICS AND SIMULANTS

Fluid inclusions in synthetic diamond crystals. A. A. Tomilenko, A. I. Chepurov, A. I. Turkin, A. P. Shebanin, and N. V. Sobolev, *Transactions of the Russian Academy of Sciences/Earth Science Sections*, Vol. 353, No. 2, 1997, pp. 247–250.

In the ongoing investigations of the geologic environments in which diamonds form, the authors studied fluid inclusions in synthetic diamonds. Microscopic examination and Raman microspectrometry were performed on diamonds from five different synthetic growth experiments, one of which had a shorter growth time at slightly lower temperature and pressure than the other four. The Raman spectra from the fluid inclusions were inconclusive for indicating the presence of water and carbon dioxide; nitrogen, hydrogen and carbon were not found. Evidence for methane was found in fluid inclusions from all samples, and a graphite film was present in the inclusions within synthetic diamonds that formed over longer growth times. The authors consider this work the first good evidence that hydrocarbons such as methane are important in diamond crystallization. Whether or not hydrocarbons play a similar role in natural diamond crystallization processes needs to be examined in future studies. Jeff Lewis

MISCELLANEOUS

Ground zero. R. Weldon, *Professional Jeweler*, Vol. 1, No. 8, September 1998, pp. 30–31.

Using the "American Ideal Cut" as its base, the American Gem Society (AGS) evaluates seven factors that define a good cut; five of the factors deal with proportions, and the other two quality factors are polish and symmetry. Diamond cut grades range from "0" to "10," with "0" being the highest. Diamonds must exhibit excellent polish and symmetry to merit a high grade. In the last year, there has been a 200% increase in the number of stones submitted to the AGS laboratory for cut grading, due to a growing interest in cut as a diamond quality factor. MM